

DOT/FAA/TCTT-25/15

Federal Aviation Administration
William J. Hughes Technical Center
Aviation Research Division
Atlantic City International Airport
New Jersey 08405

Advanced Early Fire Detection in Aircraft Cargo with MACD And Passive UHF RFID Temperature Sensing While Maintaining False Alarm Resistance

April 2025

Technical Thesis

The research described in this report was funded by the FAA as part of its mission to improve aircraft safety. The views and opinions expressed are those of the author alone and do not necessarily represent the views of the FAA. The FAA assumes no liability for the contents or use thereof. The FAA has not edited or modified the contents of the report in any manner.



U.S. Department of Transportation
Federal Aviation Administration

NOTICE

This document is disseminated under the sponsorship of the U.S. Department of Transportation in the interest of information exchange. The U.S. Government assumes no liability for the contents or use thereof. The U.S. Government does not endorse products or manufacturers. Trade or manufacturers' names appear herein solely because they are considered essential to the objective of this report. The findings and conclusions in this report are those of the author(s) and do not necessarily represent the views of the funding agency. This document does not constitute FAA policy. Consult the FAA sponsoring organization listed on the Technical Documentation page as to its use.

This report is available at the Federal Aviation Administration William J. Hughes Technical Center's Full-Text Technical Reports page: actlibrary.tc.faa.gov in Adobe Acrobat portable document format (PDF).

Form DOT F 1700.7 (8-72)

Reproduction of completed page authorized

1. Report No. DOT/FAA/TCTT-25/15		2. Government Accession No.		3. Recipient's Catalog No.	
4. Title and Subtitle Advanced Early Fire Detection in Aircraft Cargo with MACD And Passive UHF RFID Temperature Sensing While Maintaining False Alarm Resistance				5. Report Date April, 2025	
				6. Performing Organization Code	
7. Author(s) Matthew Eugene Karp				8. Performing Organization Report No. DOT/FAA/TCTT-25/15	
9. Performing Organization Name and Address Graduate Program in Mechanical and Aerospace Engineering Rutgers University New Brunswick, NJ				10. Work Unit No. (TRAIS)	
				11. Contract or Grant No.	
12. Sponsoring Agency Name and Address Federal Aviation Administration William J. Hughes Technical Center Aviation Research Division Atlantic City International Airport New Jersey 08405				13. Type of Report and Period Covered	
				14. Sponsoring Agency Code	
15. Supplementary Notes					
16. Abstract This study introduces a novel approach to enhance fire protection in aircraft cargo compartments, motivated by the urgency to address catastrophic in-flight fires recorded between 2006 and 2011. The method uses ultra-high frequency (UHF) radio frequency identification (RFID) temperature sensing tags and advanced algorithmic analysis to enhance fire detection capabilities within unit load devices (ULDs). This approach significantly reduces detection times while minimizing false alarms. The first objective was to create an economical, battery-free fire detection system with UHF RFID temperature sensing tags installed within ULDs. This positions the temperature sensing tags closer to potential fire sources than traditional cargo compartment ceiling-mounted smoke detectors. Wireless temperature sensing tags allow the ULDs to move in and out of aircraft. Passive sensors address the challenges of battery-powered systems, such as battery changes and thermal runaway risks. The second objective sought to enhance the RFID-based system with near real-time temperature monitoring capabilities within ULDs. The system provides accurate temperature trend analysis by incorporating a moving average convergence divergence (MACD) algorithm adapted from financial markets. This significant advancement improves fire detection times and supports communication of conditions within ULDs to flight crews, enabling quicker response actions.					
17. Key Words Aircraft Fire Safety -- Protection Aircraft Fire Safety -- Detection			18. Distribution Statement This document is available to the U.S. public through the National Technical Information Service (NTIS), Springfield, Virginia 22161. This document is also available from the Federal Aviation Administration William J. Hughes Technical Center at actlibrary.tc.faa.gov .		
19. Security Classif. (of this report) Unclassified		20. Security Classif. (of this page) Unclassified		21. No. of Pages 179	19. Security Classif. (of this report) Unclassified

ADVANCED EARLY FIRE DETECTION IN AIRCRAFT CARGO WITH MACD AND PASSIVE UHF
RFID TEMPERATURE SENSING WHILE MAINTAINING FALSE ALARM RESISTANCE

By

MATTHEW EUGENE KARP

A dissertation submitted to the

School of Graduate Studies

Rutgers, The State University of New Jersey

In partial fulfillment of the requirements

For the degree of

Doctor of Philosophy

Graduate Program in Mechanical and Aerospace Engineering

Written under the direction of

Francisco Javier Diez-Garias

And approved by

New Brunswick, New Jersey

May 2024

ABSTRACT OF THE DISSERTATION

ADVANCED EARLY FIRE DETECTION IN AIRCRAFT CARGO WITH MACD AND PASSIVE UHF RFID TEMPERATURE SENSING WHILE MAINTAINING FALSE ALARM RESISTANCE

by MATTHEW EUGENE KARP

Dissertation Director:
Francisco Javier Diez-Garias

This study introduces a novel approach to enhance fire protection in aircraft cargo compartments, motivated by the urgency to address catastrophic in-flight fires recorded between 2006 and 2011. The method uses ultra-high frequency (UHF) radio frequency identification (RFID) temperature sensing tags and advanced algorithmic analysis to enhance fire detection capabilities within unit load devices (ULDs). This approach significantly reduces detection times while minimizing false alarms.

The first objective was to create an economical, battery-free fire detection system with UHF RFID temperature sensing tags installed within ULDs. This positions the temperature sensing tags closer to potential fire sources than traditional cargo compartment ceiling-mounted smoke detectors. Wireless temperature sensing tags allow the ULDs to move in and out of aircraft. Passive sensors address the challenges of battery-powered systems, such as battery changes and thermal runaway risks.

The second objective sought to enhance the RFID-based system with near real-time temperature monitoring capabilities within ULDs. The system provides accurate temperature trend analysis by incorporating a moving average convergence divergence (MACD) algorithm adapted from financial markets. This significant advancement improves fire detection times and supports communication of conditions within ULDs to flight crews, enabling quicker response actions.

The third objective aimed to reduce false alarms through an algorithm capable of identifying significant temperature differences between separate ULDs. To achieve this, RFID temperature sensors were installed across all ULDs for continuous environmental monitoring. Under normal conditions, only minimal temperature variance is expected among ULDs. However, if the system detects a notable temperature differential between any two ULDs, it issues an alert. This method significantly enhances fire detection accuracy and reduces the likelihood of false alarms.

Experimental results reveal a linear correlation between heat input and the algorithm's response. This correlation is crucial for near real-time monitoring of varying fire conditions within ULDs. Additionally, the RFID system outperformed traditional external smoke detectors by reducing smoldering fire detection times to an average of 11.7 minutes. For specific 12.08 Wh lithium-ion fire configurations, the RFID system detected them in 5.4 minutes on average, whereas traditional external smoke detectors failed to detect them at all.

Acknowledgments

I am deeply grateful to God, whose guidance and strength have supported me throughout this journey. I am profoundly thankful for my wife, Lydia's unwavering love and encouragement. I owe a heartfelt thanks to my parents, Scott and Mary Karp. Their love and sacrifices have shaped me into the person I am today. I fondly remember my father, who unexpectedly passed away in 2021, just a day after receiving his COVID-19 booster. Ecclesiastes 1:18 states, "For in much wisdom is much grief: and he that increaseth knowledge increaseth sorrow." His memory and spirit have been a guiding light. My son, Luke, deserves special recognition for his endless curiosity and joy, which have inspired and motivated me. I am thankful for the love my brothers, Shane and David, and the rest of my family and friends have shown me; they also helped shape me into who I am today.

I extend my deepest gratitude to my academic advisor, Javier Diez, for his invaluable guidance and to my committee members, Dick Hill, Gary Hunter, and Yogesh Jaluria, for their essential feedback. Special thanks to Gino Zazenski, Will Zazenski, and Patrick Monaghan for their critical contractor support and our IT team, Frank Hahn and Michael Donio, for their indispensable technical assistance.

I am also thankful for the consulting insights from James Quintiere, Jo Major, Richard Lyon, Richard Walters, and Jamie Lessard. I appreciate the managerial support from Carleen Houston, Robert Ochs, and Michael Givens, whose guidance has been crucial in this project. To everyone who has contributed, including the entire Fire Safety Branch, your help has been integral to my professional and personal growth. Thank you.

Table of Contents

ABSTRACT OF THE DISSERTATION	ii
Acknowledgments	iv
Table of Contents	v
List of Tables	x
List of Illustrations	xi
Acronyms.....	xiv
1. Introduction	1
2. Literature Review	5
2.1. Aircraft Fire Protection.....	6
2.1.1. Aircraft Cargo Compartments	7
2.1.2. Regulatory Framework for Cargo Smoke Detection Systems.....	8
2.1.2.1. Smoke Generators.....	9
2.1.2.2. False Alarms	11
2.1.3. Cargo Compartment Fire Suppression and Halon 1301 Substitute	12
2.2. Fire Types and Detection Challenges	13
2.2.1. Smoldering Fires	14
2.2.2. Lithium Battery Fires.....	15
2.2.3. Heat Release Rate	17

2.3.	Fire Detection Methodologies	18
2.3.1.	Smoke Detectors	19
2.3.2.	Heat Detection.....	20
2.3.3.	Gas Detection	21
2.4.	Unit Load Device Safety and Technology	22
2.4.1.	Fire Hardened ULDs	24
2.4.2.	ULD Related Aircraft Accidents and NTSB Recommendations.....	25
2.4.3.	Study of ULD Fire Characteristics and Implications for Fire Safety	26
2.4.4.	Advancements in ULD Fire Detection and Suppression Measures	27
2.5.	RFID Technology.....	29
2.5.1.	Frequency Bands for RFID.....	30
2.5.2.	Signal Propagation and Attenuation in RFID Systems.....	32
2.5.3.	Radiation Patterns and Antenna Characteristics	33
2.5.4.	Orientation Sensing	36
2.5.5.	Environmental Considerations	37
2.5.6.	RFID Technology in Airline Baggage and Cargo Management	39
2.6.	Literature Review Conclusion.....	41
3.	Research Methodology.....	43
3.1.	Description of Test Scenarios	45

3.1.1.	Controlled Fire Scenario.....	46
3.1.2.	Smoldering Fire Scenario	47
3.1.3.	Lithium-Ion Battery Scenario	49
3.2.	Experimental Setup.....	50
3.2.1.	Mock Cargo Compartment Ceiling Setup	51
3.2.2.	ULD Configuration.....	51
3.3.	Instruments Used in Research	52
3.3.1.	Instrument Installation.....	57
3.4.	Smoke Detection Analysis.....	60
3.5.	Heat Detection Analysis	62
3.5.1.	Traditional MACD Stock Analysis Background	63
3.5.2.	Repurposed MACD for Heat Detection Background.....	66
3.5.3.	MACD Heat Detection Test Example	68
3.5.4.	MACD Heat Detection Performance Metrics	73
3.5.5.	MACD Heat Detection Operational Use	75
3.6.	Research Methodology Conclusions	77
4.	Results and Analysis.....	79
4.1.	Analysis of Moving Average Configurations	80
4.1.1.	MACD Configuration and Activation Threshold Analysis	81

4.1.2.	MACD Configuration and Sensor Maximum Analysis	84
4.1.3.	MACD Configuration and Detection Time Analysis	88
4.1.4.	Practical Implications and Optimizing MA Intervals Summary	92
4.2.	Analysis of Heat Sensor Location	94
4.2.1.	Heat Sensor Location and Sensor Maximum Analysis	95
4.2.2.	Heat Sensor Location and Detection Time Analysis	96
4.2.3.	Practical Implications and Optimizing Heat Sensor Location Analysis ..	98
4.3.	Analysis of Smoke Sensor Configurations	99
4.3.1.	Smoke Sensor Location Analysis	100
4.3.2.	Optimizing Smoke Sensor Location Analysis	102
4.4.	Evaluation of Controlled Fire Scenarios	103
4.4.1.	Heat Detection Analysis for Controlled Fire Scenarios	105
4.4.2.	Smoke Detection Analysis for Controlled Fire Scenarios	107
4.4.3.	Fire Detection Comparison for Controlled Fire Scenarios	110
4.5.	Evaluation of Smoldering Fire Scenarios	113
4.5.1.	General Test Observations for Smoldering Fire Scenarios	114
4.5.2.	20-50 and 5-20-min MA Heat Detection Analysis for Smoldering Fires	120
4.5.3.	Fire Detection Comparison for Smoldering Fire Scenarios	122

4.6.	Evaluation of Lithium-Ion Thermal Runaway Scenarios	124
4.6.1.	General Test Observations for Lithium-Ion Fires	125
4.6.2.	20-50 and 5-20-min MA Heat Detection Analysis for Lithium-Ion Fires	130
4.6.3.	Fire Detection Comparison for Lithium-Ion Fires	132
4.7.	Results and Analysis Conclusions	133
5.	Cost Benefit Analysis.....	135
5.1.	Cost Analysis	135
5.2.	Benefit Analysis.....	138
5.3.	Cost Benefit Analysis Conclusions.....	139
6.	Conclusion and Future Directions.....	141
6.1.	Summary of Key Findings.....	143
6.2.	Future Research	146
6.3.	Extended Applications Beyond Aviation Fire Detection	148
	References.....	150

List of Tables

Table 1 AAY and AKE Container Information.....	24
Table 2 Frequency and Wavelength of Various Frequency Bands.....	30
Table 3 Breakdown of Various Tested Moving Average Configurations	80
Table 4 Interaction Between Moving Averages and Activation Thresholds	81
Table 5 Interaction Between Moving Averages and Maximum Sensor Response.....	85
Table 6 Interaction Between Moving Averages and Detection Times.....	89
Table 7 Effect of Short-Term and Long-Term Moving Average Configurations on RFID Heat Detection System Performance Parameters	93

List of Illustrations

Figure 1 Schematic of Standard Smoke Generator 11

Figure 2 Relationship Between Cell Energy and Vent Gas Volume at Various SOCs..... 17

Figure 3 Spatial Orientation Map Example 34

Figure 4 Radiation Pattern Example (a) Azimuth Patten (b) Elevation Pattern..... 35

Figure 5 Beamwidth Example 36

Figure 6 Schematic Layout of Test Setup Components (Not to Scale)..... 45

Figure 7 Aviator 440 Smoke Generator Piped into Fire ULD 47

Figure 8 Insulated Aluminum Pipe Containing Wood Pellets for Smoldering..... 48

Figure 9 Arrangement for Battery Testing..... 49

Figure 10 Schematic Representation of Battery Short-Circuit Test Setup 50

Figure 11 Design of Mock Cargo Compartment Ceiling with Vinyl Smoke Cover 51

Figure 12 Comparative View: Fire ULD (Left) and Reference ULD (Right) 52

Figure 13 Axzon RFM3200-AFR Temperature Sensing RFID Tag..... 54

Figure 14 SensThys SensArray Enterprise UHF RFID Reader Configuration..... 56

Figure 15 Placement of Temperature Sensing RFID Tags within Fire ULD 58

Figure 16 Distribution of Light Obscuration Meters in Test Environment (Top-Down View)
..... 60

Figure 17 (a) Daily Stock Prices with 12-Day and 26-Day EMAs Over Time..... 65

Figure 18 Analysis of Temperature Fluctuations and Moving Averages During 89W Test....
..... 69

Figure 19 Analysis of Short-Term (5-min ma) and Long-Term (20-min ma) MACD..... 69

Figure 20 Analysis of Short-Term (20-min ma) and Long-Term (50-min ma) MACD.....	70
Figure 21 MACD, Signal, and Histogram Analysis (5-20-min MA Configuration).....	71
Figure 22 MACD, Signal, and Histogram Analysis (20-50-min Configuration)	72
Figure 23 Overview of Key Performance Metrics in RFID-Based Detection	75
Figure 24 Grid Layout Example of ULDs.....	76
Figure 25 Activation Thresholds for Varying Short-Term Moving Averages	82
Figure 26 Activation Thresholds for Varying Long-Term Moving Averages	83
Figure 27 Maximum Sensor Response for Varying Short-Term Moving Averages.....	86
Figure 28 Maximum Sensor Response for Varying Long-Term Moving Averages.....	87
Figure 29 Detection Time for Varying Short-Term Moving Averages	90
Figure 30 Detection Time for Varying Long-Term Moving Averages	91
Figure 31 Sensor Height vs. Maximum Sensor Response Analysis (20-50min MA).....	96
Figure 32 Correlation Between Sensor Height and Detection Time (20-50min MA).....	97
Figure 33 Placement of Temperature Sensing RFID Tags within Fire ULD Emphasizing the 6.4mm Mount	99
Figure 34 Light Obscuration in Relation to Sensor Distance from ULD Fire Door.....	101
Figure 35 Optimal Smoke Sensor Placement and Smoke Flow Dynamics in Cargo Compartment.....	103
Figure 36 Correlation of Heat Input to Max Sensor Response in Simulated Fire Tests...	106
Figure 37 Analysis of Heat Input vs. Smoke Detection and Light Obscuration.....	108
Figure 38 Comparison of Heat and Smoke Detection Times Relative to Heat Input	111

Figure 39 (a) Comparative Ratio of Response Times Between Heat and Smoke Detection	
(b) Comparative Detection Times Between Heat and Smoke Detection.....	112
Figure 40 Temperature Profile Analysis of Smoldering Fire Tests in ULDs.....	117
Figure 41 Study of Correlation Between Heat Generation and Smoke Propagation.....	118
Figure 42 Maximum Sensor Temperature Response in Smoldering Fires	120
Figure 43 Detection Time Analysis for Smoldering Fires (5-20 vs. 20-50-min MA)	121
Figure 44 Comparison of ULD Heat and Aircraft Smoke Detection in Smoldering Fires.	123
Figure 45 Temperature Monitoring of Lithium-Ion Cells During Thermal Runaway.....	126
Figure 46 Sensor Response to Thermal Runaway (5-20-min MA Configuration)	128
Figure 47 (a) Light Obscuration within ULD During Lithium-Ion Thermal Runaway (b)	
Smoke Detection in Cargo Compartment During Lithium-Ion Thermal Runaway	129
Figure 48 Comparison of Detection Times in Lithium-Ion Fires (5-20 vs. 20-50-min MA)	
.....	131
Figure 49 ULD Heat Detection vs. Aircraft Smoke Detection in Lithium-Ion Fires.....	132

Acronyms

A4A	Airlines for America
AS	Aerospace Standard
ATA	Aerospace Transportation Association
ASSD	Air sampling smoke detectors
CNT	Carbon nanotube
CAAS	Civil Aviation Authority Singapore
CASA	Civil Aviation Safety Australia
CFR	Code of Federal Regulations
EPC	Electronic product code
EASA	European Aviation Safety Agency
ETSI	European Telecommunications Standards Institute
FAA	Federal Aviation Administration
FCC	Federal Communications Commission
FCSRG	Fire and Cabin Safety Research Group
FCC	Fire containment cover
FSS	Fire suppression system
FRC	Fire-resistant container
FSPL	Free space path loss
FWHM	Full width at half maximum
GPIO	General-purpose input/output
HRR	Heat release rate
IC	Integrated circuit
IATA	International Air Transport Association
LCO	Lithium cobalt oxide
LFP	Lithium iron phosphate
LF	Low frequency
MA	Moving average
MLR	Mass loss rate
MPS	Minimum performance standards
MACD	Moving Average Convergence Divergence

ANAC	National Civil Aviation Agency – Brazil
NTSB	National Transportation Safety Board
%obs/m	Percent light obscuration per meter
PPE	Personal protective equipment
PoE+	Power over ethernet plus
Li-Ion pBVG	Premixed lithium-ion battery vent gas
RF	Radio frequency
RFID	Radio frequency identification
RAIN	Radio frequency identification and networking
ROR	Rate of rise
RSSI	Received signal strength indicator
RJ-45	Registered jack-45
RHCP	Right-hand circular polarization
SMPS	Scanning mobility particle sizer
SAE	Society of Automotive Engineers
SOC	State of charge
SMA	Sub-miniature version A
SAW	Surface acoustic wave
TID	Tag identifier
TSO	Technical Standard Order
HF	High frequency
TCP/IP	Transmission control protocol/internet protocol
TCCA	Transport Canada Civil Aviation
UHF	Ultra-high frequency
UV/VIS	Ultraviolet-visible spectroscopy
ULDs	Unit load devices
ULDR	Unit Loading Device Regulations
CAA	United Kingdom Civil Aviation Authority
VSWR	Voltage standing wave ratio
Wh	Watt-hours
WBM	Weight and balance manual

1. Introduction

Timely fire detection within aircraft cargo compartments, particularly involving fires originating within unit load devices (ULDs), remains a persistent challenge in the aviation industry. ULDs, required for cargo transport, can unintentionally hinder the timely detection of fires. This hindrance is due to the inherent design of ULDs that encase cargo, potentially trapping smoke inside. When a fire starts inside a ULD, the resulting smoke needs to find its way out of the container before potential detection. This is because traditional smoke detectors are outside the ULDs and typically mounted on the ceilings of cargo compartments. Consequently, there is a delay in detecting the smoke, as it must travel from inside the ULD to the open cargo space where the detectors are located.

Between 2006 and 2011, three catastrophic in-flight cargo fires originating within ULDs highlighted the dire consequences of delayed fire detection [1] [2] [3]. These incidents revealed a critically short response time between fire warning indications to the flight deck and subsequent system failures, highlighting an urgent need for improved detection methods.

This thesis introduces an innovative approach to address this issue, focusing on developing and implementing an ultra-high frequency (UHF) radio frequency identification (RFID) fire detection system. This system uses RFID temperature sensing tags strategically placed within ULDs, combined with the novel application of the moving average convergence divergence (MACD) algorithm. The MACD algorithm, traditionally

used in financial markets for trend analysis, is repurposed here to monitor and analyze temperature variations. This algorithm enhances the heat detection system's ability to detect fires that might not have reached the thresholds required to trigger traditional heat detectors. This thesis includes a comparative analysis of the effectiveness of the RFID heat detection system against traditional smoke detection systems used in aircraft cargo compartments, focusing on the speed of fire detection for various fire scenarios.

The necessity for improved fire protection in cargo compartments has been recognized by the National Transport Safety Board (NTSB), leading to recommendations for enhanced fire detection systems [4] [5]. These recommendations have informed the focus of this research, which aims to address the gaps identified in current fire safety measures. Studies conducted by the NTSB and the Federal Aviation Administration (FAA) have provided insights into the limitations of existing fire detection systems [4] [5] [6] [7] [8]. Additionally, efforts by private entities, such as Telair and FedEx Express, to develop ULD fire detection systems have been considered [9] [10]. However, air carriers have yet to adopt these advanced technologies widely, indicating a significant opportunity for improvement in early detection of onboard fires for ULDs.

In collaboration with the FAA William J. Hughes Technical Center, this research has the following objectives:

- **Cost-effective, Battery-Free Fire Detection System:**

The first objective focuses on creating a cost-effective, battery-free fire detection system using UHF RFID and temperature sensing tags within ULDs. This placement strategy brings the sensors closer to potential fire sources than traditional ceiling-mounted smoke detectors in aircraft cargo compartments. By utilizing wireless temperature sensing tags, the system facilitates the movement of ULDs in and out of aircraft.

- **Near real-time Fire Monitoring and Early Detection:**

The second objective is to provide flight crews near real-time data on fire status and location within the aircraft's cargo compartment's ULDs. The system will integrate near real-time monitoring with enhanced detection capabilities, designed to alert the crew faster than current systems used in aircraft cargo compartments. Additionally, it offers information regarding the potential fire's location and severity.

- **False Alarm Reduction and System Reliability:**

The third objective is to develop an algorithm that reduces false alarms to improve the fire detection system's reliability. This algorithm balances high sensitivity to actual fire events and minimal false positive rates, which is crucial for maintaining the trust of fire detection systems in aviation settings.

Collectively, these objectives aim to address the current limitations in fire safety within aircraft cargo compartments. It offers a path towards safer and more efficient in-flight fire detection and management. The expected outcomes include technological advancements and improvements in safety protocols and operational procedures in the aviation industry.

2. Literature Review

This section examines the challenges and advancements in fire detection within aircraft cargo compartments, focusing on ULDs. It highlights the lessons learned from past catastrophic in-flight fire incidents, notably those between 2006 and 2011, which exposed the inadequacies of current aircraft fire protection systems. This literature review identifies critical gaps in current fire detection technologies and regulatory frameworks, setting the stage for exploring UHF RFID technology to enhance fire safety protocols.

Central to this review is exploring a UHF RFID-based fire detection system. This system leverages RFID temperature sensing tags within ULDs and employs a MACD algorithm for temperature monitoring. This novel approach represents a significant shift from conventional methods. The exploratory phase included assessing the potential of RFID gas sensors. Despite their promising capabilities in detecting gases indicative of fire before visible smoke or significant heat generation, their commercial unavailability has limited their application.

The literature review encompasses an analysis of existing fire safety regulations, studies by authoritative bodies like the NTSB and FAA, and the latest advancements in fire detection technology, focusing on RFID applications in aviation. This overview sets the stage for understanding the state of fire safety in aircraft cargo compartments and the potential of RFID technology to address existing gaps and enhance overall fire safety protocols.

2.1. Aircraft Fire Protection

Aircraft fire protection research aims to prevent fatal accidents caused by in-flight fires and improve survivability during post-crash fires. The Fire and Cabin Safety Research Group (FCSRG) is an international group of Airworthiness Authorities. It directs cabin and fire safety research projects [11]. Member authorities include the FAA, Transport Canada Civil Aviation (TCCA), United Kingdom Civil Aviation Authority (CAA), European Aviation Safety Agency (EASA), National Civil Aviation Agency – Brazil (ANAC), Civil Aviation Safety Australia (CASA), and Civil Aviation Authority Singapore (CAAS). The FCSRG meets 2-3 times yearly with the International Aircraft Materials Fire Test Working Group and the International Aircraft Systems Fire Protection Working Group [12]. These meetings are open to the public and include international aviation authorities, government agencies, airframe manufacturers, systems and parts manufacturers, airlines, and academia.

The FAA has distinct but interrelated research areas in its Fire Protection Branch. These include cargo fire protection, propulsion fire suppression, power and fuel fire protection, cabin interiors and passenger survivability, and advanced fire research. The goal of cargo fire protection research is to reduce the risks due to cargo fires by performing tests to support the development of new standards for fire detection, containment, and suppression in cargo containers and cargo compartments and tests to evaluate new fire suppression agents and systems for aircraft cargo compartments. The

scope of cargo fire protection research also includes tests to characterize the hazards of various cargo commodities, such as lithium-ion batteries.

2.1.1. Aircraft Cargo Compartments

Title 14 CFR §25.857 outlines six classifications for aircraft cargo compartments, ranging from Class A to Class F, each with distinct fire protection measures to ensure safety during flight operations [13]. Class C and E compartments are relevant to this report as they are the primary standards employed on large airplanes for transporting cargo and passenger baggage.

Class A compartments are designed for easy fire detection and manual extinguishment by crew member due to their proximity to the crew station.

Class B compartments are accessible in flight with a smoke or fire detection system to alert the crew. Using a handheld fire extinguisher, a designated access point allows for fighting fires in these compartments.

Large passenger aircraft contain Class C compartments. They are equipped with an approved smoke or fire detection system that provides warnings to the flight deck. Additionally, these compartments have an approved built-in fire suppression system controllable from the flight deck. Measures are in place to control ventilation and drafts to ensure the suppression agent's effectiveness in controlling fires. These compartments also prevent hazardous quantities of smoke, flames, or suppression agents from entering any occupied area.

As of March 19, 1998, Class D compartments became obsolete due to Amendment 25-93 to 14 CFR §25.857 [14]. Their initial design aimed to control fires by depleting oxygen, but several uncontrollable fires led to removing this class from the regulations.

Class E, or main deck cargo compartments, are exclusively found in freighter aircraft designed for cargo transport. They feature a separate approved smoke or fire detection system to alert the flight crew. Unique to Class E is the capability to shut off ventilating airflow to, or within, the compartment, with controls accessible to the flight crew. However, research reveals that depressurization may not prevent flashover in cargo fires, though Halon 1301 significantly reduces fire risks [15]. Additionally, measures are in place to prevent hazardous smoke, flames, or noxious gases from reaching occupied compartments. The design also ensures that required crew emergency exits are accessible under cargo loading conditions, providing quick and safe evacuation for the crew in case of ground emergencies.

2.1.2. Regulatory Framework for Cargo Smoke Detection Systems

FAA regulations require the cargo smoke detection system to detect a fire within one minute after the start of a fire and before it can threaten the airplane's structural integrity [16]. Airframe manufacturers use calibrated smoke generators that produce an aerosol at critical locations within the coverage area to certify cargo compartment smoke detection systems. Furthermore, the detector must alarm within 60 seconds after the start of aerosol production used to simulate a fire onset [16] [17] [18]. However,

there is a discrepancy between this regulatory requirement and the practical challenges ULDs cause in cargo compartments, which can delay smoke detection.

The detection time is dependent on multiple variables. These variables include thermal buoyancy, the density of smoke production, smoke particle size, the volume and ceiling height, the number of smoke detectors and their locations, and other contributing factors [18] [19] [20] [21].

There is ongoing work within an international working group (Cargo Smoke Detection Task Group) involving major airframe manufacturers and Airworthiness Authorities to create a handbook to outline a qualification procedure for smoke generators [18]. The group aims to define values and tolerances for aerosol production and transport to achieve an international agreement on the performance of smoke generators for aircraft use.

2.1.2.1. Smoke Generators

FAA regulations require that the smoke detection systems in commercial aircraft cargo compartments be capable of alerting the flight crew with a visual signal within one minute of a fire's start. Furthermore, FAA guidance states that the design of the inflight smoke detection certification testing is to demonstrate that the smoke detection system will detect a smoldering fire that produces a small amount of smoke.

Experiments were conducted to determine which smoke generator adjustable settings affect smoke detection time, intending to develop test methods to characterize

smoke generators [18] [19] [20] [21]. The studies showed that increasing the gas propellant pressure in smoke generators results in a higher smoke output. The volumetric flow rate of the smoke exiting the smoke generator is sensitive to several factors, including the wattage of the chimney heater, the gas propellant pressure, and the type of gas propellant. The chimney heater wattage is the primary contributor to this flow rate, aiding in quicker detection of fires. Using carbon dioxide as the gas propellant instead of nitrogen or helium produces smoke that is more effective at activating size-discriminating smoke detectors and is resistant to false alarms. Full-scale tests validated these findings, demonstrating that increases in smoke production and transport lead to earlier detection times of simulated fires.

Additional experiments focused on revealing the properties of smoke generators used by four major aircraft manufacturers for certifying smoke detection systems for cargo compartments [18] [19] [20] [21]. These tests found that these smoke generators' average volumetric flow rate was around $15 \pm 2.6 \text{ ft}^3/\text{min}$, with an average steady-state light obscuration of $32 \pm 17\%/ft$.

The smoke generators detailed in this discussion are specialized units designed to produce temperature-resistant artificial smoke (Figure 1). Smoke generators use inert gas to propel mineral oil into a heat exchanger. The heat exchanger vaporizes the mineral oil and creates a nontoxic fog similar in appearance to smoke. The smoke exits through a chimney incorporated with heaters to create a thermally buoyant plume.

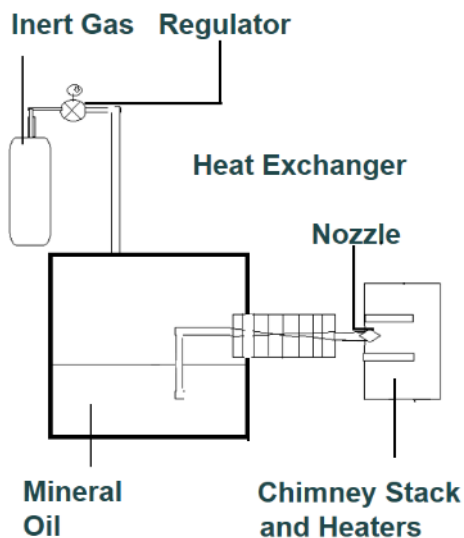


Figure 1 Schematic of Standard Smoke Generator

The relevant parameters for the performance qualification of internationally standardized smoke generators include considerations such as particle size, volumetric flow rate, and transient and steady-state light obscuration [18] [19] [20] [21]. The values of these parameters vary depending on the smoke generator model and its operation. The gas propellant, gas propellant pressure, and heater wattage affect these measured metrics.

2.1.2.2. False Alarms

Between 2002 and 2011, an average of seventy fire or smoke detector events occurred annually in inaccessible cargo areas for passenger and freighter aircraft [22]. Approximately 1% of these flight deck warnings of smoke or fire in inaccessible cargo areas resulted from actual fires [22]. The typical procedure of an inflight warning from

fire detection systems is to discharge the fire suppression agent into the cargo compartment and divert the aircraft to the nearest suitable airport [16]. False alarms can result in losing faith in the fire detection system, inconvenience passengers, and a financial burden on the airlines.

To reduce the frequency of false alarms, the FAA issued Technical Standard Order (TSO) C1e in 2014 to adopt the minimum performance standards (MPS) outlined in the Society of Automotive Engineers (SAE) Aerospace Standard (AS) 8036, which includes criteria for smoke detectors resisting alarms from nuisance sources such as water vapor, insecticide aerosols, dust, and light [23].

False alarm-resistant smoke detectors onboard aircraft typically use redundant smoke detectors that require the simultaneous activation of two individual detectors in one location or multi-wavelength light-scattering smoke detectors that use size discrimination to reject nuisances. Size discrimination is effective because smoke particles are typically less than one micron, while false alarm nuisances are usually larger than one micron [19] [21].

2.1.3. Cargo Compartment Fire Suppression and Halon 1301 Substitute

The Montreal Protocol is an international agreement designed to cut ozone-depleting agents. The international agreement led to a production ban on Halogenated fire suppressants such as Halon 1301 in 1994 [24]. Although production has stopped, the use of recycled Halon 1301 for the aviation industry continues. Halon 1301 is a highly

effective fire suppressant and has been the aviation standard since the 1960s. Since 2018, aircraft requiring a new type of certification must have a non-ozone-depleting agent for their cargo fire suppression system [25]. The European Commission mandates this to fly within European airspace. Additionally, the European Commission requires that aircraft with Halon 1301 cargo fire suppression systems retrofit their fire suppression system with a non-ozone-depleting agent by 2040 to fly within European airspace [24].

There is a requirement for the Halon 1301 substitute to pass the minimum performance standard (MPS) test. Prerequisites to the MPS test are that the agent must pass the environmental and toxicology guidelines [25]. The design of the MPS is to show that the replacement agent provides the same or a higher level of protection as Halon 1301. Cargo MPS comprises four fire test scenarios in a 56.6 m³ simulated aircraft cargo compartment. These include a bulk load fire, containerized fire, flammable liquid fire, and aerosol can explosion test.

2.2. Fire Types and Detection Challenges

This section examines smoldering and lithium battery fires and their challenges in aircraft cargo compartments. It also underscores the importance of heat release rate (HRR) in this context. The HRR measures a fire's energy output, informing the design of detection systems by quantifying fire intensity and potential severity.

2.2.1. Smoldering Fires

Smoldering fires are unique fires characterized by their flameless combustion process. Unlike typical flaming fires, smoldering fires burn slower and at lower temperatures. However, they pose a significant hazard, as they can escalate into more dangerous flaming fires when exposed to increased levels of oxygen [26] [27]. This transition from a smoldering to a flaming fire is critical, especially in confined spaces like aircraft cargo compartments.

The primary mechanism driving smoldering fires is fuel oxidation, which generates heat. This heat is the crucial element that sustains combustion, even without flames. A smoldering fire may remain contained and less intense when oxygen levels are lower.

One of the most challenging aspects of smoldering fires is their early detection. Due to their low-temperature, flameless nature, they can often go undetected by traditional fire detection systems, which are typically designed to respond to higher temperatures and flames or smoke. In the context of aircraft cargo compartments, this poses a significant risk, as the delay in detecting such fires can lead to situations where they have already transitioned into flaming fires, which are far more hazardous and difficult to manage.

2.2.2. Lithium Battery Fires

The transport of lithium batteries as cargo onboard freighter aircraft creates a potential hazard to aircraft safety. Between January 23, 2006, and June 30, 2021, 322 aviation events with smoke, fire, extreme heat, or explosions involving lithium batteries occurred while boarding, in flight, after transport, or before loading for passenger and freighter aircraft [28].

A *cell* is a single-encased electrochemical component, and a *battery* is two or more cells electrically connected [29]. Lithium batteries can undergo a process called thermal runaway. Common causes include packaging damage, improper packaging, or excess heat. A thermal runaway can occur because of a manufacturing defect after production without a proximate environmental or mishandling cause.

A crucial factor related to the hazard of thermal runaway is an event called *thermal runaway propagation*. Propagation occurs when the heat from one battery or cell causes an adjacent battery or cell to overheat [30]. The propagation persists until all batteries undergo thermal runaway or until the system removes enough heat to stop the chain reaction. This process can create enormous amounts of heat, smoke, and flammable gasses. Therefore, mitigation techniques are crucial to prevent the propagation of thermal runaway.

The outcome of thermal runaway varies depending on the cell chemistry, the size of the cell or battery, the state of charge (SOC), and the manufacturer's design [31].

Additionally, the orientation and configuration of the package affect the thermal runaway. The more hazardous outcomes can include flames, violent ejection of cell components, emission of flammable gas that can build up and later explode, or an explosion of the cell itself. Less hazardous outcomes include the emission and dissipation of combustible gases without ignition or the accumulation of flammable gases with ignition that self-extinguish.

Currently, all lithium-ion batteries transported onboard aircraft but not packed with or contained within equipment (UN 3480) must be discharged to a level less than 30% SOC [32] [33] [34]. Although a positive correlation exists between the SOC and the volume of flammable vent gases for specific cell types, this correlation breaks down when comparing cells of different sizes [35] [36]. For instance, a lithium iron phosphate (LFP) cell with a capacity of 122 watt-hours (Wh) charged to 30% SOC can produce more flammable gases than a 12 Wh lithium cobalt oxide (LCO) 18650 cell at 100% SOC, as demonstrated in Figure 2 [36]. Figure 2 represents unpublished data but follows the method detailed in relevant studies [37] [35]. The data suggests that cell energy, rather than SOC, may be a more accurate indicator of a cell's fire hazard.

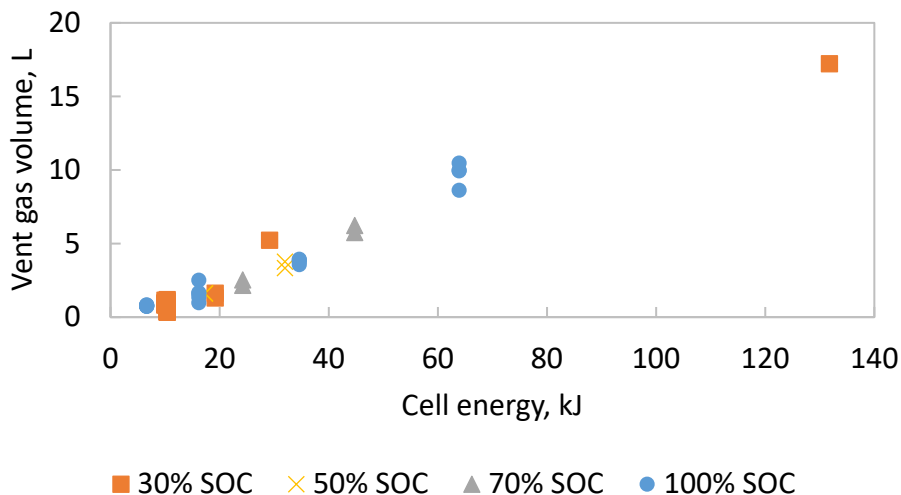


Figure 2 Relationship Between Cell Energy and Vent Gas Volume at Various SOC

The smoke detection and fire suppression systems in lower cargo compartments can detect and suppress most fires. However, the current suppression systems may need to be improved to protect against lithium battery fires [38] [39]. One reason for this is that the 5%vol Halon 1301 knockdown concentration and the sustained 3%vol Halon 1301 in a Class C cargo compartment may not be sufficient for inerting lithium-ion battery vent gas and air mixtures [38] [39] [40]. At 5%vol Halon 1301, the flammability limits range from 13.80%vol to 26.07%vol of a premixed lithium-ion battery vent gas (Li-Ion pBVG) in air [39]. Testing indicates that rendering all ratios of the Li-Ion pBVG in air inert requires 8.59% vol Halon 1301 [39].

2.2.3. Heat Release Rate

The HRR is the most critical parameter in assessing the hazard of fire [27] [41]. The HRR provides insights into the energy output of the combustion process, which is

crucial for designing effective detection and suppression systems. It is related to the effective heat of combustion (Δh_c) and the mass loss rate (MLR) with the following equation:

Equation 1
$$HRR = \Delta h_c * MLR$$

The effective heat of combustion quantifies the energy produced by the mass of fuel burned. In other words, it captures the inherent energy content of the fuel and is a fundamental property of the combustible material. The mass loss rate quantifies the mass of fuel burned per unit time. This description conveys the fuel consumption rate during combustion. The relationship between the effective heat of combustion and the mass loss rate describes the dynamics of fire growth and intensity.

2.3. Fire Detection Methodologies

A fire detector is a device that alarms when a fire is present. There are three types of fire detectors outlined within this report. They are smoke detectors, heat detectors, and gas detectors. Aircraft cargo compartments use smoke detectors for their fire detection systems. The detection time is dependent on multiple variables. These variables include thermal buoyancy, the density of smoke production, particle size, the volume and ceiling height, the number of fire detectors and their locations, fire detector sensitivity, and other contributing factors [18] [19] [20] [21] [42].

2.3.1. Smoke Detectors

A *smoke detector* is a fire detector that alarms when smoke is present. Smoke detectors typically alarm at 12.5 percent obscuration per meter (%obs/m) [43]. Still, the sensitivity can vary by application, and increasing the sensitivity will decrease detection time but increase the likelihood of false alarms. This report briefly describes four types of smoke detectors: ionization smoke detectors, photoelectric smoke detectors, multi-wavelength light scattering smoke detectors, and aspirating smoke detectors.

An ionization smoke detector uses electrically charged plates and a small amount of radioactive material to ionize the air between the charged plates in a chamber. The charged plates attract smoke particles, causing a disturbance in the flow of ions. This ion flow disruption results in a current decrease, triggering an alarm. Ionization smoke detectors are typically better at detecting flaming fires than other smoke detector methods.

A photoelectric smoke detector uses a collimated light source and a photosensitive sensor in a chamber. Smoke particles scatter the light, which causes the photodetector to measure an increase in light intensity and, consequently, an alarm. Photoelectric smoke detectors are typically better at detecting smoldering fires than other smoke detector methods.

A multi-wavelength light-scattering smoke detector uses collimated light sources of two distinct wavelengths and two photodetectors to measure the scattered light. Like

the photoelectric smoke detector, smoke particles scatter the light, which causes the photodetectors to measure an increase in light intensity. Multi-wavelength light-scattering smoke detectors use particle size discrimination to reduce the likelihood of false alarms. Smoke particles are typically less than one micron, while smoke detectors' nuisance sources, such as water vapor, insecticide aerosols, dust, and light, are greater than a micron [44]. Mie Scattering Theory governs light scattering by sub-micron particles where scattering intensity is a function of the wavelength of the incident light, refractive index, and particle radius. Therefore, to ensure that the smoke detector alarms only with smaller-sized smoke particles, the system approximates the smoke particle size by measuring the scattering intensity from known multi-wavelength light sources.

An aspirating smoke detector uses fans or pumps to pull air samples to a centralized smoke detector through tubing. The centralized smoke detector uses one or a combination of the previously mentioned smoke detection methods. Aspirating smoke detectors are typically more sensitive than other smoke detection methods and can have the added benefit of sampling from multiple areas simultaneously.

2.3.2. Heat Detection

A *heat detector* is a fire detector that alarms when heat is present. Three types of heat detectors briefly described in this discussion are fixed temperature, rate-of-rise (ROR), and combination heat detectors.

A fixed-temperature heat detector triggers an alarm when the sensor's temperature reaches a specified threshold. Fixed heat detectors typically alarm when the temperature exceeds 58°C and are ideal for detecting slowly developing fires.

ROR heat detectors alarm when the temperature rise reaches a specified threshold. ROR heat detectors typically alarm when the heating rate exceeds 8.3°C/min and are better at detecting rapidly growing fires.

A combination of fixed temperature and ROR heat detectors uses a set temperature and a temperature rise threshold. The advantage of using both heat detection strategies is that a ROR detector will respond quickly to rapidly developing fires. In contrast, the fixed temperature detector will react to slowly growing fires.

While increasing the sensitivity of the heat detection system may allow for earlier fire detection, it is also vital to be resistant to false alarms. Therefore, the heat detection algorithm should compensate for expected changes in ambient temperature. The difference between the fixed temperature threshold and the expected ambient temperature should exceed 14°C [42]. Heat detectors have the added benefit over smoke detectors in that they are less affected by nuisance sources such as water vapor, insecticide aerosols, dust, and light.

2.3.3. Gas Detection

A *gas detector* is a fire detector that alarms when gas species associated with combustion are present. Typical fires consume oxygen and produce carbon dioxide and

carbon monoxide. For this reason, manufacturers commonly use carbon dioxide and carbon monoxide sensors in gas detectors. Gas detectors typically exhibit greater sensitivity than other detection methods because they can sense gases a fire produces before they emit visible smoke or generate significant heat [45].

In addition to traditional gas detection methods, this study explored the potential of wireless gas detection for early fire detection. Notably, the investigation considered RFID gas sensing tags, which, despite showing promise, currently face limitations in commercial availability. Furthermore, surface acoustic wave (SAW) chemical sensor systems and carbon nanotubes (CNTs) based gas sensors were reviewed. SAW sensors, using a polymeric-coated array to detect chemical vapors indicative of fire threats, offer a novel approach to fire detection by identifying the materials involved in fire incidents [46]. Additionally, CNT gas sensors leverage the unique properties of CNTs for sensitive and rapid gas detection, highlighting the potential of these technologies in enhancing early fire detection systems [47].

2.4. Unit Load Device Safety and Technology

The primary purpose of a ULD is to secure cargo inside an aircraft so that the shipment does not move during flight [48]. Additionally, ULDs increase efficiency in loading and unloading cargo.

A ULD is a general term referring to a pallet or a container. A pallet typically has an aluminum base due to its lightweight and durable properties. Pallets usually have a

flexible cover made of high-strength synthetic materials like nylon or polyester to securely contain and protect the cargo. This makes it suitable for handling irregular or oversized shipments.

Containers also usually incorporate aluminum in their framing. Their panels can include aluminum, polycarbonate, or composite materials to protect cargo against impacts and environmental factors. Typically, containers have a fabric door for access. The design of the fabric door is to facilitate easy handling and access but is also the section in which smoke can most readily escape in the event of a fire within the container.

ULDs are removable parts and are subject to various requirements. For example, TSO-C90 and SAE AS36100 specify strength and safety criteria [49] [50]. The Airlines for America (A4A), formerly the Aerospace Transportation Association (ATA), and the International Air Transport Association (IATA) classify the distinct types of ULDs. The Unit Loading Device Regulations (ULDR) specify the 2-inch minimum clearance between the ULD and the cargo liner, and the weight and balance manual (WBM) provides instructions on how to load and unload a ULD into the aircraft [51]. The 2-inch clearance allows smoke to circulate to the smoke detectors and the fire suppressant to circulate to the fire.

Airlines select specific types of ULDs based on the aircraft's design and cargo needs. For instance, AAY containers fit into most main deck cargo compartments. Meanwhile, half-sized AKE (ATA code LD-3) containers fit into the lower deck

compartments of wide-body aircraft. Table 1 shows the dimensions for the AAY and AKE containers.

Table 1 AAY and AKE Container Information

	AAY	AKE
Operational max gross weight: kg (lb.)	6,033 (13,300)	1,588 (3,500)
External volume: m ³ (ft ³)	15.6 (550)	4.8 (168)
Internal volume: m ³ (ft ³)	13.9 (492)	4.3 (153)
External dimensions (W x L X H) mm (in)	2,235 (88) x 3,175 (125) x 2,083 (82)	1,534 (60.4) x 2,007 (79) x 1,626 (64)
Aircraft and Deck	Standard Body - Main Deck	Wide Body -Lower Deck

2.4.1. Fire Hardened ULDs

Fire-hardening is possible for both pallet and container-type ULDs. A fire-hardened pallet uses a fire containment cover (FCC), and a fire-hardened container is a fire-resistant container (FRC). Typically, these FCCs and FRCs consist of fire-resistant polymer composites. These fire-hardened ULDs undergo testing to ensure their materials meet all flammability requirements. The FCC faces tests according to the MPS set by SAE AS6453, and the FRC gets tested to the MPS defined by SAE AS8992 [52] [53]. Previous FAA experiments have demonstrated that the FCC and FRC can suppress class-A fires for four hours but may not suppress bulk shipments of lithium batteries [54] [55].

2.4.2. ULD Related Aircraft Accidents and NTSB Recommendations

Between the years 2006 and 2011, three catastrophic in-flight cargo fires originated within ULDs [1] [2] [3]. Two of the three investigations found a short time between the fire warning indication to the flight deck and the failure of the flight control systems [2] [3]. These accidents led to research to better understand the root cause of the accidents and ways to mitigate future accidents. The NTSB and FAA investigated these three accidents and conducted research to characterize fires originating within ULDs [4] [5] [6] [7] [8].

The NTSB concluded that the current fire protection measures for cargo compartments are inadequate and recommended the FAA to “Develop fire detection system performance requirements for the early detection of fires originating within cargo containers and pallets and, once developed, implement the new requirements” and “Ensure that cargo container construction materials meet the same flammability requirements as all other cargo compartment materials in accordance with Title 14 *Code of Federal Regulations* (CFR) 25.855”, and “Require the installation and use of active fire suppression systems in all aircraft cargo compartments or containers, or both, such that fires are not allowed to develop” [4].

The focus of this research is on the development and implementation of a UHF RFID temperature measuring system for the early detection of fires originating inside ULDs. However, mitigating fires originating within ULDs is a multipronged approach consisting of early detection, fire containment, and fire suppression.

2.4.3. Study of ULD Fire Characteristics and Implications for Fire Safety

The NTSB conducted a study to measure various aspects of ULD fires, including detectability, growth rate, and energy output [5]. The study used a standardized fire load of cardboard boxes filled with 2.5 pounds of shredded paper to simulate fire conditions within cargo ULDs. The NTSB study compared two types of ULDs: the rigid A2N containers and the collapsible DMZ pallets. The results showed significant differences in the time taken to detect a fire and the speed at which fires reached their peak intensity.

The study aimed to measure the time it takes for smoke to become visible and dense enough to trigger smoke detection alarms on an aircraft after a fire starts. Rigid A2N containers are constructed from aluminum and polycarbonate and have fabric roll-up doors. The roll-up doors facilitate quick smoke egress in case of a fire. The study found that smoke capable of triggering aircraft smoke detection systems started to emerge between 2 minutes 30 seconds and 3 minutes 19 seconds after the fire became visible in these containers. Conversely, collapsible DMZ pallets are made of fire-resistant polypropylene and are designed to be collapsible for easy storage when not in use. When deployed, they are covered with a lightweight, impermeable material, significantly delaying smoke egress. Consequently, it takes longer for smoke to reach sufficient levels to activate external smoke alarms, ranging from 5 minutes 10 seconds to 18 minutes 30 seconds after visible smoke is detected inside the ULD.

This distinction in detection times is crucial, given that the FAA regulation Title 14 CFR §25.858 mandates cargo compartment smoke detection systems to identify a fire

within one minute from its start [16]. The NTSB's findings indicate a discrepancy between this regulatory requirement and the reality of smoke detection delays caused by ULD design.

The duration from smoke detection to peak energy release is critical to fire suppression efforts. The A2N containers offer a period of 7 minutes and 30 seconds to 10 minutes and 30 seconds from when smoke is first detected to when the fire reaches its peak intensity, presenting a crucial but brief window for beginning fire suppression measures. Conversely, the DMZ pallets provide a much narrower window for action, ranging from just 1 minute and 54 seconds to 2 minutes and 12 seconds.

Additionally, despite the DMZ pallets' construction from materials claimed to be fire-resistant, these tests revealed a higher peak energy release rate and total energy output than the A2N containers. Fire-resistant additives usually work well for single-burning items that prevent propagation and self-extinguish. However, they do nothing in a fully involved fire and can counterintuitively add fuel to it.

In conclusion, the NTSB analysis indicates that the design and construction materials of ULDs influence smoke detection and in-flight fire suppression in aircraft [5].

2.4.4. Advancements in ULD Fire Detection and Suppression Measures

The FAA conducted three studies with specific objectives: characterizing fires originating within ULDs, testing potential ULD-installed fire detection systems, and

comparing these ULD-installed systems to aircraft-installed fire detection systems [6] [7] [8].

The first study, which remains unpublished, aimed to compare smoke detection times for fires originating inside ULDs versus those outside ULDs, assessing whether ULDs impede smoke detection [6]. Like the NTSB study, this FAA study concluded that fires originating within ULDs could have significantly delayed smoke detection.

The second FAA study evaluated potential ULD-installed fire detection systems, including an ASSD, a multi-wavelength smoke detector, and gas detectors designed for detecting smoldering and flaming fires within ULDs [7]. The study found that the smoke detectors responded quickly to the array of fire sources forming within the ULD.

Following this investigation, a subsequent iteration of the FAA study compared ULD-installed smoke detection systems, such as the ASSD and a battery-powered wireless fire detector, to aircraft-installed smoke detection systems [8]. The study measured an average of approximately five minutes of delay between ULD-installed and aircraft-installed fire detection systems for smoldering fires originating within ULDs.

Telair and FedEx Express have each developed innovative ULD fire detection and suppression systems. Telair incorporated temperature sensors into the power drive of wide-body cargo aircraft and placed them directly underneath each ULD position [10]. The temperature sensors enable the detection of irregular temperature increases by providing a visual indication to the cockpit.

FedEx Express released an automatic fire suppression system (FSS) in 2009. This system uses a network of infrared thermal sensors with an overhead injector mechanism [9]. It autonomously dispenses a fire-suppressing foam upon detecting heat into the affected cargo container. This technology provides FedEx aircraft with the ability to suppress fires promptly.

These advancements by Telair and FedEx Express illustrate progress in the development of ULD fire safety technologies. However, other air carriers have yet to adopt these technologies widely, so there is still a gap in onboard early fire detection for ULDs.

2.5. RFID Technology

A basic RFID system comprises a reader (interrogator), tag (transponder), and antennas. The reader is the data-capturing device, and the tag is the data-carrying device. The reader communicates with the tags through electromagnetic radio waves transmitted and received through antennas. The information transmitted from the reader to the tag is the downlink signal, and the information backscattered from the tag to the reader is the uplink signal. The reader's antenna can be either built-in or externally connected via a cable [56] [57]. The tag combines an integrated circuit (IC) for processing and storage and an antenna for receiving and sending signals [58] [59].

2.5.1. Frequency Bands for RFID

RFID commonly uses three frequency bands. The frequency ranges are 125-134.2 kHz and 140-148.5 kHz for the low frequency (LF) band, 13.553-13.567 MHz for the high frequency (HF) band, and 858-930 MHz for the UHF band [60]. Calculations can determine the wavelength associated with each frequency band using Equation 2. Table 2 tabulates frequencies within the LF, HF, and UHF bands and their corresponding wavelengths. The characteristics and optimal application of the RFID system vary by the frequency band.

Equation 2
$$\lambda = \frac{c}{f}$$

- Lambda is the wavelength.
- c is the speed of light (299,792.458 km/s).
- f is the frequency.

Table 2 Frequency and Wavelength of Various Frequency Bands

Frequency Band	Frequency	Wavelength
LF	125 kHz	2400 m
HF	13.567 MHz	22.11 m
UHF	858 MHz	0.35 m

The *LF band* has large wavelengths much larger than the antenna size. Therefore, the reader and tag communicate by magnetic coupling. Magnetic coupling occurs when the magnetic field from the reader antenna couples with a tag and changes the electrical impedance of the reader antenna [61]. Magnetic coupling does not rely on backscattering to communicate. LF RFID has a short read range of approximately 10 cm.

The LF tags are typically more expensive than HF and UHF tags and have slower read rates. However, LF RFID can penetrate thin metal and water. As a result, LF RFID finds typical applications in animal tagging, access control badges, and car key fobs [61] [62].

The *HF band* has a shorter wavelength than the LF band, and the reader and tag communicate by magnetic coupling. HF RFID has a slightly longer read range of approximately 10 cm to 1 m. Manufacturers typically use HF RFID for near-field communication (NFC). NFC is a global communication standard regulated by ISO 14443 and ISO 18000-3 [63] [64]. Personal ID cards such as passports, access control badges, data transfer, and ticketing typically use this technology.

The *UHF band* has wavelengths that are comparable to the size of the antenna. Therefore, UHF RFID usually uses radiative coupling to communicate between the reader and the tag. Although the short wavelengths cannot penetrate water or metal, the reader and tag can passively communicate up to 10 meters using backscatter communication [61] [62]. Passive UHF tags are less expensive than LF and HF tags due to their widespread adoption. UHF RFID is a global communication standard regulated by EPCglobal Gen2 ISO 18000-63 [65]. UHF RFID is also known as RAIN, an acronym derived from RADio frequency Identification. UHF RFID systems can collect data from one or more unpowered assets simultaneously without a line of sight (LOS). Recent advances in RFID tags allow them to sense physical parameters such as temperature, moisture, and pressure of unpowered assets [66] [67] [68]. Supply chain management and inventory tracking typically use UHF RFID.

UHF RFID tags can be active, semi-passive, or passive [61] [62]. Active tags use a battery to power the IC and transmit the radio communication back to the reader. Semi-passive tags use a battery to power the IC but still use backscattered communication to communicate with the reader. Passive tags operate by harnessing the power from the electromagnetic waves received via the reader antenna to activate the IC. Passive tags then communicate with the reader using a backscattering method.

2.5.2. Signal Propagation and Attenuation in RFID Systems

Understanding signal dynamics, specifically through the Friis Transmission Equation and free space path loss (FSPL), is essential in RFID systems. The Friis Transmission Equation, as shown in Equation 3, serves to quantify the communication efficiency between the reader and the tag [69]. This equation calculates the ratio of power received to the power transmitted. The equation is a function of the distance between the reader's antennas and the tag, the wavelength of the propagating wave, and the gains of the transponder and the receiver.

Equation 3

$$\frac{P_r}{P_t} = G_r G_t \left(\frac{\lambda}{4\pi D} \right)^2$$

Where P_r is the received power, P_t is the transmitted power, G_r is the gain of the receiving antenna, G_t is the gain of the transmitting antenna, λ is the wavelength of the electromagnetic wave, and D is the path length between the transmitting and receiving antenna.

The FSPL, quantified by Equation 4, is typically measured in decibels (dB), a logarithmic unit that quantifies the power ratio.

$$\text{Equation 4} \quad FSPL (dB) = 20 \log \frac{4\pi D}{\lambda}$$

A higher FSPL value indicates more energy loss, meaning the signal strength decreases over the distance traveled. Conversely, a lower FSPL suggests less energy loss, showing a more robust signal over the same distance.

The Friis Transmission Equation and the FSPL formula are interrelated but serve distinct purposes. The Friis Transmission Equation primarily assesses the power dynamics between the reader and the tag, factoring in the antennas' gains. In contrast, FSPL calculates the attenuation of the signal strength over distance in free space, an essential factor for determining the effective range and reliability of RFID communication.

2.5.3. Radiation Patterns and Antenna Characteristics

The *spatial orientation* maps the targeted antenna radiation intensity in different directions, as demonstrated in Figure 3 [60]. The spatial orientation defines the azimuth pattern, or phi cut, and the elevation pattern, or theta cut. The azimuth pattern is the top-down view of the antenna. The elevation pattern is the side view of the antenna. Correct orientation is crucial in RFID systems to ensure the antenna is aimed correctly for optimal signal transmission and reception.

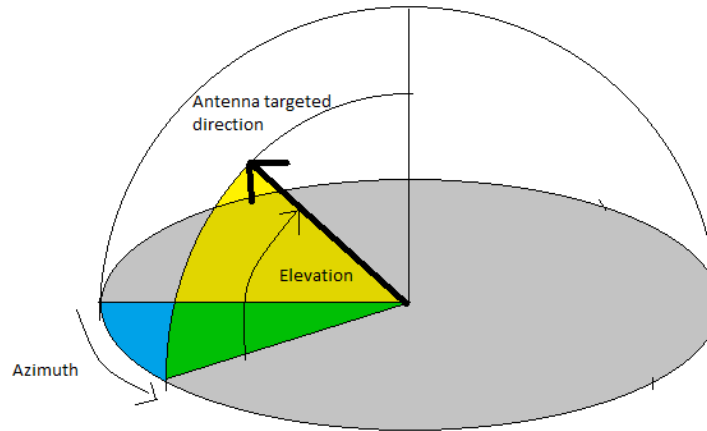


Figure 3 Spatial Orientation Map Example

The *radiation pattern* graphically represents how the antenna emits or receives energy in different directions, and an example is shown in Figure 4 [57]. Again, the radiation pattern is expressed by the azimuth and elevation pattern. The maximum available power in decibels normalizes the power value. These patterns help understand the antenna's overall coverage and directional characteristics.

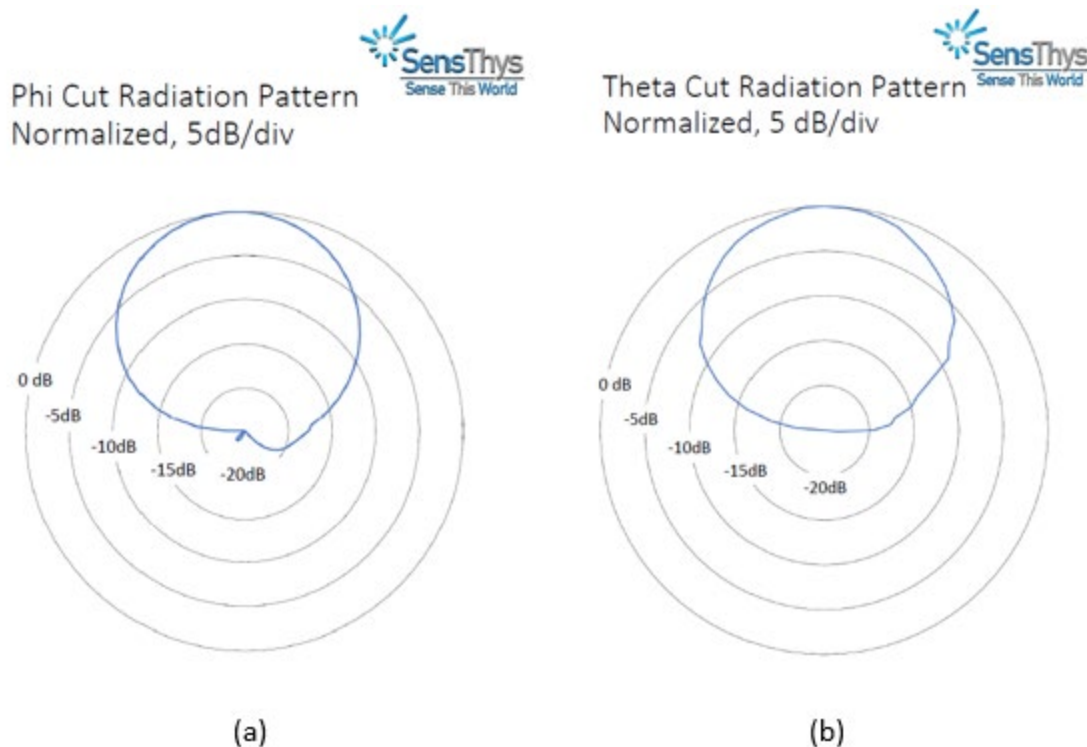


Figure 4 Radiation Pattern Example (a) Azimuth Pattern (b) Elevation Pattern

Beamwidth measures the spread of the main lobe of an antenna's radiation pattern, which is demonstrated in Figure 5. The beamwidth is the angular width between the points where the signal strength drops to half its maximum value, often referred to as the -3 dB points [70]. Beamwidth is a crucial factor in determining the antenna's directivity; a narrower beamwidth generally indicates a more focused and directive antenna, which concentrates energy in a specific direction. Therefore, antennas with wide beams have less gain for the same power output than those with narrow beams.

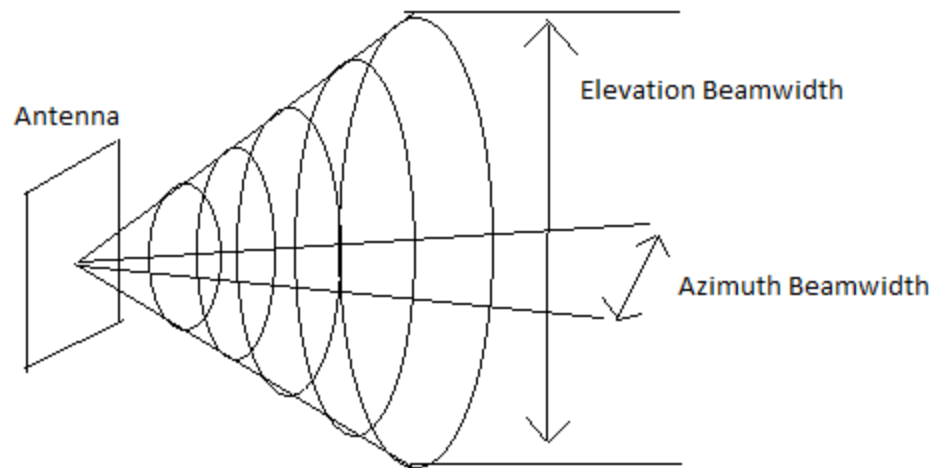


Figure 5 Beamwidth Example

RFID reader antennas are typically unidirectional and have specific beamwidths to maximize directivity. In contrast, RFID tags commonly employ dipole antennas. The dipole radiation pattern takes the shape of a donut and projects most of its energy in front and behind the surface of the tag with little energy towards the center of the tag [71]. This perpendicular emission allows for more versatile signal reception.

2.5.4. Orientation Sensing

The *reader's orientation* with respect to the tag is essential for communication [70]. The ideal orientation is fundamental, and the tags face each other to receive the maximum energy from the tag backscattered directly to the reader. The antenna azimuth angle is the angle between the direction of the antenna and a reference

direction. The antenna elevation angle is the angle between the direction of the antenna and the horizontal plane.

2.5.5. Environmental Considerations

The environment can influence the efficacy of an RFID system. Environmental contributors like absorption, penetration, reflection, refraction, and diffraction actively alter electromagnetic energy transmitted [60] [62]. The environment can create a multipath effect, changing the amplitude, phase, or frequency and resulting in null or extended read zones.

When electromagnetic waves encounter materials, their behavior changes compared to their propagation in free space. These waves can be partially reflected, attenuated, and delayed [72]. Furthermore, their polarization can be altered due to the interaction with the material. The dielectric properties of the material govern these changes in electromagnetic wave behavior. Understanding these interactions is crucial in various applications, including the design and functioning of RFID systems [70].

Materials with high dielectric constants, such as water with a dielectric constant of around 80, significantly impact electromagnetic wave propagation [73]. Water reflects almost all incident electromagnetic waves and absorbs most of the remaining energy. This leads to substantial signal attenuation in RFID applications [74].

The penetration depth (δ) is critical in understanding how electromagnetic waves interact with materials. The *penetration depth* is defined as the depth below a material's

surface at which the intensity of an electromagnetic wave decreases to $1/e$ of its original intensity at the surface. This concept is quantified by Equation 5 [75]. When the penetration depth of a material significantly exceeds its thickness at a specific frequency, the material becomes ‘transparent’ to the electromagnetic wave, allowing it to pass through with minimal attenuation [72]. Conversely, if the penetration depth is much smaller than the material’s thickness at that frequency, the material acts as an ‘opaque’ barrier, blocking the wave’s passage. In cases where the penetration depth is similar to the material’s thickness, the material behaves in a ‘translucent’ manner, partially allowing the wave to penetrate while also causing some attenuation.

Equation 5
$$\delta = \frac{1}{\sqrt{\pi f \mu \sigma}}$$

Where f is the frequency of the electromagnetic wave, μ is the magnetic permeability of the material, and σ is the electric conductivity of the material.

At 900 MHz, a common frequency for UHF RFID systems, the penetration depth varies based on the material’s properties. In materials like metals with high magnetic permeability and electrical conductivity, the skin depth is extremely small, often only a few micrometers. This results in electromagnetic waves being reflected rather than penetrating the material [74].

Although UHF RFID cannot penetrate metal, a common approach that allows RFID tags to read on metal is using a spacer made of a material with a low dielectric constant [74]. This spacer between the metal surface and the RFID tag creates a barrier

that mitigates the metal's disruptive effects on the electromagnetic field. RFMicron solves detuning by incorporating a self-adjusting mechanism within the RFID tag's chip [76]. This mechanism dynamically alters the chip's impedance to match the antenna's changing impedance. This continuous impedance matching significantly enhances tag performance and maintains consistent read ranges to overcome the detuning challenge of reading RFID tags on metal.

Unlike metal, materials with low magnetic permeability and electrical conductivity, such as plastics and composites, exhibit much greater penetration when exposed to electromagnetic waves at 900 MHz. In these materials, the penetration depth can extend to several centimeters. These materials are more 'transparent' to electromagnetic waves, allowing for deeper penetration with minimal attenuation. However, it is worth noting that there can be some absorption of electromagnetic energy, leading to a slight reduction in signal strength.

Therefore, UHF RFID electromagnetic waves will not pass through aluminum ULDs but can read tags on metal. Furthermore, electromagnetic waves can pass through composite ULDs. However, the composite material absorbs some of the electromagnetic energy.

2.5.6. RFID Technology in Airline Baggage and Cargo Management

Implementing RFID technology in the airline industry has significantly enhanced operational efficiency and accuracy of operations such as baggage handling. RFID

technology enables the quick and easy identification of the destination information for each bag on a flight. Identification is critical when bags bound for different destinations are mixed in the same ULD. This capability is essential to reducing the chances of mistakenly sending ULDs to the wrong destination, especially when mixing bags bound for different destinations in the same ULD. For instance, a ground handler can actively distinguish ULDs that contain bags for various destinations from those carrying bags for terminating passengers. RFID technology helps to streamline sorting and minimize mishandling [77].

The accuracy of RFID systems in reading tags approaches 100%. The high accuracy is a significant improvement over the best-case 85% accuracy rate of barcode systems. This enhanced tracking and logging capability reduces the manual handling of bags and the possibility of bags being routed incorrectly or lost. Additionally, RFID technology can expedite the average time to screen bags, reducing the chances of baggage missing a flight due to delays in screening [77] [78].

RFID's role also extends to managing and inventorying ULDs. Traditional methods of ULD tracking, such as manual record keeping, barcode scanning, and visual inspections, are prone to errors and can result in significant losses [48]. For example, airlines like Lufthansa and Air France report substantial percentages of their ULD inventory lost annually due to inefficient tracking, amounting to hundreds of millions of dollars in losses [79]. The introduction of RFID offers a solution by providing near real-

time tracking of ULDs, improving the accuracy of inventory management, and reducing the time and labor involved in manual data entry and error reconciliation [77] [79].

Moreover, RFID technology aligns with the IATA Resolution 753, effective June 1, 2018 [80] [81]. This resolution mandates comprehensive baggage tracking to reduce mishandling. It requires IATA members to track baggage at critical points in the journey, including loading, transfer, and arrival. This global initiative demonstrates the value of RFID tracking in enhancing baggage handling systems industry-wide [81] [80] [82].

In addition to baggage handling, RFID technology holds significant potential in various aspects of aviation operations. Boeing and Airbus have recognized the benefits of RFID in managing commercial airplane parts. Adopting RFID in this area can lead to more accurate information regarding parts demand, reductions in inventory and repair times, and the verification of genuine parts delivered [83].

Thus, RFID technology has already been in the airline industry with positive results. The advantages of the technology, especially its comparatively low cost, are already improving operations. This thesis examines its potential role in enhancing safety by improving early fire detection systems where present technology is insufficient.

2.6. Literature Review Conclusion

The literature review establishes the critical nature of fire detection in aircraft cargo compartments. It emphasizes the limitations of traditional detection systems, especially in the context of ULDs. The introduction of UHF RFID technology, combined

with the MACD algorithm, can revolutionize fire detection by offering near real-time monitoring, reduced false alarms, and improved system reliability. This innovative approach aligns with the recommendations from authoritative bodies like the NTSB and FAA, aiming to fill the void in current fire safety measures. By leveraging the advancements in RFID technology, this research seeks a safer and cost-effective fire detection system for the aviation industry.

3. Research Methodology

This section outlines the methodology for developing and validating a novel heat detection system using UHF RFID technology to detect fires in aviation cargo compartment ULDs. It is important to note that this study is focused specifically on the AAY type ULD. As described in Section 2.4.2, according to the NTSB's analysis, the ability to detect and suppress fires is affected by the design of the ULD and the materials used [5]. However, this methodology has the potential for broader application.

The RFID heat detection system integrates the MACD algorithm, a tool commonly used in financial markets for trend analysis. In this novel application, MACD is adapted to analyze temperature trends within ULDs, enhancing the RFID system's capability to detect heat changes indicative of fire events.

Alongside the RFID heat detection system, the study also incorporates a light obscuration smoke detection system placed outside the ULDs. This setup simulates traditional smoke detection systems typically found in aircraft cargo compartments. The experimental design directly compares the innovative RFID heat detection system and conventional smoke detection systems. It uses data from these tests to evaluate their respective performances in aircraft cargo compartments.

The three evaluated fire scenarios include controlled simulated fires using heaters and smoke generators, smoldering fires using wood pellets and an insulated

pipe, and hazardous material fires using lithium-ion batteries that undergo thermal runaway.

Figure 6 illustrates the experimental setup, though not to scale. The key features of the test setup are the flat plate, vinyl curtains (not depicted), fire ULD, reference ULD, UHF RFID antennas, UHF RFID temperature sensors, and light obscuration meters.

The flat plate functions as a mock cargo compartment ceiling. Additionally, a vinyl curtain hangs from this flat plate. The flat plate and the draped vinyl curtain mock up the cargo compartment. The fire ULD contains the different fire scenarios for evaluating the RFID heat detection system's responsiveness to temperature changes. At the same time, the reference ULD remains empty and provides baseline temperature measurements, which are essential for the heat detection algorithm. UHF RFID antennas attach to the mock cargo compartment ceiling directly over the center of the two ULDs. Additionally, both ULDs contain UHF RFID temperature sensing tags. Light obscuration meters mounted on the flat plate mimic the functionality of smoke detectors in aircraft cargo compartments, enabling direct comparison between internal heat detection and external smoke detection methods in aviation cargo environments.

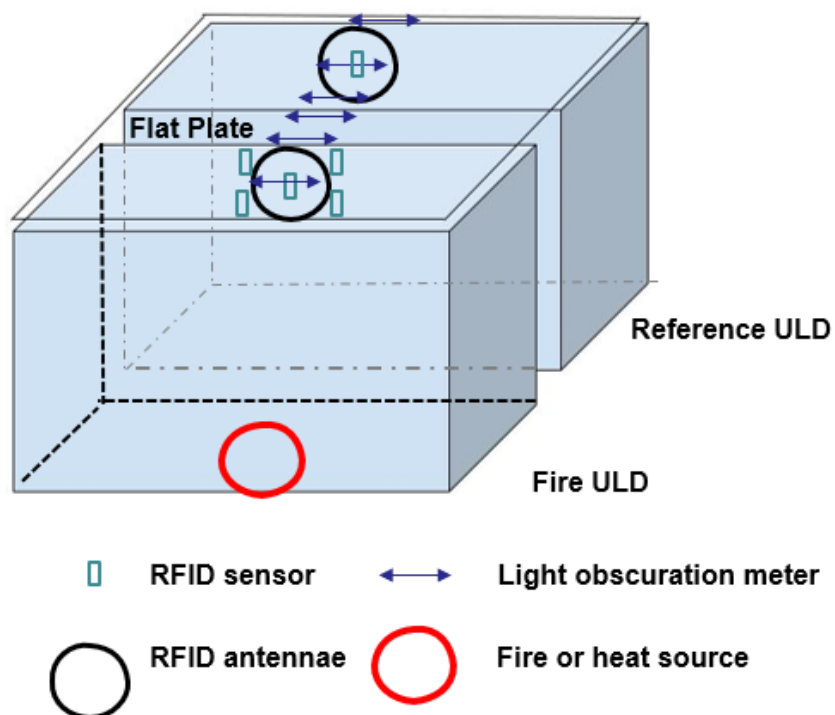


Figure 6 Schematic Layout of Test Setup Components (Not to Scale)

While the initial focus is on AAY type ULDs, the methodology and findings from this study lay a foundation for extending the heat detection system's applicability to more ULD types.

3.1. Description of Test Scenarios

This section delves into the specifics of the three fire scenarios that evaluate the RFID heat detection system within aviation ULDs, with each scenario assessing the system's response to different fire conditions and offering a comparative analysis against traditional smoke detection systems.

3.1.1. Controlled Fire Scenario

The controlled fire scenario is pivotal in evaluating the RFID heat detection system. It employs a heater and a smoke generator to simulate fire situations within a ULD, providing a controlled and measurable environment. The exact quantity of heat and smoke introduced into the ULD is critical in this scenario. It provides a benchmark to compare the responsiveness of the RFID heat detection system and the smoke detection system.

A heater and a smoke generator simulate varying fire situations within a ULD in the controlled fire scenario. The heater, located centrally on the ULD's floor, adjusts its heat output via a variable AC transformer. Simultaneously, an externally placed smoke generator pipes cold smoke inside the ULD, as shown in Figure 7. Placing the smoke generator externally ensures that the heat and smoke inputs are independent variables for a precise assessment. For testing, a smoke generator produces an aerosol for 60 seconds. This represents the test procedures outlined in the certification regulation [84]. A Concept Aviator 440, operated at 14psig of CO₂, was employed for these tests [85]. The smoke generator reflects a major airframe manufacturer's standardized smoke output and ensures the scenario's relevance to operational conditions [20].



Figure 7 Aviator 440 Smoke Generator Piped into Fire ULD

3.1.2. Smoldering Fire Scenario

The smoldering fire scenario is essential for evaluating the RFID heat detection system's aptitude in detecting slow-burning fires, which are hazardous due to their tendency to escalate unnoticed with the existing smoke detection systems used in aircraft cargo compartments. It uses a vertical aluminum pipe (15.24cm diameter, 58.88cm length) filled with 620g of low ash hardwood pellets and ignited at the bottom with a propane hand torch, as shown in *Figure 8*. To aid in sustaining the smolder, the pipe is insulated with 5.08cm thick Mineral Wool, which has an R-value of 8.7. This insulation helps maintain the fire's intensity without external heat sources.

This scenario uses a type K thermocouple positioned 10cm above the pipe's base to monitor the smoldering process [86]. The decision to move the pipe into the center of the ULD is based on achieving a self-sustaining smolder, as indicated by the thermocouple readings. This determination involves a nuanced judgment, balancing the

need for a low starting temperature with the requirement for the smolder to be self-sustaining. Moving the pipe prematurely into the ULD can result in the smolder self-extinguishing if the temperature is not sufficiently high to maintain it.



Figure 8 Insulated Aluminum Pipe Containing Wood Pellets for Smoldering

3.1.3. Lithium-Ion Battery Scenario

Given the significant hazard of transporting lithium batteries aboard cargo aircraft, a lithium-ion battery fire scenario is vital to this experimental design. Lithium batteries are prone to thermal runaway. Thermal runaway is a process where batteries overheat and can trigger adjacent batteries to do the same. This scenario seeks to evaluate the effectiveness of both the heat detection system and the smoke detection system in identifying and responding to such hazardous conditions, providing a comprehensive assessment of their capabilities in detecting fires caused by thermal runaway in lithium-ion batteries.

The lithium-ion battery fire scenario uses two LCO pouch cells, each fully charged with capacities of 5.48Wh and 6.6Wh, respectively. The insulation surrounding the cells helps to ensure that both cells go into thermal runaway, as shown in *Figure 9*.

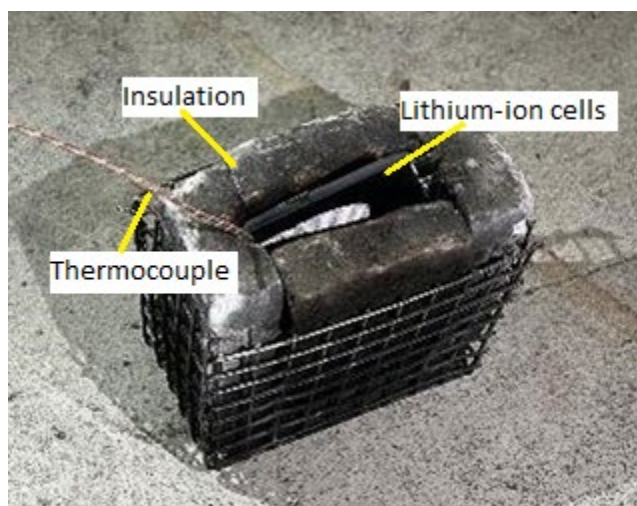


Figure 9 Arrangement for Battery Testing

In this setup, a user-activated relay triggers a short circuit, resulting in thermal runaway, illustrated in *Figure 10*. This scenario assesses the ability of the RFID-based heat detection system to identify and respond to lithium-ion thermal runaway in comparison to the performance of existing smoke detection systems used in aircraft cargo compartments.

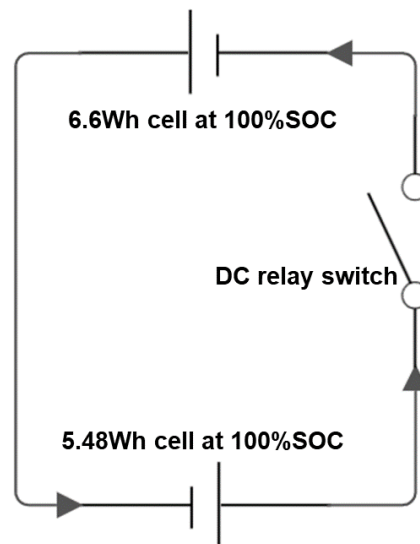


Figure 10 Schematic Representation of Battery Short-Circuit Test Setup

3.2. Experimental Setup

The design of the experimental setup for this research is to replicate the conditions found in aircraft cargo compartments. This setup is crucial for assessing the efficacy of the UHF RFID-based heat detection system under realistic conditions. It includes the creation of a mock cargo compartment ceiling and the use of two ULDs. The configuration is tailored to evaluate the RFID heat detection system's performance

compared to traditional smoke detection methods under controlled conditions that mimic aircraft environments.

3.2.1. Mock Cargo Compartment Ceiling Setup

The mock cargo compartment ceiling is a vital setup component, measuring 6.1m x 3.7m x 2.1m (L x W x H). This ceiling is positioned 7.6cm above the ULDs and is wrapped in a vinyl cover along its perimeter to maintain a controlled environment. The setup aims to mimic the conditions of an actual aircraft cargo compartment to the extent possible, ensuring the relevance and applicability of the test results. *Figure 11* depicts the overhead view of the mock cargo compartment ceiling and vinyl cover.



Figure 11 Design of Mock Cargo Compartment Ceiling with Vinyl Smoke Cover

3.2.2. ULD Configuration

The test setup employs two distinct ULDs: the fire ULD and the reference ULD. The fire ULD contains either controlled or real fire scenarios. It includes a light

obscurator meter to gauge smoke production and UHF RFID temperature sensing tags for monitoring heat generation. In contrast, the reference ULD is a control unit without heat input. It also has a temperature sensor to record the baseline temperature. This baseline data from the reference ULD is critical in the false alarm reduction algorithm, providing a comparative metric for the readings acquired from the fire ULD. *Figure 12* illustrates the location of both ULDs.



Figure 12 Comparative View: Fire ULD (Left) and Reference ULD (Right)

3.3. Instruments Used in Research

This study evaluates the effectiveness of two fire detection approaches by comparing a UHF RFID heat detection system positioned inside ULDs with a light obscuration based system that simulates the traditional smoke detectors found in aircraft cargo compartments, specifically for detecting fires that start within a ULD. The RFID heat detection system consists of RFM3200 temperature sensing tags, a SensArray

Core RFID reader, and a SensRF-101 external antenna. The traditional smoke detection system comprises a laser diode and an ultraviolet-visible spectroscopy (UV/VIS) sensor.

Installed on ULDs are RFM3200 temperature sensing tags to monitor the ambient thermal conditions for the RFID system [59]. This brings the temperature-sensing tags closer to potential fire sources than ceiling-mounted smoke detectors. These temperature sensing tags use an integrated radio frequency (RF) antenna for energy harvesting and data transmission. The SensArray Core RFID reader has an internal antenna connected to the SensRF-101 external antenna [56] [57]. They are both positioned at the cargo compartment's ceiling. In this setup, the temperature sensing tags actively collect, decode, and translate temperature signals into temperature measurements. The sensor generates temperature data, the antenna facilitates its wireless transmission, and the RFID reader decodes it for further analysis and action.

The RFM3200, shown in Figure 13, is a wireless, battery-free temperature sensor [59]. This sensor has dimensions of 31.9 x 101.7 mm. The standard operating temperature ranges from -40°C to +85°C. This sensor has a flexible design and an adhesive backing. The sensor operates within the Federal Communications Commission (FCC) and European Telecommunications Standards Institute (ETSI) frequency standards. It requires a RAIN-compliant reader for its functionality. It incorporates an integrated RF antenna for two purposes. The first is to harvest energy necessary for its temperature-sensing functionality, and the second is to facilitate communication with an RFID reader.

The antenna's configuration makes it insensitive to moisture and dirt. However, it is not suitable for use on metal.



Figure 13 Axzon RFM3200-AFR Temperature Sensing RFID Tag

The RFM3200 temperature sensing tags are powered and read by the Magnus S3 IC chip integrated within the tags. The chip encompasses a 64-bit tag identifier (TID) memory, which offers a permanent, factory-set, unique serial number for each tag [58]. The chip also includes a 160-bit electronic product code (EPC) memory that supports up to 128-bit EPC. The EPC is a globally unique identifier for a specific item, often used in tracking and inventory management applications.

Beyond these identifiers, the Magnus S3 chip generates a temperature code, signifying the chip's temperature [87]. For accurate readings, it is essential to factor in the reader's transmission frequency, power received by the sensor, averaging of readings, and command timing. Each chip contains single-point calibration data in its user memory. The calibration translates the temperature code into Celsius readings.

Averaging multiple readings can help reduce noise or fluctuations in the Temperature Code.

Furthermore, the received signal strength indicator (RSSI) code measures the power level the chip receives from the reader [87]. This metric can significantly influence the accuracy of temperature and sensor readings. Stronger signals yield more precise data interpretation when within the recommended range. However, deviating from this range can have notable impacts. If the RSSI code exceeds the recommended maximum, it can lead to power distortion, potentially causing communication failures between the reader and the chip. Conversely, if the RSSI code falls below the minimum threshold, it might result in missed reads due to insufficient signal strength.

Careful power management is essential to maintain the RSSI code within the optimal range in RFID systems utilizing Magnus S3 chips [87]. In situations where the placement of sensor tags and readers is stable, the reader's power can be set to a level that aligns with the recommended RSSI code and kept constant. In more dynamic environments, the reader must adjust its power dynamically to ensure the RSSI code stays within the desired range. The select command can also filter tag responses based on their received power levels, ensuring only tags within the appropriate range respond.

The SensArray Core plays an essential role in this research as a fourth-generation Enterprise Platform Integration Core (EPIC) RFID reader and antenna system (Figure 14) [56]. It operates under the radio frequency identification and networking (RAIN) protocol, standardizing UHF RFID technology. It features an 8.5dBic internal antenna and

three additional antenna ports. It incorporates a 4 in/4-out 30W powered general-purpose input/output (GPIO) subsystem, powered through power over ethernet plus (PoE+) inputs ranging from 30W to 90W. The device communicates via transmission control protocol/internet protocol (TCP/IP) using a registered jack-45 (RJ-45) connector. It consumes 13W when active and 3W in idle mode. Its operating frequencies align with either FCC or ETSI guidelines. With dimensions of 25.4 x 25.4 x 2.0 cm and weighing 0.79 kg, it operates effectively within a temperature range of 0°C to +50°C.



Figure 14 SensThys SensArray Enterprise UHF RFID Reader Configuration

The SensRF-101 is an external antenna designed for the SensArray Core [57]. It has a 70-degree full width at half maximum (FWHM) beamwidth and a nine dBic directivity. It utilizes right-hand circular polarization (RHCP). The antenna features a 10W power limit, a 50 Ohm input impedance, and a voltage standing wave ratio (VSWR) with a typical value of 1.2 and a maximum of 1.33. The construction is primarily

polycarbonate and measures 25.4 x 25.4 x 2.4 cm. The SensRF-101 connects to the RFID reader through a sub-miniature version A (SMA) connector.

In addition to the UHF RFID-based heat detection system described above, the research also uses a light obscuration system for fire detection outside of ULDs to simulate traditional cargo compartment smoke detection systems. This light obscuration system uses a 2.3mW, 670nm laser diode and a high-sensitivity USB UV/VIS sensor [88] [89]. The laser diode functions within a temperature range of -10 to +40°C and requires a separate power supply. At the same time, the UV/VIS sensor, connected through a 2.5m cable to a USB interface, discerns power between 10 μ W and 100mW over a wavelength spectrum of 325 - 1065 nm. This setup allows for measuring smoke density under varied fire scenarios, with calibration set to sound an alarm upon reaching a 12.5 %obs/m light obscuration threshold. This satisfies the TSO C1e criterion for optical smoke detectors [43] [23].

3.3.1. Instrument Installation

Two UHF RFID readers are placed directly above each ULD for data acquisition, as shown in Figure 6. Their positioning is critical for optimal data collection from the UHF RFID temperature sensing tags within the ULDs. This setup ensures the accuracy and reliability of the data, which is crucial for evaluating the performance of the RFID-based heat detection system.

In the fire ULD, temperature sensing tags are positioned at the ceiling center to monitor temperature variations during the test scenarios. On the interior ceiling at the center of the ULD, there is one sensor directly on the surface (0mm) and four additional temperature sensing tags at varying heights down from the ULD ceiling of 6.4mm, 25.4mm, 50.8mm, and 76.2mm. These mounts are essential in minimizing heat loss from conduction to the ULD surface, ensuring more sensitive temperature readings. Furthermore, an exterior ceiling sensor is installed at the ULD center surface (-3.175mm) to accommodate the RFID reading limitation through metal. *Figure 15* illustrates the placement of the internal temperature sensing tags. Conversely, the reference ULD has a single interior ceiling sensor mounted at the ceiling center (6.4mm) to gauge the baseline temperature. This reference temperature provides a comparative measure for the experiments conducted.

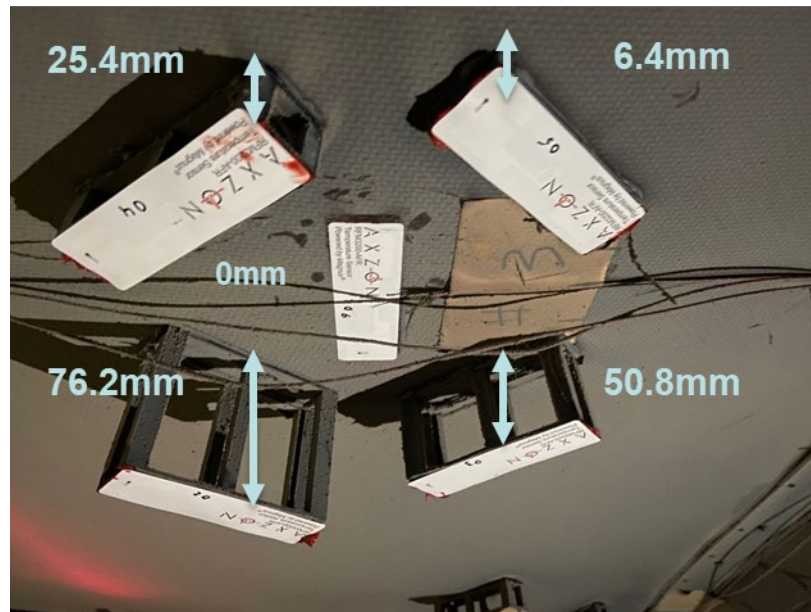


Figure 15 Placement of Temperature Sensing RFID Tags within Fire ULD

The test setup for smoke detection includes light obscuration meters, each equipped with 2.3mW 670nm laser diodes and silicon photodiode light sensors. These devices measure the degree of light obscuration, which indicates smoke presence. One of these light obscuration meters is mounted on the ceiling of the fire ULD, positioning the lasers and light sensor 1.2 meters apart. An additional five meters are mounted at various distances from the fire ULD door along the mock cargo compartment ceiling. These distances are -0.3m, 0m (directly above the ULD exit), +0.3m, +1.06m, and +3.34m. This ensures a comprehensive assessment of the smoke spread from the fire source. The consistent 1.2-meter spacing between each laser and sensor pair guarantees uniform light obscuration measurements across the entire setup. *Figure 16* offers a top-down view, illustrating the distribution of these meters on the mock cargo compartment ceiling. The smoke detection system is set to trigger an alert when the light obscuration level reaches a threshold of 12.5% per meter.

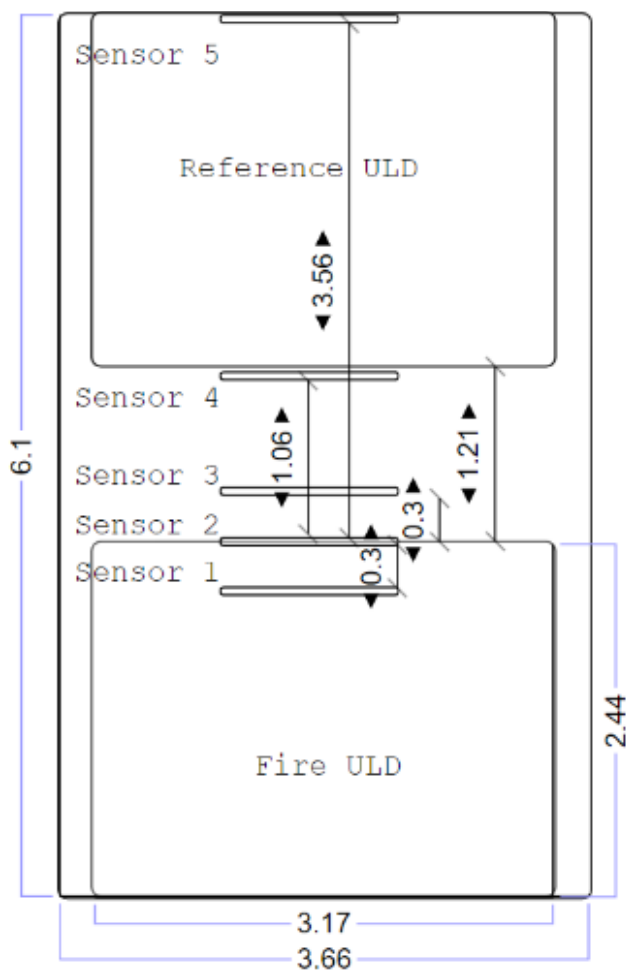


Figure 16 Distribution of Light Obscuration Meters in Test Environment (Top-Down View)

3.4. Smoke Detection Analysis

The smoke detection approach in the test setup uses light obscuration meters placed within the fire ULD and on the ceiling of the mock cargo compartment to measure light obscuration as an indicator of smoke presence. These meters, equipped with a 2.3mW, 670nm laser diode and silicon photodiode light sensors, quantitatively assess the density and presence of smoke particles under varied fire scenarios. This setup continuously collects data at a rate of 1Hz.

The analytical method to quantify particles is through light obscuration, using the ratio of measured light intensity with particles to the light intensity of a cleared path between the laser diode and the silicon photodiode. The Beer-Lambert law calculates the light obscuration per unit length during the test as follows:

$$\text{Equation 6} \quad O_u = \left[1 - \left(\frac{T_s}{T_c} \right)^{\frac{1}{d}} \right] 100$$

O_u is the percent obscuration at distance d ,

d is the distance between the laser diode and the photodiode,

T_s is the aerosol density meter reading with smoke,

T_c is the aerosol density reading with clear air.

The test setup has a light obscuration meter within the fire ULD, positioned at the ceiling, with a maintained distance of 1.2 meters between the laser diodes and the silicon photodiode light sensors. The setup includes placing five additional light obscuration meters along the ceiling, with each meter maintaining 1.2 meters between its respective lasers and light sensors. *Figure 16* illustrates the setup. Calibrating the light obscuration meters before each test involves turning off the lasers, zeroing the sensor, and then turning on the laser.

A critical metric in this analysis involves measuring the time it takes from test initiation to reach the 12.5 percent light obscuration per meter (%obs/m) threshold. This lapse in time is the smoke detection time. The threshold aligns with the UL 268 safety

standard guidelines for fire alarm system smoke detectors [43]. This threshold is essential for ensuring a balanced and accurate detection of smoke. This allows a fair analysis of the RFID heat detection system's performance against existing smoke detection systems in aircraft cargo compartments under various fire scenarios.

The UL 268 standard outlines specific materials and procedures for smoke detection, including controlled test fires and the criteria for alarm response times. The detailed smoke profile and obscuration levels provide a structured framework for evaluating smoke detection.

3.5. Heat Detection Analysis

Heat detection within ULDs is essential for early detection and mitigation of fire incidents. The innovative application of the MACD method, traditionally employed in stock market analysis, has been repurposed to enhance the sensitivity and timeliness of heat detection systems. This section elaborates on the MACD-based heat detection algorithm, its background, and the analysis of heat detection activation within the testing environment.

During these experiments, the RFID-based heat detection system gathered an average of 15 temperature measurements for each tag within a 15-second interval. The RFID system was purposely stressed with extra tags to simulate a more demanding operational environment, aligning with the study's goal to validate the implementation of UHF RFID temperature sensing tags in ULDs. While this study used only two ULDs,

operational applications would typically involve instrumenting more ULDs. Therefore, two antennas read twenty-two tags to replicate these more complex conditions. However, the analysis focused only on the relevant seven tags outlined in section 3.3.1. The RFID readers collected temperature data for one hour before initiating the fire scenarios to collect baseline data for MACD analysis.

3.5.1. Traditional MACD Stock Analysis Background

MACD is a technical indicator traditionally used in stock market analysis to determine changes in price momentum, trend direction, and potential buy or sell signals. MACD operates through three fundamental components: the MACD line, signal line, and histogram line.

To calculate the *MACD line*, subtract the long-term moving average (typically a 26-day exponential moving average (EMA)) from the short-term moving average (typically a 12-day EMA) of a stock's price. A rising MACD line suggests that the short-term momentum is outpacing the long-term momentum, which might indicate a bullish or upward trend, while a falling MACD line could signal a bearish or downward trend.

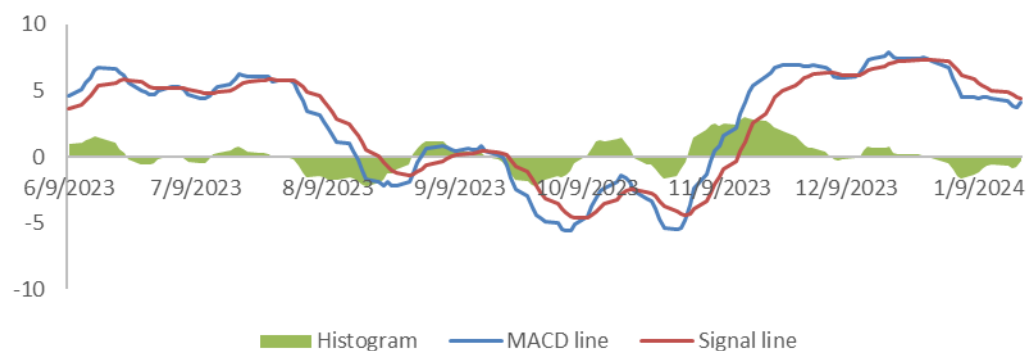
The *signal line*, often a 9-day EMA, of the MACD line triggers buy or sell signals. A bullish signal occurs when the MACD line crosses above the signal line, indicating a buy signal. Conversely, a bearish signal occurs when the MACD line crosses below the signal line, indicating a sell signal.

The *histogram line* is the difference between the MACD and signal lines. It helps to assess the magnitude and direction of momentum. When the histogram is above zero, it implies that the MACD line is above the signal line, potentially indicating bullishness. Conversely, when it is below zero, it suggests that the MACD line is below the signal line and potentially indicates bearishness. The histogram can also reflect momentum strength. Larger histogram bars represent stronger momentum, while smaller bars or a diminishing size of bars could signal a weakening momentum.

Figure 17 (a) shows the stock's closing price, 12-day and 26-day EMAs. These EMAs help smooth out price data over a specified period and are vital in calculating the MACD line. Figure 17 (b) displays the MACD line, the signal line, and the histogram. The MACD line is the difference between the 12-day and 26-day EMAs, and the signal line is a 9-day EMA of the MACD line. The histogram represents the difference between the MACD and signal lines and helps identify bullish or bearish momentum.



(a)



(b)

Figure 17 (a) Daily Stock Prices with 12-Day and 26-Day EMAs Over Time

(b) MACD Line, Signal Line, and Histogram Analysis Over Time

By analyzing the direction and crossing points of the MACD and signal lines, along with the expansion or contraction of the histogram, investors can infer information about the potential continuation or change in market trends. In a *bullish trend*, the MACD line exceeds the signal line, accompanied by an increasing histogram. This pattern indicates a potential uptrend in stock price. In a *trend reversal*, the MACD line approaches the signal line and the histogram contracts. This pattern suggests a possible reversal in stock price. In a *bearish trend*, the MACD line dips below the signal line, accompanied by a decreasing histogram. This indicates a likely downtrend in stock price.

The MACD is a lagging indicator that relies on past price action to signal market trends. Therefore, MACD's signals are not predictive but confirmatory. The MACD helps to confirm the establishment of a trend rather than indicating the exact moment it begins. Nevertheless, lagging indicators are valuable for providing evidence of a trend's stability and potential continuation.

3.5.2. Repurposed MACD for Heat Detection Background

The MACD analyzes trends over time. The ability to analyze trends makes it a valuable tool for monitoring temperature variations within ULDs. This novel application of MACD in heat detection works through three fundamental components, like its financial counterpart: the MACD line, signal line, and histogram line.

To calculate the *MACD line for heat detection*, subtract the long-term moving average from the short-term moving average of temperatures within the fire ULD. A rising MACD line suggests that the short-term momentum is outpacing the long-term momentum, which might indicate an escalation in temperature or a fire event. In contrast, a falling MACD line could signal a decrease in temperature or fire suppression.

The *signal line for heat detection* is the difference between a short-term moving average and a long-term moving average of temperatures within the reference ULD. It is a comparative reference to the MACD line, distinguishing between normal and abnormal temperature variations.

The *histogram line for heat detection* represents the difference between the MACD and signal lines. It indicates the temperature differential between the fire and reference ULDs. A larger bar on the histogram line in heat detection could signify a growing temperature differential between the fire and reference ULDs, potentially indicating a thermal hazard. Conversely, smaller bars or a reducing histogram line could represent a narrowing temperature differential and indicate stabilizing conditions.

This repurposing of the MACD for heat detection mirrors its traditional role in financial markets. In ULD heat detection, the MACD line's relative position to the signal line and its impact on the histogram are critical. For example, a rising MACD line above the signal line, akin to a bullish stock trend, could indicate a rising temperature trend and a fire within a ULD. Conversely, a descending MACD line towards the signal line, akin to a trend reversal in stocks, could indicate a cooling temperature trend and fire suppression within a ULD.

An essential aspect to acknowledge when adapting MACD for heat detection is its nature as a lagging indicator. This implies that the MACD bases its insights on historical data. As a result, its indications are confirmatory rather than predictive. It verifies the establishment of a trend rather than its start. In the context of heat detection within ULDs, this lagging nature of the MACD does not detract from its efficacy. Instead, it offers dependable confirmation of ongoing temperature trends.

3.5.3. MACD Heat Detection Test Example

This section uses a collection of figures to highlight the effectiveness of MACD in identifying temperature changes and trends over time. The section demonstrates the innovative application of MACD in a new field. Each figure contains temperature data during an 89W heating scenario initiated at 0 seconds.

Figure 18 shows the raw temperature data and the 5-min moving average (MA), 20-min MA, and 50-min MA. The main observations are that this approach can effectively smooth short-term temperature fluctuations with moving averages while preserving the sensitivity to more significant temperature trends. The shorter moving average reflects short-term temperature movements and is more responsive to recent temperature changes. The more extended moving average represents longer-term trends and is less sensitive to short-term temperature fluctuations.

Notably, the maximum observed temperature of 30°C and the rate of temperature rise of 0.4°C/min are well beneath the typical thresholds of heat detectors, which are 57°C and 6 °C/min, respectively. This highlights the limitations of traditional heat detection methods in identifying early-stage fire development.

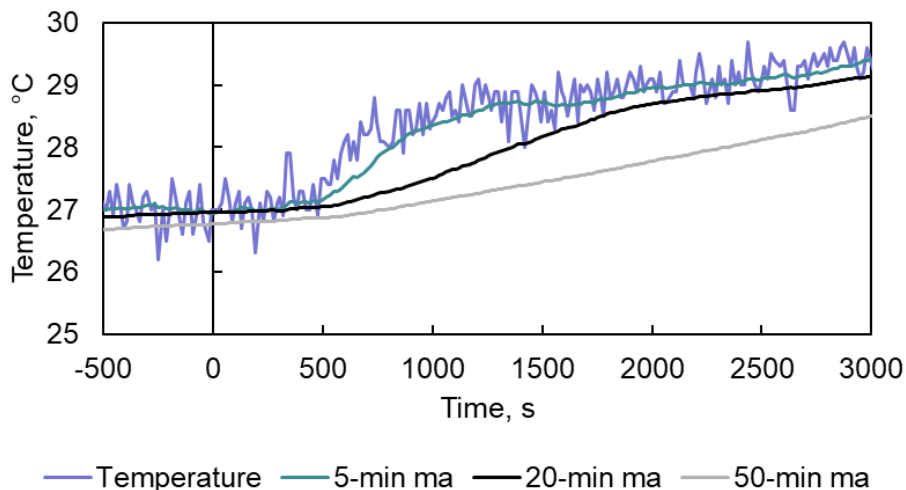


Figure 18 Analysis of Temperature Fluctuations and Moving Averages During 89W Test

Figure 19 illustrates the relationship between time and temperature. It includes legends indicating the short-term (5-min) and long-term (20-min) moving averages and the MACD 5-20-min MA. The secondary axis represents the time against the temperature differential between the short-term and long-term moving averages.

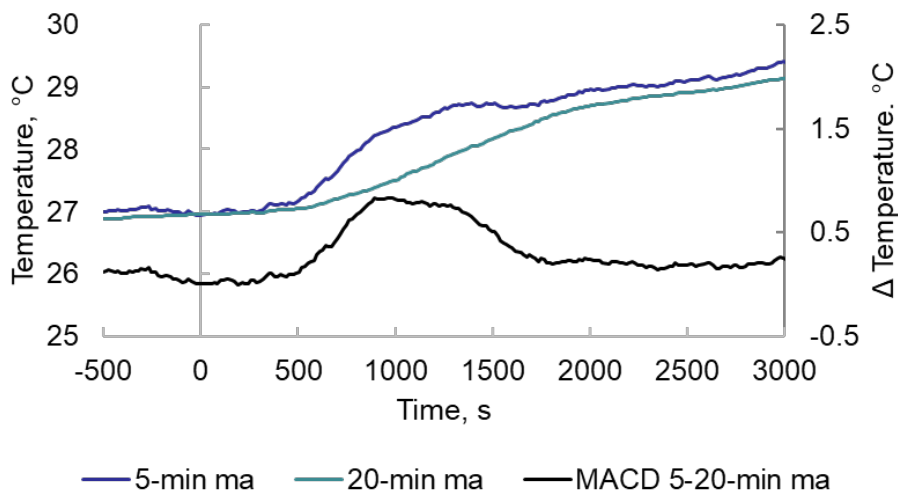


Figure 19 Analysis of Short-Term (5-min ma) and Long-Term (20-min ma) MACD

Figure 20 also shows the correlation between time and temperature. It features legends denoting the short-term (20-min) and long-term (50-min) moving averages and the MACD 20-50-min MA. Similarly, the secondary axis is time against the temperature differential between the short and long-term moving averages.

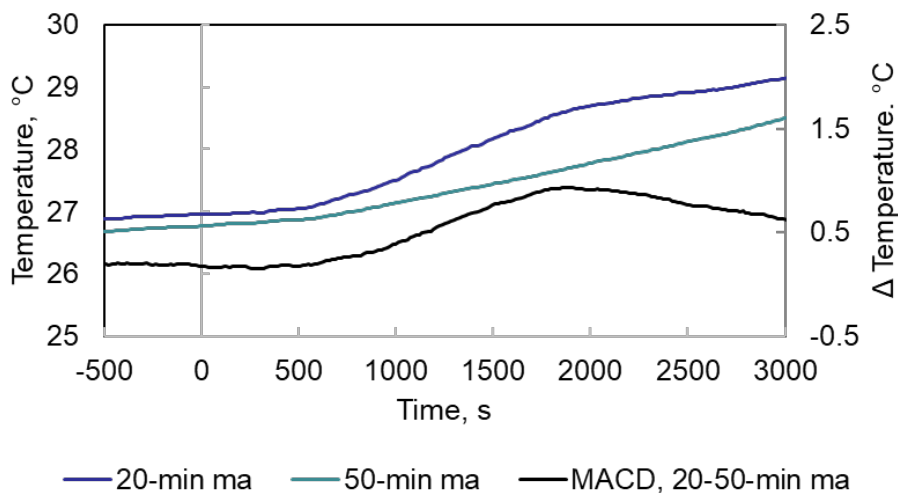


Figure 20 Analysis of Short-Term (20-min ma) and Long-Term (50-min ma) MACD

Figure 19 and Figure 20 show the MACD line's capability to detect momentum changes by determining whether recent temperature trends deviate from long-term trends. This MACD representation also normalizes the temperature fluctuations over time. Data normalization yields a more straightforward comparative analysis of temperature trends between ULDs. It is of note that the 5-20-min MACD responds quicker than the 20-50-min MA MACD. However, it also has more fluctuations.

Figure 21 and Figure 22 show time against temperature differential, with legends indicating the MACD line for the fire ULD, the signal line for the reference ULD, and the

histogram line, which is the difference between the MACD and signal lines. *Figure 21* uses the 5-20-min MA, and *Figure 22* uses the 20-50-min MA.

The histogram line is a near real-time indicator of the temperature trend differential between the fire and reference ULDs. This temperature differential is vital for minimizing false alarms. Initially, the MACD and signal lines remain parallel until the onset of heating in the fire ULD. The small temperature differential signifies a consistent temperature trend in both ULDs. Additionally, both lines are above zero before heat initiation, indicating an upward temperature trend within the mock cargo compartment, with minimal difference between them, as depicted by the flat histogram line. An observable divergence occurs between the MACD and signal lines within the fire ULD as the rising histogram line captures the heating effect. The divergence indicates a temperature differential between the fire and reference ULDs and is vital for accurate heat detection.

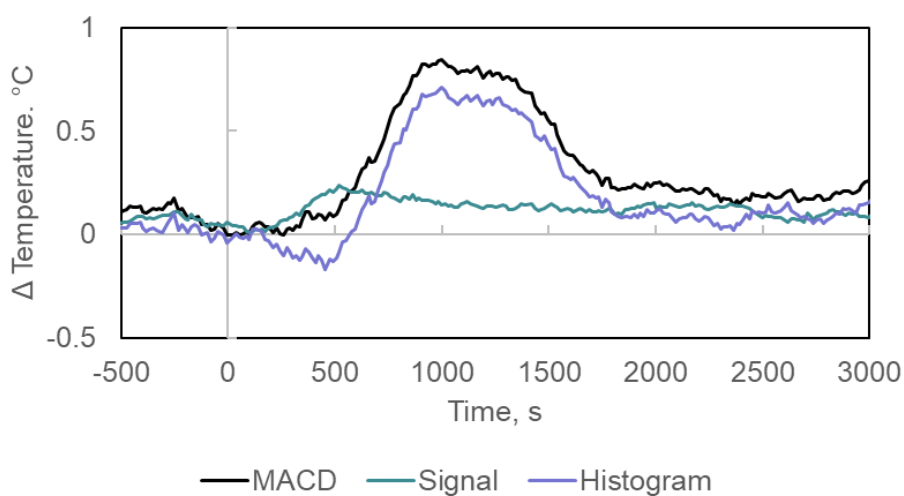


Figure 21 MACD, Signal, and Histogram Analysis (5-20-min MA Configuration)

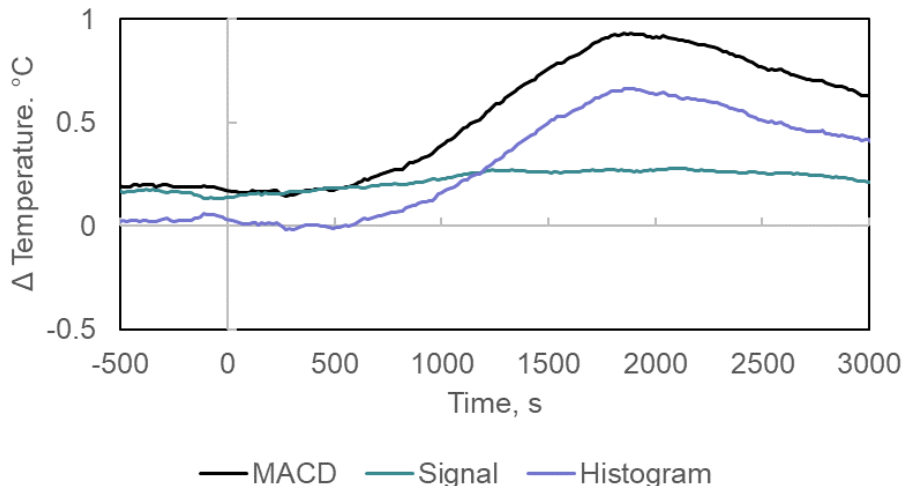


Figure 22 MACD, Signal, and Histogram Analysis (20-50-min Configuration)

The MACD heat detection algorithm displays an exceptional ability to recognize subtle changes in temperature trends within ULDs, highlighting its advantage over traditional heat detector algorithms that rely on fixed temperature or rate-of-rise thresholds. This sensitivity allows the MACD algorithm to detect early-stage fire development that might not trigger conventional heat detectors, which typically activate at higher temperature thresholds, such as 57°C, or significant rates of temperature rise, around 6 °C/min. The nuanced approach of the MACD, employing moving averages to smooth short-term fluctuations while remaining attuned to significant temperature shifts, ensures a more refined and responsive detection mechanism. This capability is crucial for early fire detection, where the early identification of incremental temperature increases can lead to timely interventions, potentially averting larger-scale fire incidents.

3.5.4. MACD Heat Detection Performance Metrics

In this and subsequent sections, the term “sensor response” specifically refers to the behavior of the histogram line, as outlined in sections 3.5.2 and 3.5.3. This histogram line, derived from the MACD heat detection analysis, is crucial in identifying and quantifying temperature variations within the ULDs. The metrics discussed here are based on the analysis of this histogram line, offering a precise method to evaluate the RFID heat detection system’s performance under varying thermal conditions.

The term *noise* refers to the random temperature fluctuations observed in the collected data. These fluctuations do not contribute to the overall trends within the ULDs but may reflect minor environmental changes, sensor inaccuracies, or other unknown factors. Identifying and quantifying the noise is essential for the data analysis because it helps distinguish between genuine temperature variations and false alarms.

The *activation threshold* is another critical metric defined as a deviation in sensor response exceeding fifteen standard deviations (15σ) from the norm during 11 hours in ambient conditions. This methodology acknowledges the presence of random temperature fluctuations inherent in the data due to minor environmental changes, sensor inaccuracies, or other indeterminate factors. Setting the activation threshold well above the noise level ensures that only substantial and sustained temperature changes trigger an alert, reducing the likelihood of false alarms. This approach effectively filters out minor temperature variances that do not correlate with the fire risk, focusing on statistically significant deviations likely to represent a real threat.

Maximum sensor response measures the peak response of the histogram line with heat added to the fire ULD. It represents the apex of temperature variation detected by the RFID heat detection system during the test scenario. Evaluating the maximum sensor response is essential for assessing the system's sensitivity and responsiveness to increasing thermal conditions within the ULD.

Detection time is another critical metric. The detection time calculates the duration from the initiation of heat within the fire ULD until the histogram line crosses the activation threshold. This metric captures the timeliness of the heat detection system in identifying and responding to adverse thermal conditions.

Figure 23 exemplifies these concepts by illustrating time against temperature differential for a 337 W test. The heater in this test starts at zero seconds. The figure highlights three critical parameters: maximum sensor response (indicating peak temperature variation), the 15σ activation threshold (defining the detection benchmark), and detection time (showing the system's speed in identifying threshold-exceeding signals). Analyzing these parameters is essential in evaluating the heat detection system's effectiveness and capacity for timely and accurate detection in varying operational scenarios.

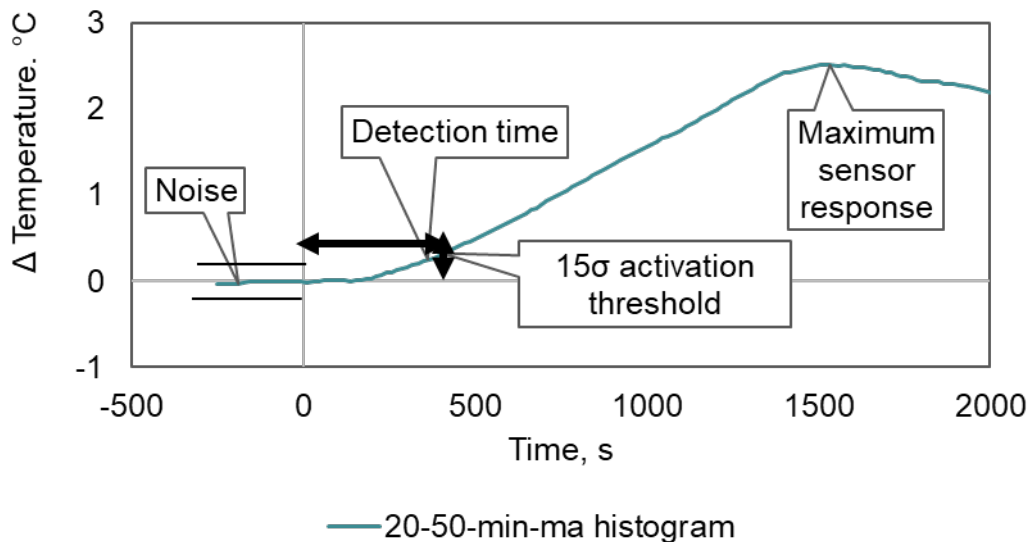


Figure 23 Overview of Key Performance Metrics in RFID-Based Detection

3.5.5. MACD Heat Detection Operational Use

In operational use, the adaptation of MACD for heat detection in ULDs employs a dynamic approach to identify potential fire hazards. Initially, each ULD operates as an independent sensor, analyzing its temperature fluctuations and as part of a communal baseline for comparative analysis. This dual functionality significantly enhances the network's sensitivity and precision in identifying temperature anomalies.

Each ULD computes its own MACD line by calculating the difference between its short-term and long-term temperature moving averages. Each ULD constructs its signal line by averaging the MACD lines from its neighboring ULDs. This aggregated signal line then serves as a communal baseline, enabling each ULD to continuously compare its temperature trends and detect any significant deviations from the established group norm. The deviation between an individual ULD's MACD line and this communal signal

line forms the histogram line. This histogram line quantifies the deviation and enables the identification of outliers potentially indicating thermal hazards. Consider ULD 3's position within a grid layout for illustration purposes, shown in Figure 24.

ULD 1	ULD 2
ULD 3	ULD 4
ULD 5	ULD 6

Figure 24 Grid Layout Example of ULDs

The signal line for ULD 3 is the average of the MACD lines from ULDs 1, 2, 4, 5, and 6, which surround it. This average provides a communal baseline for assessing ULD 3's temperature trends. The histogram line measures the temperature difference between ULD 3's MACD line and the average signal line of its neighbors. Therefore, the heat detection system can identify significant outliers that may pose fire risks. For example, a notable temperature increase in ULD 3, indicated by an elevated histogram value, prompts a fire alarm activation.

This approach allows temperature monitoring for each ULD and leverages the collective data from the aircraft cargo compartment to enhance detection accuracy. Concentrating on significant deviations within this monitored network helps minimize false alarms while detecting authentic thermal hazards.

Performing an activation threshold analysis within an actual cargo compartment during operational scenarios is critical. Operational scenarios include loading the ULDs into a cargo compartment, flight operations, and the unloading phase. The dynamics and environmental conditions encountered in operational settings differ from those in a

controlled test laboratory setting. Therefore, the activation thresholds deduced from laboratory tests may not accurately reflect the typical sensor responses during airplane operations.

3.6. Research Methodology Conclusions

This chapter outlined the research methodology for developing and validating a novel UHF RFID heat detection system to enhance fire detection capabilities within aviation cargo compartment ULDs. This system analyzes temperature trends by integrating the MACD algorithm, traditionally used in financial markets to improve early fire detection.

The experimental setup included the simulation of traditional smoke detection systems. This setup allowed for directly comparing the new RFID heat detection system against conventional smoke detection systems under various fire scenarios. Fire scenarios included controlled simulated fires, smoldering, and hazardous material fires involving lithium-ion batteries.

The methodology section included an examination of the instrumentation used. This includes UHF RFID antennas, RFID temperature sensing tags, and light obscuration meters to emulate the operational environment of an aircraft cargo compartment. This ensured the collection of accurate and relevant data for evaluating the RFID system's performance against traditional smoke detection methods.

Additionally, the methodology section included details regarding the MACD heat detection algorithm that can detect small temperature changes that traditional heat detectors might miss due to their reliance on fixed temperature or rate-of-rise thresholds. This capability is crucial for enhancing the safety and reliability of fire detection systems in aviation cargo compartments, where early detection can be the difference between a manageable incident and a catastrophic accident.

This study aims to detect heat in AAY type ULDs and monitor the smoke's egress from fires inside these ULDs. While it is possible to apply this study's methodology to other types of ULDs, the outcomes will vary based on the ULD's construction and materials used.

4. Results and Analysis

Chapter 4 presents the experimental evaluation of the RFID heat detection system for fire detection within AAY type ULDs. This chapter outlines the findings from various experimental setups, examining the efficacy of moving average configurations, optimal placement of heat and smoke sensors, and the system's performance across different fire scenarios.

Initial experiments focus on the heat based MACD algorithm to determine optimal parameters that enhance heat detection efficiency. Detailed analyses investigate the MACD configuration's impact on activation thresholds, sensor maximums, and detection times, providing insights into how moving average intervals can be optimized for AAY type ULDs.

Furthermore, the analysis involves assessing various sensor placements to understand their effects on detection sensitivity and timeliness.

Subsequently, the performance of the RFID system is tested across several fire scenarios. These fire scenarios include controlled simulations of fires, smoldering incidents, and lithium-ion battery fires. The variety of controlled fire scenarios allows for a comparative assessment of the heat-based fire detector against existing smoke detection systems in aircraft cargo compartments to highlight potential advantages and limitations.

4.1. Analysis of Moving Average Configurations

The analysis of MACD presented in Chapter 3 laid the foundation for monitoring temperature variations within ULDs, utilizing the MACD line, signal line, and histogram line. The insights from the MACD analysis are instrumental in this chapter, where we explore the behavior of six distinct moving average configurations under simulated controlled fire scenarios. Table 3 displays the six moving average configurations. Each composition, consisting of a short-term moving average and a long-term moving average, undergoes evaluation regarding key parameters: activation threshold, maximum sensor response, and detection time. This evaluation aims to optimize the MACD algorithm to minimize the activation threshold, maximize the sensor response, and reduce the detection time.

Table 3 Breakdown of Various Tested Moving Average Configurations

Configuration	Short Term MA	Long Term MA
1-5-min MA	1-min MA	5-min MA
1-20-min MA	1-min MA	20-min MA
1-50-min MA	1-min MA	50-min MA
5-20-min MA	5-min MA	20-min MA
5-50-min MA	5-min MA	50-min MA
20-50-min MA	20-min MA	50-min MA

4.1.1. MACD Configuration and Activation Threshold Analysis

This section expands on understanding the activation threshold described in Chapter 3.5.4. It details how various configurations of these moving averages influence the thresholds required to trigger an RFID heat detection system alert. A lower activation threshold effectively reduces the needed heat to trigger an alarm. Table 4 tabulates the interaction between long-term and short-term moving averages and their corresponding experimental activation thresholds.

Table 4 Interaction Between Moving Averages and Activation Thresholds

Short Term MA	Long Term MA	Activation Threshold, $\Delta^{\circ}\text{C}$
1-min MA	5-min MA	1.2
1-min MA	20-min MA	1.4
1-min MA	50-min MA	1.4
5-min MA	20-min MA	0.6
5-min MA	50-min MA	0.7
20-min MA	50-min MA	0.3

The activation threshold for a heat detection system responds significantly to variations in the short-term moving average. Figure 25 shows that increasing this short-term moving average interval from 1 to 5 minutes and further to 20 minutes consistently significantly lowers the activation threshold. Transitioning from a 1-minute to a 5-minute short-term moving average particularly highlights a steep drop in the activation threshold. This trend persists across all considered long-term moving average intervals.

For instance, with the long-term moving average set at 50 minutes, the activation threshold reduces from 1.42°C for a 1-minute short-term moving average to 0.72°C for 5 minutes and 0.27°C for 20 minutes.

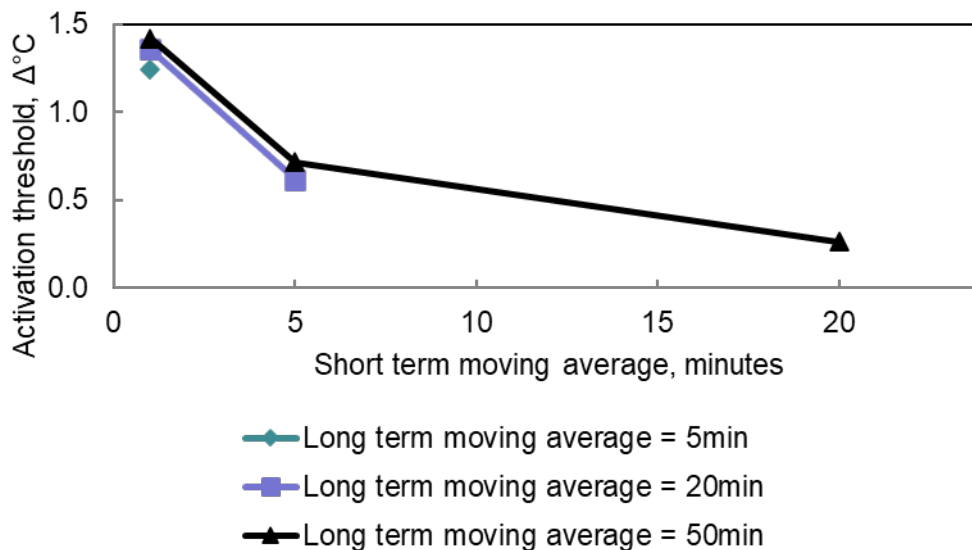


Figure 25 Activation Thresholds for Varying Short-Term Moving Averages

Conversely, the impact of altering the long-term moving average intervals on the activation threshold is more moderate. As shown in Figure 26, extending the long-term moving average from 5 to 20 minutes and further to 50 minutes results in only incremental increases in the activation threshold. This is evident across all examined short-term intervals. Specifically, while maintaining a 1-minute short-term moving average, the threshold experiences a slight increase from 1.24°C for a 5-minute long-term moving average to 1.36°C with a 20-minute interval. Then, it increases to 1.42°C for a 50-minute interval.

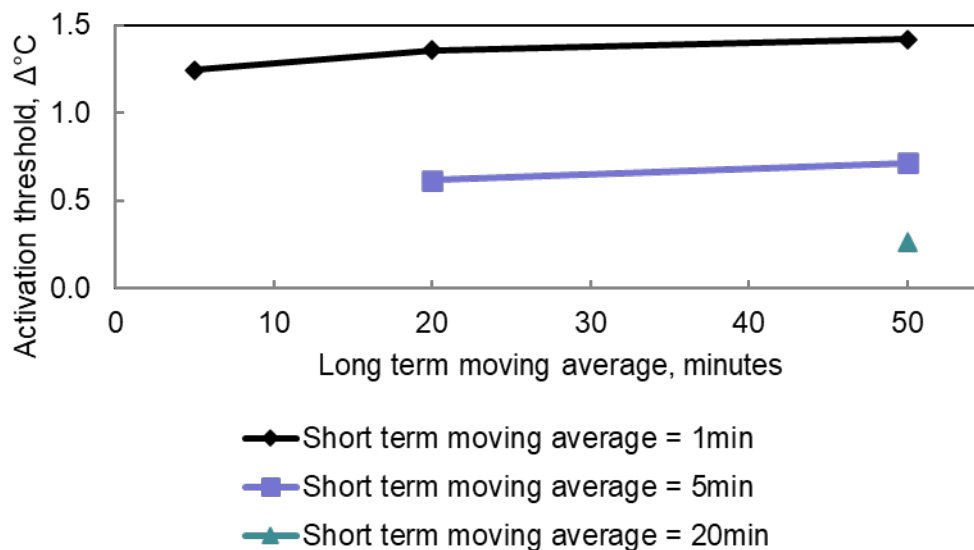


Figure 26 Activation Thresholds for Varying Long-Term Moving Averages

This data shows that the activation threshold is particularly sensitive to adjustments in the short-term moving average compared to variations in the long-term moving average. Increasing the short-term moving average duration significantly decreases the activation threshold, and increasing the long-term moving average moderately increases the activation threshold.

Intuitively, increasing the length of the short-term and long-term moving averages would decrease both the activation threshold and the noise. Longer averages should smooth out fluctuations more effectively, leading to a more stable signal and a lower activation threshold.

However, the experimental results show a nuanced interaction between moving average lengths and activation thresholds. With a longer long-term moving average, the system becomes more susceptible to short-term temperature fluctuations due to its

design to smooth out longer trends. Consequently, transient temperature spikes stand out more against this smoothed baseline, potentially leading to pronounced histogram bars that may not reflect significant temperature changes. The MACD's application for heat detection further amplifies this by actively comparing temperature trends between a fire ULD and a reference ULD. A longer long-term moving average can exaggerate the histogram's differential for any short-term noise not concurrently present in both ULDs, leading to discrepancies that may not signify a genuine thermal hazard.

4.1.2. MACD Configuration and Sensor Maximum Analysis

This section expands on understanding the maximum sensor response introduced in Chapter 3.5.4. The maximum sensor response quantifies the highest temperature variation detected by the RFID heat detection system for a given heat input. Table 5 demonstrates the interaction between long-term and short-term moving average configurations and their effect on the maximum sensor response. The tabulated results are from test experiments with heat inputs of 390W and 230W into the fire ULD.

Table 5 Interaction Between Moving Averages and Maximum Sensor Response

Short Term MA	Long Term MA	Maximum Sensor Response, $\Delta^{\circ}\text{C}$
1-min MA	5-min MA	0.99
1-min MA	20-min MA	2.55
1-min MA	50-min MA	3.60
5-min MA	20-min MA	2.11
5-min MA	50-min MA	3.35
20-min MA	50-min MA	2.35

The maximum sensor response for a heat detection system responds significantly to variations in the short-term moving average. Figure 28 shows that increasing this interval from 1 to 5 minutes and further to 20 minutes consistently significantly lowers the maximum sensor response. This trend persists across all considered long-term moving average intervals. For instance, with the long-term moving average set at 50 minutes, the activation threshold reduces from 3.60°C for a 1-minute short-term moving average to 3.35°C for 5 minutes and 2.35°C for 20 minutes.

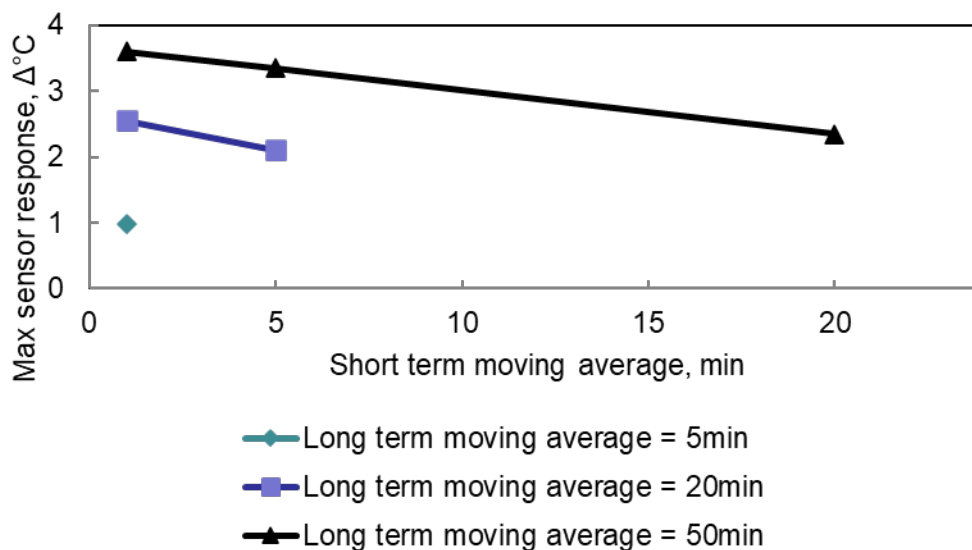


Figure 27 Maximum Sensor Response for Varying Short-Term Moving Averages

Similarly, the maximum sensor response for a heat detection system responds significantly to variations in the long-term moving average. As illustrated in Figure 28, lengthening the long-term moving average from 5 to 20 minutes and subsequently to 50 minutes correlates with notable rises in the maximum sensor response. This trend is consistent across various short-term moving average intervals. Transitioning from a 5-minute to a 20-minute long-term moving average particularly highlights a steep increase in the maximum sensor response. Specifically, for a 1-minute short-term moving average, the maximum sensor response rises from 0.99°C with a 5-minute long-term moving average to 2.55°C at 20 minutes and to 3.60°C at a 50-minute interval.

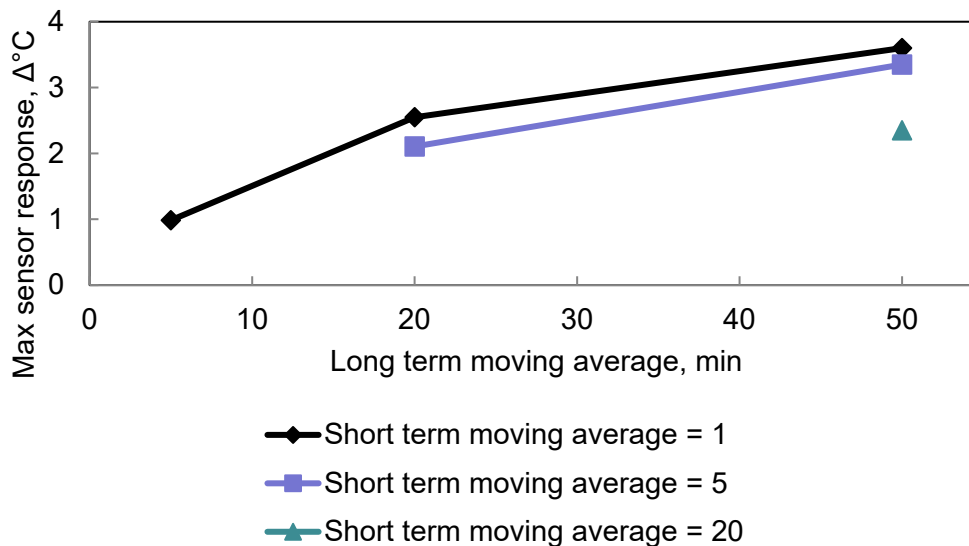


Figure 28 Maximum Sensor Response for Varying Long-Term Moving Averages

This data shows that the maximum sensor response is sensitive to adjustments in the short-term and long-term moving averages. Increasing the short-term moving average duration decreases the maximum sensor response, and increasing the long-term moving average moderately increases the maximum sensor response.

Intuitively, lengthening the long-term moving average in a MACD-based heat detection system accentuates the maximum sensor response. Extending the long-term moving average provides a more consistent and stable baseline, smoothing out longer-term temperature trends. Against this stable baseline, short-term temperature increases, captured by the short-term moving average, become more pronounced. The rationale is that while the long-term average slowly incorporates temperature changes, any rapid temperature rise becomes starkly evident, leading to a more significant

differential between the short-term and long-term averages, thus amplifying the maximum histogram sensor response.

This intuition aligns with the experimental data observed. As the long-term moving average lengthens, its role as a baseline magnifies deviations from normal temperature behavior. This effect is particularly evident when rapid temperature increases occur, which take time to reflect in the smoothed long-term trend. These increases cause the short-term moving average to spike relative to the long-term average, resulting in a larger histogram bar that indicates a significant temperature differential.

4.1.3. MACD Configuration and Detection Time Analysis

This section expands on the comprehension of detection time, as explained in Chapter 3.5.4. This metric is critical as it captures the timeliness of the RFID heat detection system in identifying and responding to adverse thermal conditions. Table 6, derived from experimental data with a heat input of 390W into the fire ULD, illustrates how various configurations of short-term and long-term moving averages influence detection times. The 1-5-min MA configuration notably failed to surpass the activation threshold, resulting in the absence of a recorded detection time for this setting.

Table 6 Interaction Between Moving Averages and Detection Times

Short Term MA	Long Term MA	Detection Time, min
1-min MA	5-min MA	Did Not Detect
1-min MA	20-min MA	2.85
1-min MA	50-min MA	3.10
5-min MA	20-min MA	4.10
5-min MA	50-min MA	4.35
20-min MA	50-min MA	6.83

In examining the detection time for the RFID heat detection system, it becomes evident that changes in the short-term moving average significantly influence this metric. As shown in Figure 29, adjusting the short-term moving average from 1 to 5 to 20 minutes markedly extends the detection time. This consistent trend is observed across all considered long-term moving average intervals. For instance, with a long-term moving average of 50 minutes, the detection time lengthens from 3.10 minutes for a 1-minute short-term moving average to 4.35 minutes for a 5-minute interval and further to 6.83 minutes for a 20-minute interval.

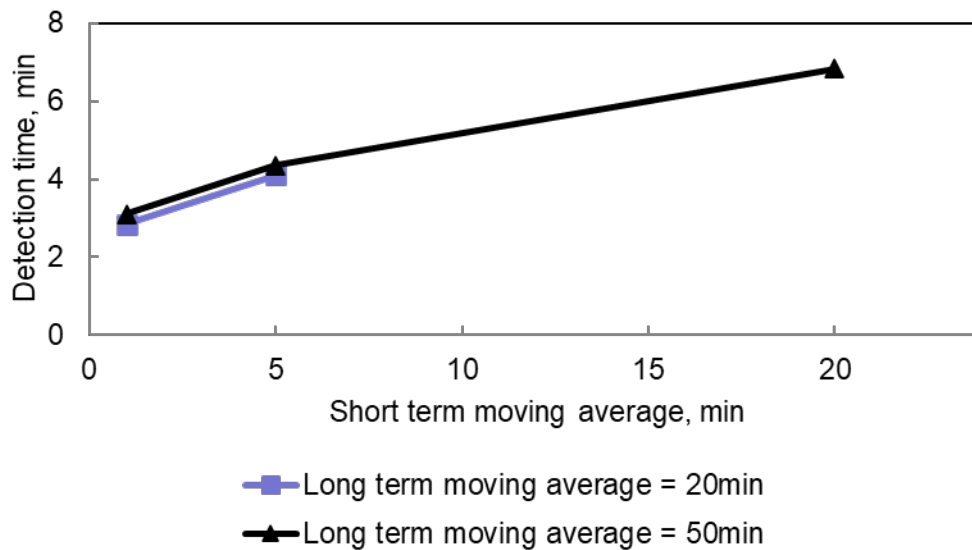


Figure 29 Detection Time for Varying Short-Term Moving Averages

In contrast, the impact of varying the long-term moving average is less pronounced but still evident. Figure 30 shows that increasing the long-term moving average results in a modest increase in detection time. For example, the detection time slightly increases from 2.85 minutes at a 20-minute interval to 3.10 minutes at a 50-minute interval.

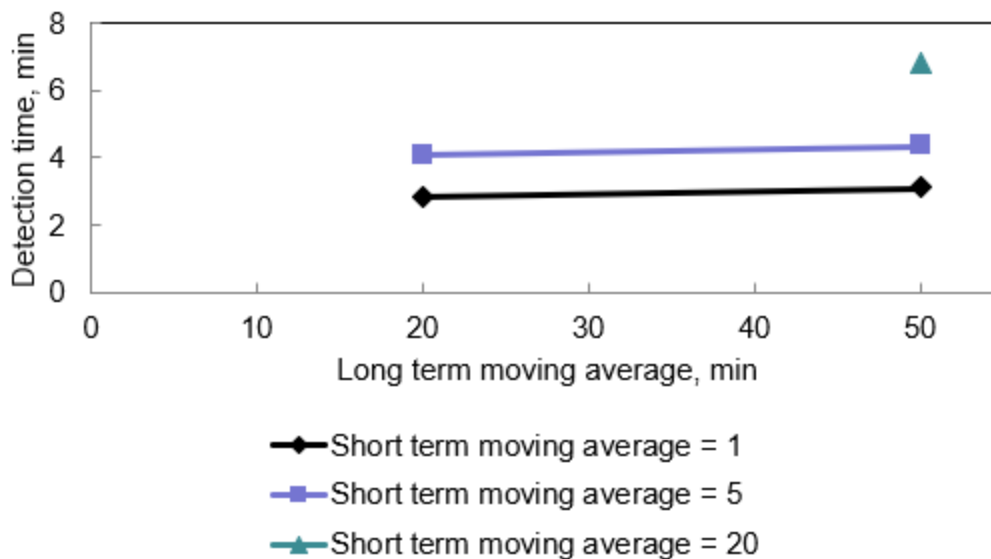


Figure 30 Detection Time for Varying Long-Term Moving Averages

The study reveals that lengthening the short-term moving average significantly extends the detection time. In contrast, increasing the long-term moving average only moderately increases the detection time.

Shortening the short-term moving average in a MACD-based heat detection system intuitively leads to faster detection times, as it heightens sensitivity to immediate temperature shifts, quickly identifying deviations from established long-term trends. This rapid response is crucial for early fire event detection. Experimental evidence aligns with this intuition, demonstrating that reduced short-term moving average lengths correlate with shorter detection times. However, the minimal short-term and long-term moving average pairing (1-5-min MA) did not detect the event, suggesting a practical limit to shortening averages for effective detection.

The experiments highlight a nuanced relationship between moving average lengths and detection efficiency. While shorter short-term averages expedite anomaly detection, optimal system performance requires a balanced approach with the long-term average to ensure specificity and sensitivity.

4.1.4. Practical Implications and Optimizing MA Intervals Summary

The key performance parameters to optimize the RFID heat detection system include the activation threshold, maximum sensor response, and detection time.

For the activation threshold, which is pivotal in determining when the system triggers an alarm, the configuration of the short-term moving average has a pronounced effect. A reduced short-term moving average interval leads to a higher activation threshold, requiring a more significant temperature change to trigger the system. Contrarily, the activation threshold has a marginal variation when increasing the long-term moving average intervals.

Both short-term and long-term moving averages influence the maximum sensor response, which signifies the system's capacity to detect the highest temperature variation. Reduced short-term moving averages tend to register higher maximum sensor responses due to their ability to capture rapid temperature spikes. In contrast, increased long-term moving averages reflect higher sensor responses by capturing broader temperature trends, which can be essential for identifying slow-developing fire hazards.

The detection time represents the interval from heat initiation to alarm activation. Longer short-term moving averages increase detection time, delaying the system's response to heat events. While an extension of the long-term moving average only marginally increases detection time, its effect is less significant than changes in the short-term moving average.

Table 7 summarizes the effects of adjusting short-term and long-term MAs on these critical performance parameters to clarify these results. This table demonstrates the nuanced effects of MA adjustments on system performance.

Table 7 Effect of Short-Term and Long-Term Moving Average Configurations on RFID Heat Detection System Performance Parameters

Parameter	Effect of Increasing Short-Term MA	Effect of Increasing Long-Term MA
Activation Threshold	Significantly decreased	Marginally increased
Maximum Sensor Response	Decreased	Increased
Detection Time	Significantly increased	Moderately increased

Based on the experimental data from Sections 4.1.1, 4.1.2, and 4.1.3 the 5-20-min and 20-50-min MA configurations emerge as optimal choices, each catering to distinct operational needs. The 5-20-min MA effectively responds to rapid temperature increases, while the 20-50-min MA is better suited for responding to slowly developing fires.

In practical operational settings, the time needed to establish baseline measurements for the long-term MA is a crucial factor. A dynamic approach can address

this by initially employing a 1-5-min MA configuration for rapid baseline establishment, followed by a transition to the 5-20-min MA to maintain heightened sensitivity while improving detection reliability. As the flight progresses and baseline measurements stabilize, combining the 5-20-min MA and 20-50-min MA configurations can offer a balanced solution, effectively monitoring quick and slow-developing fires.

The data presented provides a foundational understanding, but specific operational needs and constraints should guide the final determination of the most suitable MA intervals.

4.2. Analysis of Heat Sensor Location

This section aims to identify which RFID temperature sensing tag placement within the mock cargo compartment is most likely to trigger an alarm during a fire event. The findings here contribute to comprehensively comparing traditional smoke detection systems with the RFID heat detection system in subsequent sections.

Section 4.1 investigates varying moving average durations used in the MACD heat detection algorithm. The 20-50-min MA configuration, as described in Section 4.1.4, is used as the analytical benchmark for evaluating sensor performance across different ceiling configurations.

As outlined in Section 3.3.1, on the interior ceiling at the center of the fire ULD, there is one sensor placed directly on the surface (0mm), and four additional temperature sensing tags are mounted at varying heights of 6.4mm, 25.4mm, 50.8mm,

and 76.2mm (*Figure 15*). The mounts assist in minimizing heat loss from conduction to the ULD surface. Reducing heat loss to the ULD provides a more accurate temperature reading of the ambient environment. Furthermore, an exterior ceiling sensor is installed at the fire ULD center surface (-3.175mm) to compensate for the RFID reading limitation through metal. This provides insights into fire detection capabilities for aluminum ULDs, where it is challenging to place temperature sensing tags inside the ULD because the UHF electromagnetic waves cannot penetrate metal.

4.2.1. Heat Sensor Location and Sensor Maximum Analysis

This section expands on the maximum sensor response outlined in Chapter 3.5.4. The maximum sensor response is representative of the peak temperature variation detected by the RFID heat detection system during a specified test scenario. Understanding the maximum sensor response is essential in assessing the system's sensitivity and responsiveness to thermal variations within the fire ULD.

Figure 31 illustrates the relationship between sensor height and the maximum change in temperature. The graph represents the average signal sensitivity across five tests, employing the 20-50-min-ma histogram line, with varying heat inputs (80, 141, 249, 337, and 584W) introduced to the fire ULD.

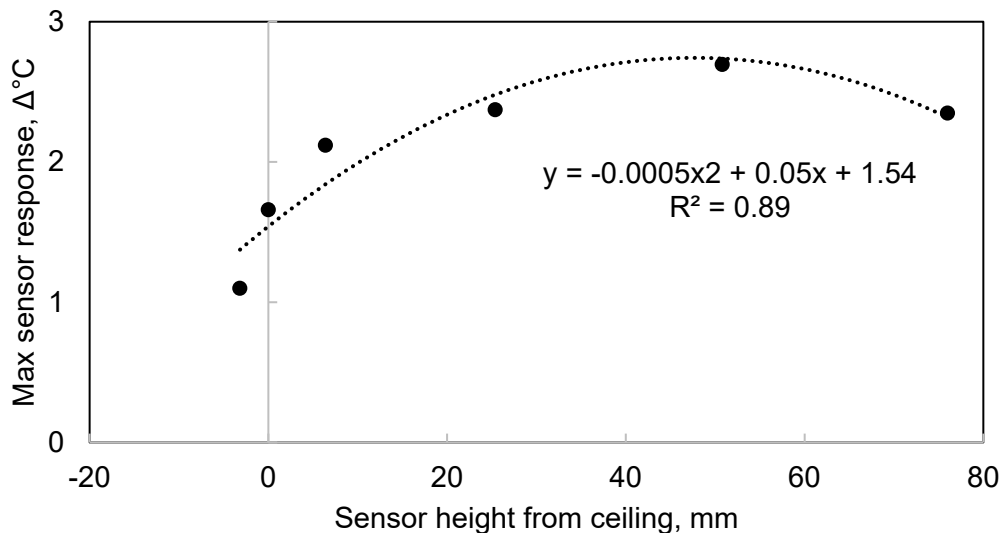


Figure 31 Sensor Height vs. Maximum Sensor Response Analysis (20-50min MA)

The graph condenses the key observations into a quadratic function: $y = -0.0005x^2 + 0.05x + 1.54$, with a coefficient of determination (R^2) of 0.89. They demonstrate an excellent fit to the data points. This quadratic function exhibits a concave-down shape, explaining the relationship between sensor height and maximum sensor response. Additionally, by solving for x (sensor height) to find the maximum y (max sensor response), a sensor height of 50.4mm is the optimal sensor height for maximizing sensor response.

4.2.2. Heat Sensor Location and Detection Time Analysis

This section focuses on analyzing how different sensor locations affect the detection time. Expanding the concept of detection time outlined in Chapter 3.5.4, the detection time here signifies the duration from the onset of heat within the fire ULD until the point when the 20-50-min MA histogram line crosses the activation threshold.

The activation threshold is set at fifteen standard deviations above the norm over 11 hours in ambient conditions, specifically applied to the histogram line. This threshold accounts for random temperature fluctuations due to minor environmental changes, sensor inaccuracies, or other variables. The primary aim is to assess the RFID heat detection system's efficiency in promptly identifying heat anomalies across various sensor placements within the ULD.

Figure 32 displays the relationship between sensor height and detection time, with each data point symbolizing a specific sensor height. The results are from an average of five tests using the 20-50-min MA histogram line, with varying heat inputs (80, 141, 249, 337, and 584W) to the fire ULD. In other words, it shows how changing sensor heights influence the system's promptness in detecting thermal events within the fire ULD.

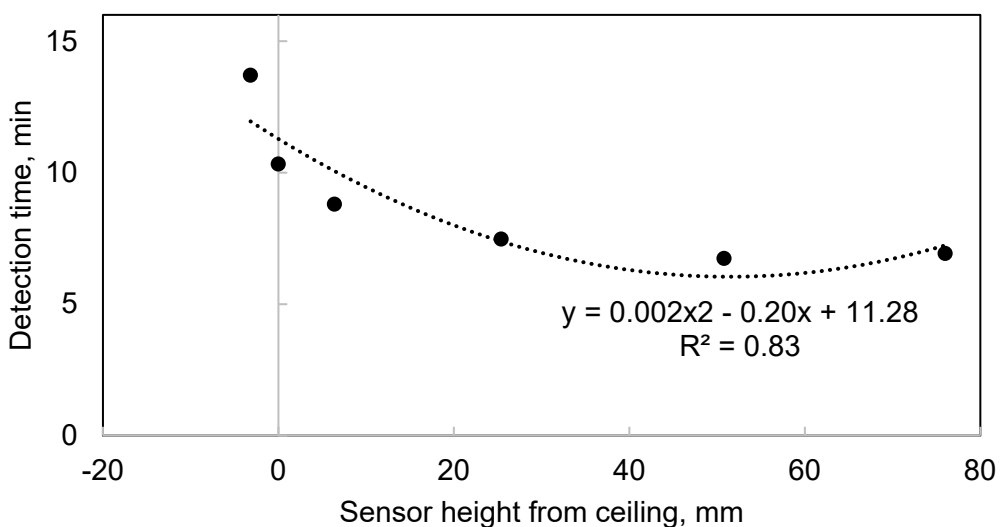


Figure 32 Correlation Between Sensor Height and Detection Time (20-50min MA)

The graph represents the quadratic function expressed as $y = 0.002x^2 - 0.20x + 11.28$, with an R^2 value of 0.83, and exhibits a concave-up shape. This R^2 value signifies a robust positive correlation between sensor height and detection time. Solving for x (sensor height) to discover the minimum y (detection time) results in calculating an optimal sensor height of 50.9mm for minimizing detection time.

4.2.3. Practical Implications and Optimizing Heat Sensor Location Analysis

The key objectives in sections 4.2.1 and 4.2.2 were to find a sensor position that minimizes detection time, maximizes signal sensitivity, and adheres to spatial constraints within the ULD. Sensor location influences detection time and maximum sensor response. Strategic sensor positioning is important for the accuracy and reliability of temperature readings and is essential for early fire detection and timely intervention in thermal threats.

The data supports the importance of sensor location in optimizing the RFID heat detection system. The maximum sensor response for the exterior surface sensor is 1.1 $\Delta^\circ\text{C}$, the interior surface sensor on the ceiling is 1.6 $\Delta^\circ\text{C}$, the 6.4mm sensor is 2.1 $\Delta^\circ\text{C}$, and the 50.8mm sensor is 2.8 $\Delta^\circ\text{C}$. Correspondingly, the detection time for the exterior surface sensor is 13.7 minutes, the interior surface sensor is 10.3 minutes, the 6.4mm sensor is 8.8 minutes, and the 50.8mm sensor is 6.7 minutes. Even though the 50.8mm sensor appears to be the optimal sensor location, it impedes significantly more space within the ULD that may be used in flight operations than the 6.4mm sensor.

This analysis led to selecting the sensor positioned on the 6.4mm mount for deeper analysis. Figure 33 encircles the 6.4mm mount for emphasis and clarity. The 6.4mm mount has balanced features, specifically for its response time, high signal sensitivity, and minimal spatial intrusion within the ULD. The increased response time is crucial for timely detection and reaction to potential fire hazards. Additionally, high signal sensitivity highlights the system's ability to respond to minimal temperature variations. Furthermore, the minimal spatial intrusion within the ULD ensures that the sensor setup does not impinge on the available cargo space.

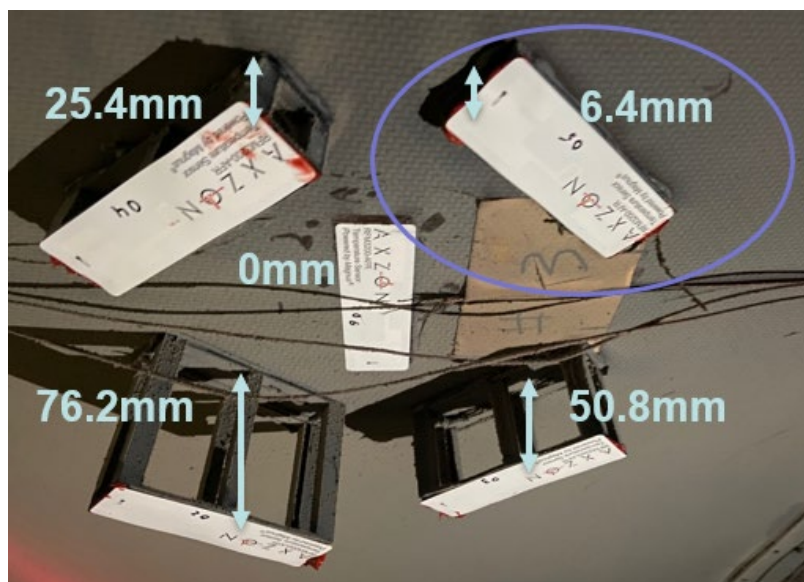


Figure 33 Placement of Temperature Sensing RFID Tags within Fire ULD Emphasizing the 6.4mm Mount

4.3. Analysis of Smoke Sensor Configurations

This section aims to identify which smoke sensor placement within the mock cargo compartment has the highest likelihood of triggering an alarm during a fire event.

Identifying and selecting the smoke sensor most likely to trigger an alarm enables a reasonable comparison between traditional smoke detection systems and the RFID heat detection system under investigation.

To better visualize the arrangement and proximity of the sensors to the fire ULD, refer to the schematic provided in *Figure 16* from Section 3.3.1. This schematic details the sensor distribution, offering a clear top-down perspective of the experimental setup and aiding in understanding the subsequent analysis of sensor performance.

The controlled fire scenario within the fire ULD uses an externally positioned smoke generator alongside a heater placed at the interior center floor of the ULD, as shown in Figure 7 from Section 3.1.1. A variable AC transformer controls the heater's output. For the tests, the smoke generator produces an aerosol for 60 seconds, following the testing procedures required for certification.

4.3.1. Smoke Sensor Location Analysis

This subsection examines how the positioning of smoke sensors within the cargo compartment influences their maximum response. Figure 34 shows the relationship between the sensor horizontal distance from the ULD fire door and the maximum 60-second average in light obscuration, based on nineteen tests with various heat inputs and consistent smoke inputs introduced to the fire ULD. This choice provides a clearer visualization of the trend and a more precise interpretation of the data. Notably, the

peak %obs/m is higher than the 60-second time average, making this a conservative representation of the smoke detection capability.

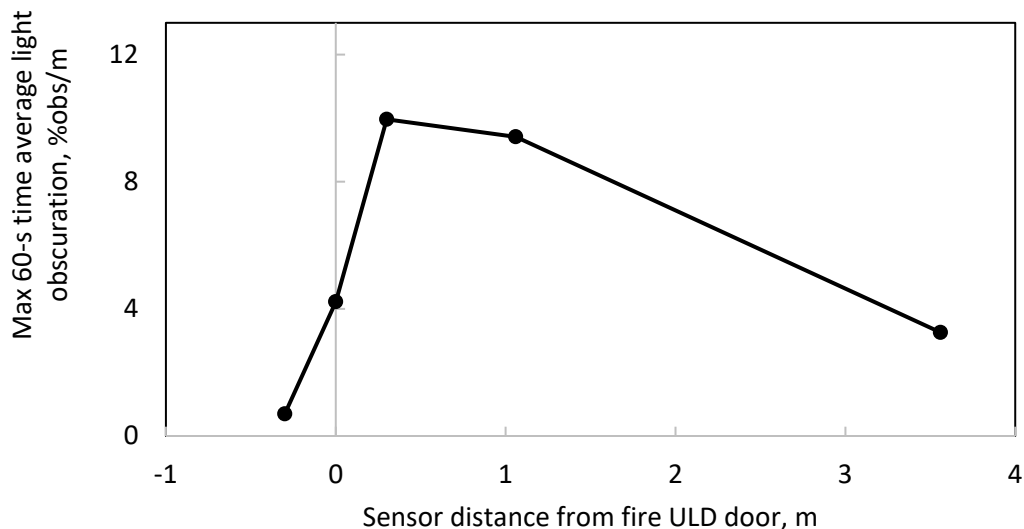


Figure 34 Light Obscuration in Relation to Sensor Distance from ULD Fire Door

A distinct trend demonstrated in the graph is the horizontal propulsion of smoke as it exits the fire ULD. Specifically, the sensor located at +0.3m from the ULD door measures significantly more smoke compared to the sensor at -0.3m from the ULD door. The sensor at 0.3m demonstrates the greatest maximum 60-second average in light obscuration. Furthermore, there is a measurable decrease in smoke detection capability at intermediate distances between +0.3m and the two ends of the mock cargo compartment as the sensors are situated farther away. Additionally, the sensor aligned directly above the ULD door does not capture as much smoke as the sensor positioned at 1.06m from the door, with the -0.3m sensor measuring the least amount of smoke.

4.3.2. Optimizing Smoke Sensor Location Analysis

This subsection identifies the optimal location for the smoke sensor to respond to fire threats. The sensor at +0.3 meters from the ULD door is selected for further analysis due to its high signal sensitivity. The smoke exhibits forward momentum as it exits the ULD, reaching the end of the mock cargo compartment before reverting towards the aft sensor.

Figure 35 illustrates the setup within the cargo compartment, highlighting the reference ULD and the fire ULD and indicating the typical smoke flow pattern during a test scenario. The sensor at +0.3 meters is encircled to underscore its importance in detecting the forward movement of smoke. This behavior of smoke, where it initially moves forward before reversing direction, aligns with findings reported by the FAA regarding smoke transport in aircraft cargo areas [90].

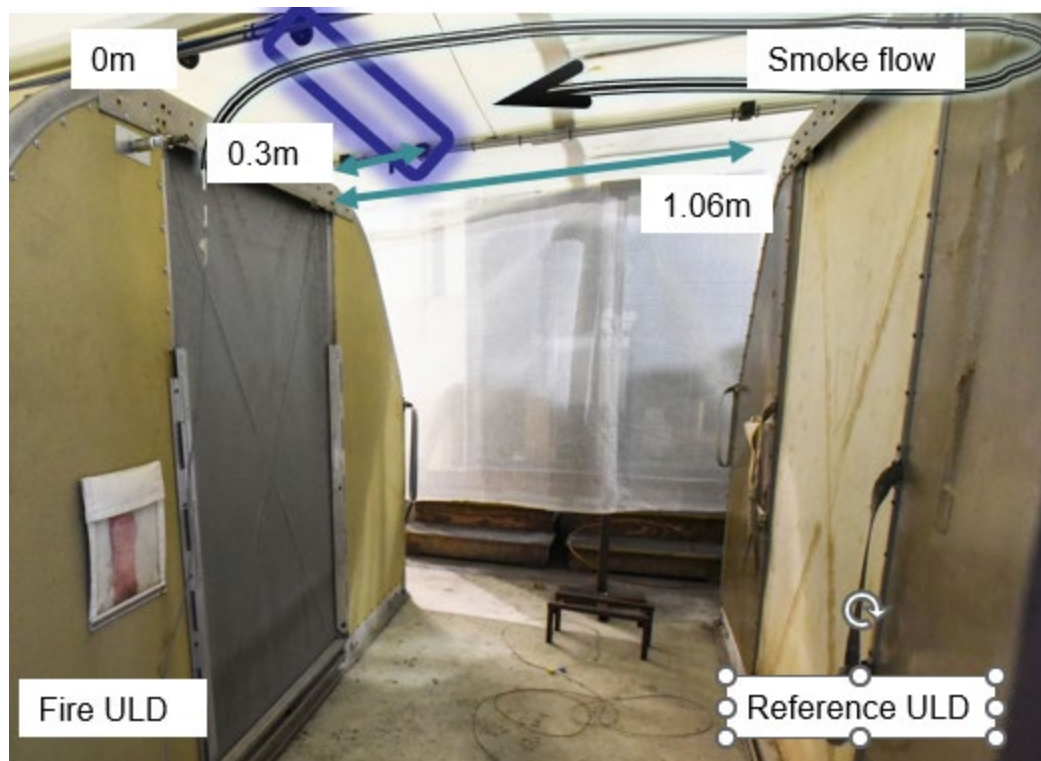


Figure 35 Optimal Smoke Sensor Placement and Smoke Flow Dynamics in Cargo Compartment

Selecting the smoke sensor location at +0.3 meters from the ULDB door aims to ensure sufficient signal sensitivity. The aim is to maximize the probability of prompt fire alarm activation. This optimized sensor location is essential in allowing the smoke detectors the best chance of early fire detection and enabling a fair comparison between the RFID heat detection system and existing smoke detection systems in aircraft cargo compartments.

4.4. Evaluation of Controlled Fire Scenarios

This section evaluates the RFID heat detection system and the cargo smoke detection system across controlled fire scenarios within ULDBs. The structured

experimental setup allows for observations and assessments of the system's responses under varying fire conditions to evaluate its ability for early fire detection. Subsections 4.4.1 and 4.4.2 provide an in-depth heat and smoke detection analysis. The goal is to assess the heat and smoke detection systems based on the acquired test data. The research seeks to understand the correlation between the heat input to the fire ULD and the resulting sensor responses in heat and smoke detection. Furthermore, this analysis aims to highlight the strengths and limitations of the heat detection system, allowing for informed recommendations for its further development.

Section 3.1.1 describes the controlled fire scenarios. The experiments use a heater and a smoke generator to simulate varying fire situations within a ULD. The heat and smoke detection analyses in the following subsections, 4.4.1 and 4.4.2, respectively, are derived from the data collected from twenty-one tests. However, two of those tests malfunctioned, with the smoke sensor missing smoke measurements. For the testing protocol, the smoke generator is activated to produce an aerosol for 60 seconds. The aerosol production remained constant across all tests, and the heat input varied from 55W to 669W. The optimized configurations in previous sections, 4.1.4, 4.2.3, and 4.3.2, were used. The optimized configuration includes the 6.4mm sensor mount and the +0.3m smoke meter. The 5-20-min MA configuration was selected for this section for its rapid detection time. However, it should be noted that the 20-50-min MA configuration has a lower activation threshold and can detect slowly developing fires that the 5-20-min MA configuration may miss.

The following subsection introduces two added terms. They are *the minimum heat input for heat detection* and the *minimum heat input for smoke detection*. The minimum heat input for heat detection denotes the lowest heat input required to activate an RFID heat detection system alarm. The minimum heat input for smoke detection indicates the lowest heat input needed to eject the aerosol from the ULD and activate a smoke detection system alarm.

4.4.1. Heat Detection Analysis for Controlled Fire Scenarios

This subsection aims to determine the relationship between the amount of heat input to the fire ULD and the resultant sensor response. This relationship is vital for understanding the efficacy of the RFID heat detection system across varying fire scenarios. The analysis contains data from twenty-one tests with heat inputs ranging from 55W to 669W.

Figure 36 shows a linear correlation between the heat input to the fire ULD and the resulting maximum temperature change. The mathematical expression of the linear relationship is $y = 0.01x + 0.19$, where x denotes the heat input in watts, and y represents the maximum temperature change in degrees Celsius. The sensor detects the temperature change, and the 5-20-min MA calculates the histogram signal. The high R^2 is 0.97, showing a strong linear correlation between the two variables. The strong correlation between heat input and sensor response demonstrates the sensor's effectiveness in estimating the heat within the ULD.

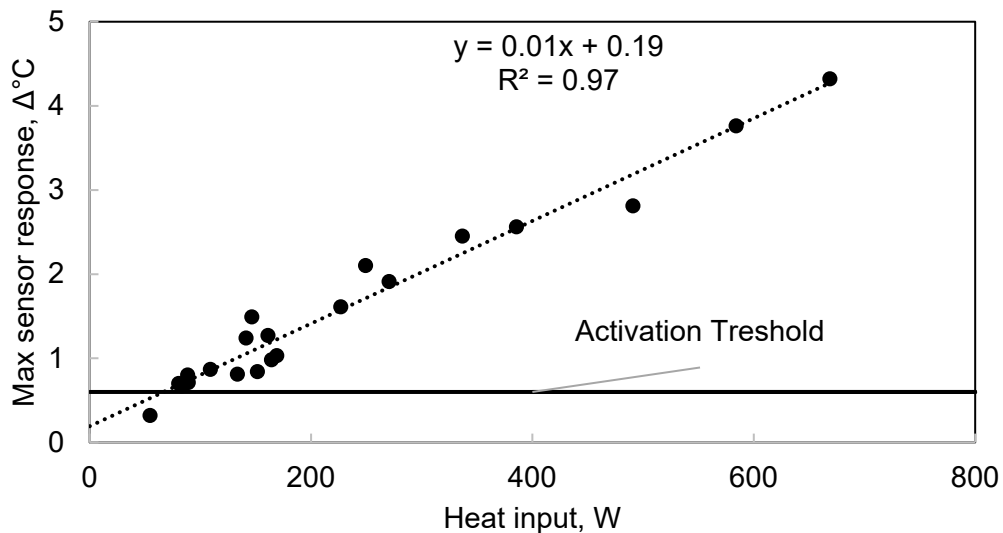


Figure 36 Correlation of Heat Input to Max Sensor Response in Simulated Fire Tests

The system's design is to provide near real-time fire status and location data to flight crews, allowing them to determine the effectiveness of fire suppression measures. The linear model extrapolated from the data suggests that it is a reliable tool for evaluating the heat detection system's performance under an array of fire scenarios.

As determined in section 4.1.1, the activation threshold for the 5-20-min MA was set at 0.6, as shown in Table 4. The minimum heat input for detection was calculated to be 67W using the equation $y = 0.01x + 0.19$ alongside the activation threshold of 0.6. The minimum heat input for detection is essential in understanding the system's sensitivity to varying heat inputs.

4.4.2. Smoke Detection Analysis for Controlled Fire Scenarios

This subsection aims to find the relationship between the heat input to the fire ULD and the smoke production, as quantified by the maximum 60-second average in light obscuration. Analyzing the signal sensitivity with varying heat inputs helps to find the threshold at which smoke detection occurs. The results include data from nineteen tests executed with varying heat input while ensuring consistent aerosol production, as detailed in section 3.1.1.

The constant aerosol production isolates the impact of varying heat input on smoke detection. Therefore, it provides a clearer insight into the smoke detection capability under different fire scenarios. The constant aerosol generation ensures that the heat input variations influence the variations in smoke detection. Thus, it establishes a controlled experimental environment that aligns with the simulated fire situations within the ULD.

Figure 23 shows the relationship between the heat input to fire ULD and the maximum 60-second average in light obscuration, with a secondary axis indicating the occurrence of smoke detection. The data in the primary axis fits a sigmoid function, as shown in Equation 7:

$$\text{Equation 7} \quad y = 18.2 + \frac{0.5 - 18.2}{1 + \frac{x}{146}^{6.7}},$$

X represents the heat input in watts and y represents the maximum 60-second average in light obscuration.

The R^2 is 0.87 and suggests a correlation between the heat input into the fire ULD and the smoke measurement, representing smoke escaping the fire ULD. Furthermore, it shows the potential predictive capacity of this model for aircraft-level fire detection building from this simulated fire scenario.

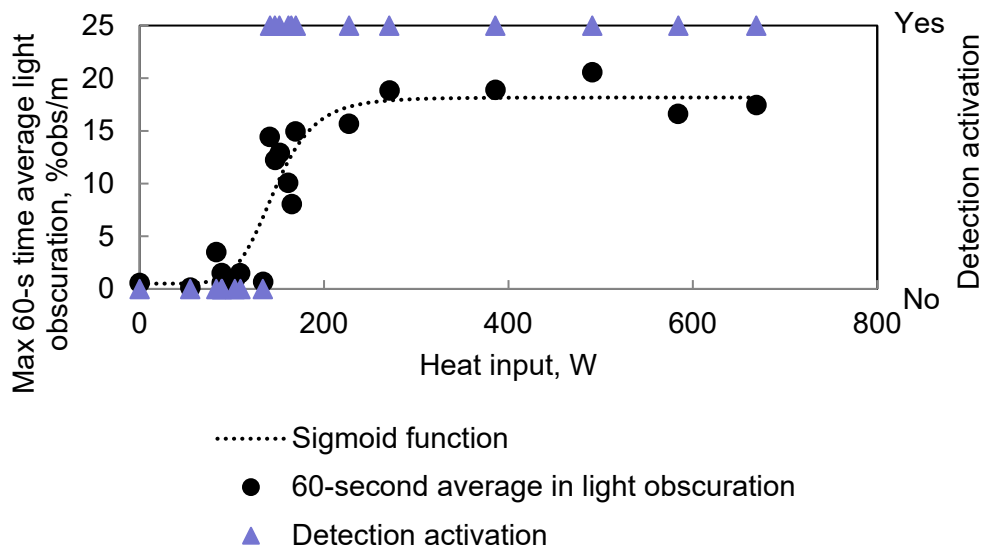


Figure 37 Analysis of Heat Input vs. Smoke Detection and Light Obscuration

The sigmoid curve in Figure 37 shows a typical S-shaped curve. Initially, minimal smoke escapes the fire ULD at low heat input, resulting in lower smoke detection capability in the cargo compartment. As heat input increases, there is a sharp rise in smoke measurement, marking a transition to effective smoke detection in the cargo compartment. The curve eventually levels off, indicating a phase of reliable detection where further heat input changes have a marginal impact on the smoke measurement. This curve explains the behavior of smoke propagation with varying heat inputs, aiding in understanding operational thresholds and reliability of the smoke detection system.

The minimum heat input for smoke detection was experimentally calculated by averaging the highest heat input without activation (134W) and the lowest with activation (141W), resulting in an approximate threshold of 137.5W. Simultaneously, a mathematical approach was employed, solving the sigmoid function for x when y equaled 12.5%obs/m for the max 60-s time average in light obscuration, yielding a value of 163.4W. This is a conservative estimate due to the 60-second data averaging, as the peak %obs/m is likely higher than the 60-s time average, illustrated by some data points triggering an alarm despite having a 60-s time average below 12.5%obs/m. Solving the sigmoid function for its minimum heat input for smoke detection is vital in understanding the system's sensitivity to varying heat inputs.

The equation derived in Section 4.4.2, $y = 0.01x + 0.19$, establishes a predictive relationship between the heat input to the fire ULD and the maximum temperature change detected by the sensor using the 5-20-min MA. This equation predicts the rise in temperature at which smoke will escape the ULD. When applying this model to the minimum heat inputs for smoke detection, 137.5W for the experimental value and 163.4W for the mathematical value, it is possible to infer the minimum sensor temperature response required to push smoke out of the ULD. The minimum sensor temperature responses are 1.6°C for the experimental value and 1.8°C for the mathematical value.

4.4.3. Fire Detection Comparison for Controlled Fire Scenarios

This section compares the minimum heat input required to activate heat and smoke detection systems. In subsection 4.4.1, the minimum heat input for heat detection is mathematically determined to be 67W. In subsection 4.4.2, the minimum heat input for smoke detection is higher, with experimental and mathematical estimations at 137.5W and 163.4W, respectively.

The heat detection system exhibits a linear response to increasing heat input. This is important for near real-time monitoring and early detection of thermal threats. A sigmoid function characterizes the mock cargo compartment smoke detection system's behavior. This inherently includes a delayed response during its initial phase at lower heat input levels before transitioning into a rapid response phase. This initial phase represents a zone where the heat input is insufficient to eject smoke from the ULD, delaying smoke detection.

Figure 38 shows the response dynamics of the heat and smoke detection systems to varying heat input levels within the fire ULD. Additionally, the figure includes a close-up inset of the ULD heat detection's response to varying heat input levels. The mathematical expressions of the relationships governing the detection times are $y = 83x^{0.5}$ for heat detection and $y = 390136x^{-1.8}$ for smoke detection. Both functions have inverse relationships between the heat input and detection time. The mathematical functions signify that an increase in heat input corresponds to a decrease in detection time.

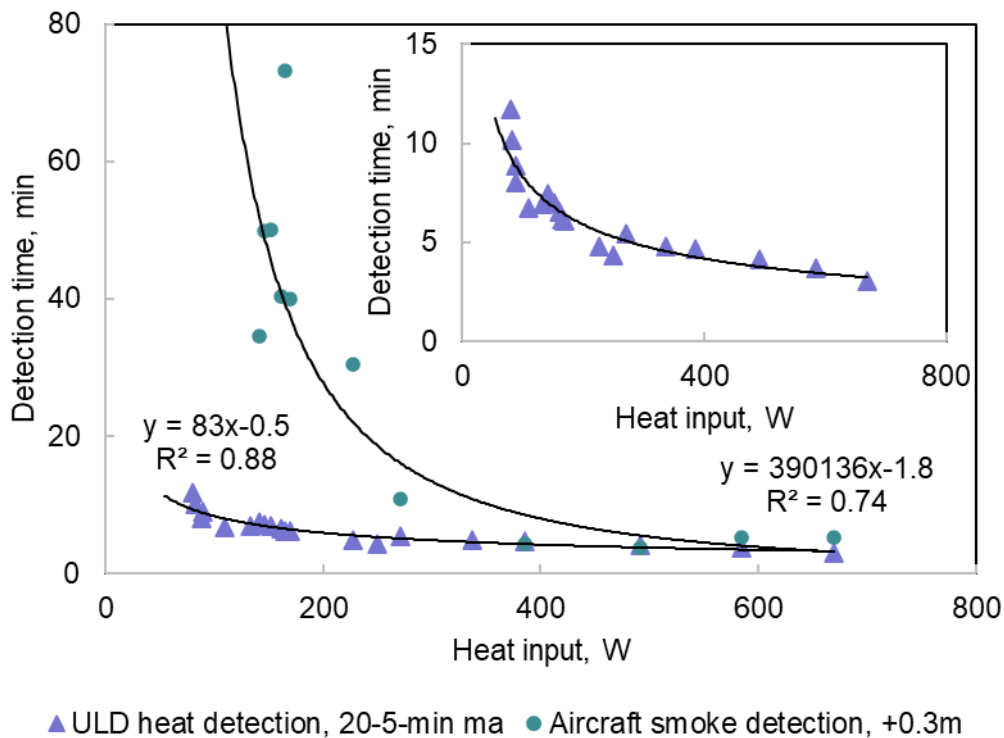


Figure 38 Comparison of Heat and Smoke Detection Times Relative to Heat Input

The coefficients and exponents in these power functions represent the rate at which detection time decreases with increasing heat input. Notably, the exponents -1.8 and -0.5 indicate the rate of decrease in detection time for smoke and heat detection systems, respectively. Smoke detection has a steeper decline, as represented by its lower exponent value. Additionally, the R^2 values of 0.74 for smoke detection and 0.88 for heat detection indicate a reasonable fit of these power functions to the actual data.

Figure 39 (a) and (b) compare RFID heat detection and traditional smoke detection system performance across different heat input levels based on Figure 38's power functions, accompanied by actual data points and estimates. Figure 39 (a) displays the response ratio, calculated as the smoke detection time divided by the RFID

It is important to note that smoke detection was non-responsive at heat inputs less than 141W, whereas heat detection was operational at points below that threshold but not below 67W. The lowest heat input at which smoke detection occurred is 141W.

4.5. Evaluation of Smoldering Fire Scenarios

This section evaluates the RFID heat detection system for smoldering fires in ULDs. Smoldering fires exhibit gradual heat release and minimal smoke production. This challenge necessitates a system capable of early identification to mitigate the risk of escalation to uncontrollable fires within the cargo compartment.

The experimental setup is consistent with the protocols outlined in Section 3.1.2 and utilizes a smoke pipe filled with hardwood pellets. This setup replicates the slow and low-heat combustion process typical of smoldering materials. UHF RFID temperature sensing tags are placed at predetermined locations within the ULD to capture the temperature profiles and validate the performance of the heat detection system. These locations originate from the optimized sensor placements discussed in sections 4.1.4, 4.2.3, and 4.3.2.

Additionally, data is collected from the light obscuration meter located at the ceiling of the fire ULD, as described in Section 3.3.1. The internal ULD light obscuration data serves solely for demonstrative purposes, illustrating the buildup of smoke within the ULD until it is pushed out of the ULD.

A series of three tests assess the response of the heat detection system using both 5-20 and 20-50-min MA intervals. These intervals are essential for detecting the incremental temperature changes associated with smoldering fires. The data analysis will focus on the system's detection times. The detection times provide insight into the efficacy of different moving average intervals in early fire detection.

A comparative analysis compares the performance of the system by monitoring the response of the heat detection system using both 5-20 and 20-50-min MA intervals. The goal is to refine the operational capabilities of the heat detection system.

4.5.1. General Test Observations for Smoldering Fire Scenarios

This section examines the smoldering fire scenarios in ULDs. In the smoldering fire scenario, an aluminum pipe that is 15.24 cm in diameter and 58.88 cm in length is filled with 620g of low-ash hardwood pellets. This pipe is initially ignited at the bottom using a propane hand torch. Once a sustained smolder is observed, the pipe is moved to the center of the ULD floor. The temperature measurement data taken 10 cm from the bottom of the pipe reflects the drying phase of the pellets higher up in the pipe, even though the bottom may already be in the pyrolysis, or smoldering, stage. This setup allows for observing the gradual progression of the combustion process within a controlled environment.

The *heating value*, or calorific value, refers to the amount of heat energy released upon the complete combustion of a unit of fuel. The energy release in this

scenario is critical to understanding the detection capabilities of fire systems for smoldering fires. The hardwood pellets have a heating value of approximately 19.2 MJ/kg [91]. Therefore, the total potential energy from the 620 grams used is around 11.9 MJ. This quantity of heat, when released in a confined space like a ULD, is quite significant.

The pellets initiate the drying phase when subjected to heat. Typically, wood pellets contain 5 to 10 percent moisture, and the initial heat exposure leads to the evaporation of this water content [91]. This stage of moisture evaporation is endothermic, absorbing heat from its surroundings and regulating the overall temperature increase within the ULD.

As the fire intensifies within the pipe, the wood pellets undergo pyrolysis—increased heat and smoke production mark this stage [92] [93]. The insulated pipe design ensures progressive heat build-up. As the heat increases within the pipe, it can contribute to an increased pyrolysis rate, creating a feedback loop that intensifies the fire.

The subsequent gas combustion stage occurs if sufficient oxygen is present, leading to the efficient burning of the emitted gases [26]. During the gas combustion phase, the wood pellets release volatile gases such as carbon monoxide, hydrogen, and methane. These gases mix with the oxygen in the ULD and ignite upon reaching their respective ignition temperatures. This phase characterizes a more efficient and complete burning process.

Finally, the coal burnout stage involves the burning of residual carbon particles. These latter demonstrate different heat release patterns, with the gas combustion stage typically contributing to higher heat output within the ULD.

The experimental observations across three distinct tests demonstrate the variability inherent in smoldering fires. In Figure 40, the x-axis depicts time, while the y-axis illustrates the internal pipe temperature for three trials. The red dots on the graph denote the time and temperature when external smoke detection occurs. Each of the three tests presents unique temperature trajectories. The variability is indicative of the diverse nature of smoldering combustion. Test 1 shows a steep rise in temperature post the 100°C mark, suggesting a rapid transition from smoldering to flaming combustion. Test 2 and Test 3 offer different patterns of temperature escalation, attributing them to variations in factors like packing density or airflow. These variations impact the combustion dynamics [93] [92].

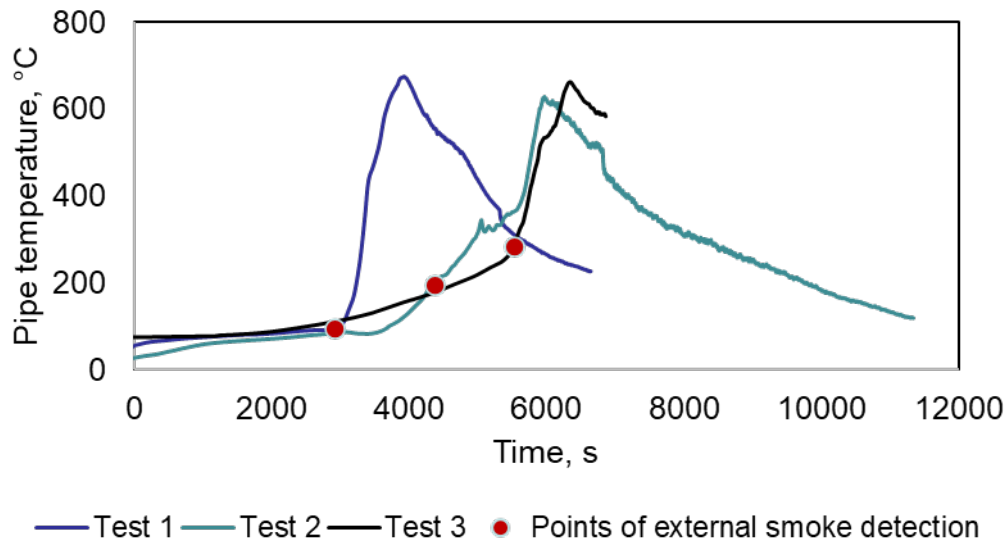


Figure 40 Temperature Profile Analysis of Smoldering Fire Tests in ULDs

A steep increase in temperature typically indicates a transition from smoldering to flaming combustion. This transition is crucial as it exhibits a significant increase in heat release, contributing to a rapid pressure build-up and smoke density inside the ULD. When the internal pressure exceeds the containment ability of the ULD, smoke begins to escape and becomes detectable by external light obscuration meters.

Test 2 presents an interesting case; the temperature reaches a plateau of around 350°C. This plateau may indicate a sustained period where the fire is in equilibrium. During this phase, the burning material's heat generation rate could balance the heat loss rate to the surroundings, resulting in a steady-state condition. Once the combustion intensifies beyond this equilibrium, we see another sharp increase in temperature.

Test 2, as demonstrated in Figure 41, exemplifies the delay in external smoke detection. In this figure, the x-axis represents time, with the primary y-axis measuring

light obscuration levels inside the ULD and in the aircraft cargo compartment. The secondary y-axis tracks the internal pipe temperature. External smoke detection occurs only after sufficient heat accumulation, which increases the internal pressure and drives the smoke outward. This delay is essential to understanding the limitations of traditional smoke detectors, which may only trigger once visible smoke is present.

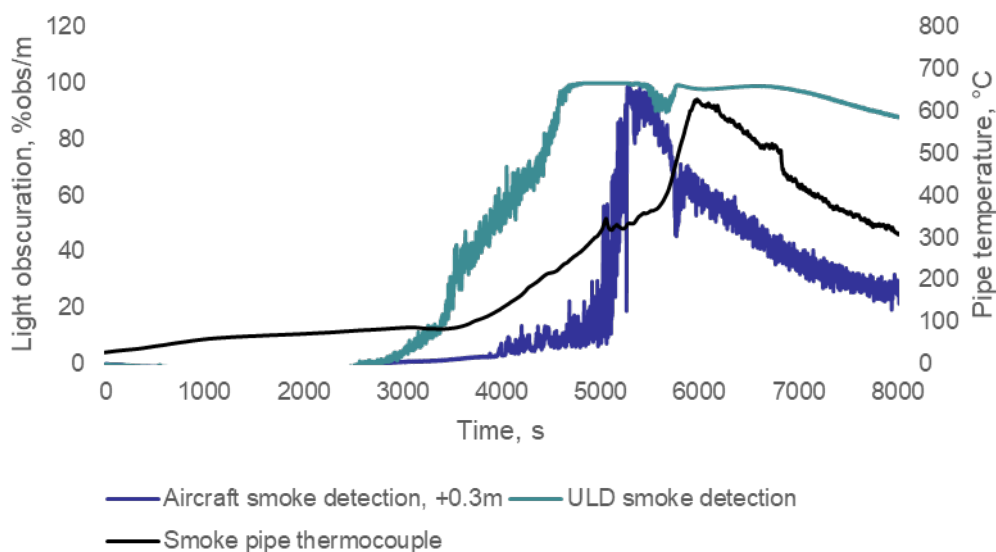


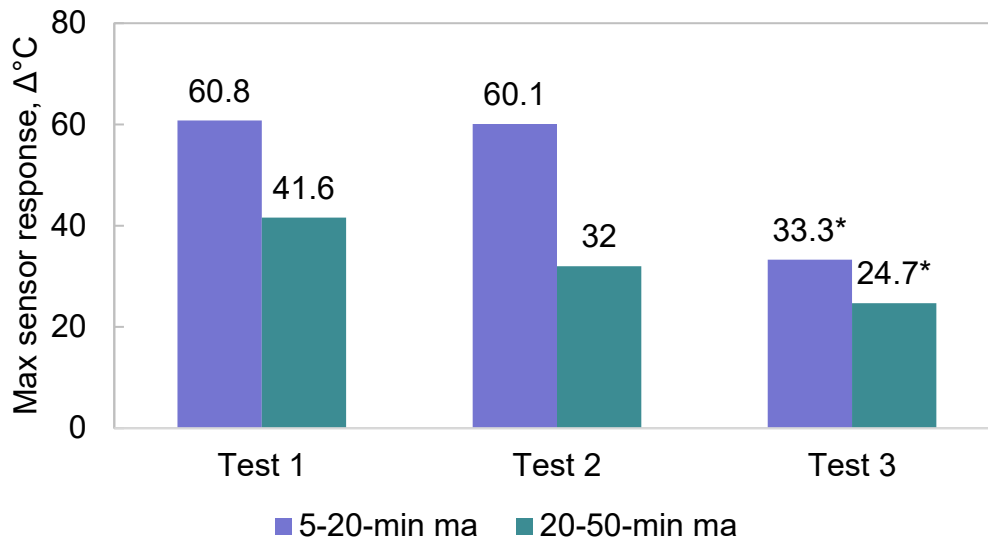
Figure 41 Study of Correlation Between Heat Generation and Smoke Propagation

Figure 42 shows the maximum sensor responses to the varying tests. Tests 1 and 2 displayed similar maximum temperatures in the 5-20-min MA, with Test 1 recording 60.8°C and Test 2 recording 60.1°C. This similarity indicates a degree of reproducibility in the initial phases of the smoldering fire as measured by this approach. In contrast, the 20-50-min MA showed more variation, with Test 1 at 41.6°C and Test 2 at 32°C. The results suggest that the fire development variation can affect the maximum sensor

response. The temperatures observed in these tests are notably higher than the maximum of 4.3°C at 668W heat input, as mentioned in section 4.4.1.

However, exercise caution when making direct comparisons. The combustion of wood pellets in the smoldering fire tests is a more dynamic process with varying heat output over time, unlike the constant heat output from the electric heater in the controlled scenarios.

In Test 3, it is crucial to mention that the UHF RFID temperature sensing tags failed to record the maximum temperature. This significant failure reveals potential difficulties in fully capturing the temperature profile during specific fire scenarios. Understanding these limitations is essential for effectively monitoring and assessing the performance of fire suppression measures. Despite this shortfall, it is noteworthy that the tags detected the fire's presence before ceasing to function.



*Figure 42 Maximum Sensor Temperature Response in Smoldering Fires
(5-20 vs. 20-50-min MA)*

In Figure 42, the presence of an asterisk (*) indicates the UHF RFID temperature sensing tags that failed during this test.

4.5.2. 20-50 and 5-20-min MA Heat Detection Analysis for Smoldering Fires

The 20-50 and 5-20-min MA configurations in RFID-based heat detection systems serve distinct purposes. The 20-50-min MA configuration is particularly effective in identifying the gradual, consistent temperature increases that characterize smoldering fires. The 20-50-min MA configuration detected temperature changes earlier than the 5-20-min MA in two of the three smoldering fire tests, as shown in Figure 43. Early fire detection can be crucial in a cargo compartment where a smoldering fire may not present immediate signs of danger but can rapidly become a significant threat if left undetected. The longer moving average allows the system to discern an actual

temperature trend from the background noise, providing a reliable alert for fires that develop over time.

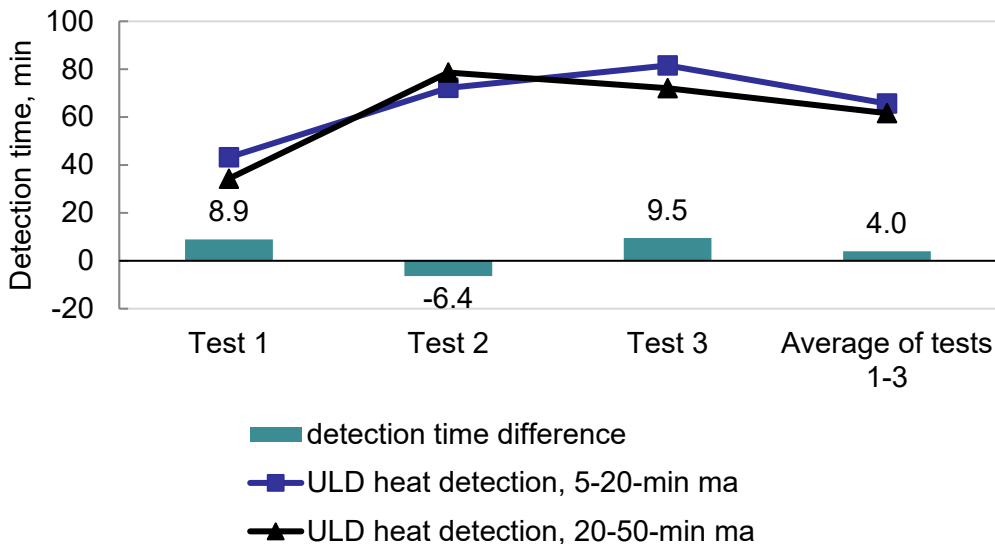


Figure 43 Detection Time Analysis for Smoldering Fires (5-20 vs. 20-50-min MA)

The data analysis reveals that the 20-50-min MA configuration typically detects smoldering fires more quickly than the 5-20-min MA, as seen in the shorter average detection times. In Tests 1 and 3, the initial, gradual rise in temperature during the smoldering stage was sufficient to surpass the activation threshold set for the 20-50-min MA, leading to early detection. However, in Test 2, this gradual temperature increase at the onset of smoldering was not enough to trigger an early detection with the 20-50-min MA threshold, resulting in earlier detection with the 5-20-min MA configuration for detection. This deviation can be attributed to the unique fire dynamics observed in Test 2, where an internal pipe temperature plateau indicated a combustion equilibrium phase. It is important to note that the internal pipe temperature offers a partial view of

the total HRR, serving as an indicator rather than a comprehensive measure. The algorithm relies on temperature measurements at the ceiling of the ULD, which may provide a more accurate representation of the overall HRR than the internal pipe temperature. This unexpected result in Test 2 underscores the challenge of accurately characterizing smoldering fires and the critical need for adaptive detection strategies. Such strategies must be versatile enough to interpret the nuanced signals from varying fire sources.

4.5.3. Fire Detection Comparison for Smoldering Fire Scenarios

This section presents a comparative analysis of detection times between the ULD heat detection system and traditional aircraft smoke detection systems. It focuses on the operational advantages of the RFID heat-based fire detection system in the context of smoldering fire scenarios within ULDs.

The experimental data highlights significant detection time advantages the ULD heat detection system offers, as shown in Figure 44. By utilizing the best-performing setting between the 5-20 and 20-50-min MAs, the system demonstrates an average detection time of 59.5 minutes. In comparison, traditional aircraft smoke detection systems recorded an average time of 71.2 minutes. The results show an average detection time saving of 11.7 minutes across all tests. The average time saving suggests a substantial improvement in the ULD heat detection system's ability to identify potential fire events promptly.

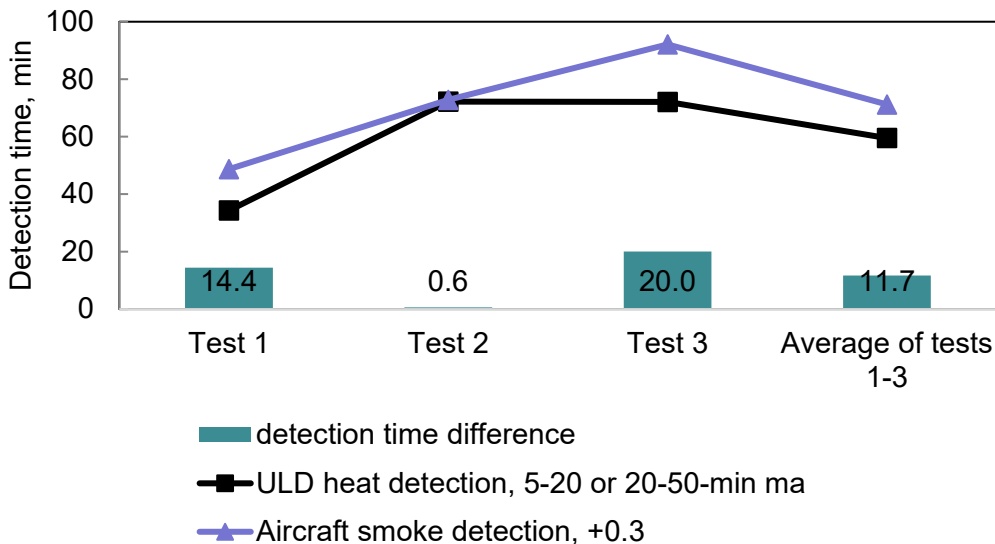


Figure 44 Comparison of ULD Heat and Aircraft Smoke Detection in Smoldering Fires

The ULD heat detection system notably outperformed the smoke detection system in Tests 1 and 3, with faster response times of 14.4 and 20.0 minutes, respectively, using the 20-50-min MA configuration. However, in Test 2, the gradual rise of the internal ULD temperature during the initial smoldering phase failed to meet the early detection threshold of the 20-50-min MA. Therefore, the 5-20-min MA configuration achieved an earlier detection, marginally surpassing the external aircraft smoke detection system by 0.6 minutes. This early detection by the 5-20-min MA configuration occurred as Test 2's internal pipe temperature rapidly escalated to a higher stable plateau, coinciding with a significant rise in heat within the ULD. This heat increase facilitated the expulsion of smoke from the ULD, enabling its near-simultaneous detection by the smoke detection system.

The quicker detection times of the ULD system have profound operational implications. In the event of a fire, the system's efficiency enables faster decision-making for flight crews, allowing more effective fire suppression actions and initiating emergency procedures if needed. This time saving is crucial, as it can contribute to the safety of the aircraft and its passengers by providing valuable minutes for a response.

The findings from these tests align with the objectives of developing a cost-effective, near real-time fire status monitoring system that offers improved detection times over existing solutions. The ULD heat detection system's performance in experimental tests underlines its potential as a superior alternative to conventional smoke detectors, particularly for detecting early smoldering fires in cargo compartments.

4.6. Evaluation of Lithium-Ion Thermal Runaway Scenarios

This section assesses the responsiveness of the RFID-based heat detection system to lithium-ion thermal runaway scenarios within ULDs through a series of two tests. Recognizing the significant threat posed by lithium-ion battery fires, this evaluation seeks to validate the system's effectiveness in a context where rapid escalation and high energy release are critical factors.

Section 3.1.3 describes the test methodology. It evaluates two LCO pouch cells, each fully charged with capacities of 5.48Wh and 6.6Wh. In this setup, a user-activated relay triggers a short circuit, simulating a dangerous event known as thermal runaway.

This initiation method ensures a controlled assessment without the addition of heat. In parallel with Sections 4.4 and 4.5, recording the system's detection times evaluates its performance relative to traditional external smoke detectors commonly used in aircraft cargo compartments.

In this comparative analysis, the external smoke detectors serve as a benchmark to measure the advanced capabilities of the RFID-based system. The comparison highlights the RFID system's potential to offer earlier warnings. Results demonstrate the RFID-based system's performance in terms of detection speed. Such capability is vital in providing timely alerts to flight crews, enabling quick action to mitigate fire events, and enhancing safety against the unique risks presented by lithium-ion batteries in aviation cargo.

4.6.1. General Test Observations for Lithium-Ion Fires

The following section investigates the dynamics of lithium-ion battery fires within ULDs. It uses experimental data to comprehend the phenomena of thermal runaway. This analysis mirrors the detailed observational approach applied in Section 4.5.1, focusing on the interplay between temperature, sensor response, and smoke release patterns during lithium-ion fires.

The experiments used two LCO pouch cells, each fully charged, with capacities of 5.48Wh and 6.6Wh. Using these identical cells in Test 1 and Test 2 ensured a controlled environment to assess thermal runaway characteristics under comparable conditions.

The experiments started with a user-activated relay inducing a short circuit, marking time zero for Figure 45 through Figure 47.

Figure 45 shows the temperature profiles over time for Test 1 and Test 2 of the lithium-ion cells undergoing thermal runaway. Both tests reach peak temperatures in a similar range. However, Test 1 has a prolonged elevated temperature phase was not observed in Test 2. The extended period of high temperature in Test 1 may be attributable to the ignition of flammable vent gases, releasing additional energy over a longer duration. In contrast, the temperature in Test 2 declines more swiftly after reaching the peak. The steeper decline in temperature suggests a less extensive or non-occurrence of vent gas ignition.

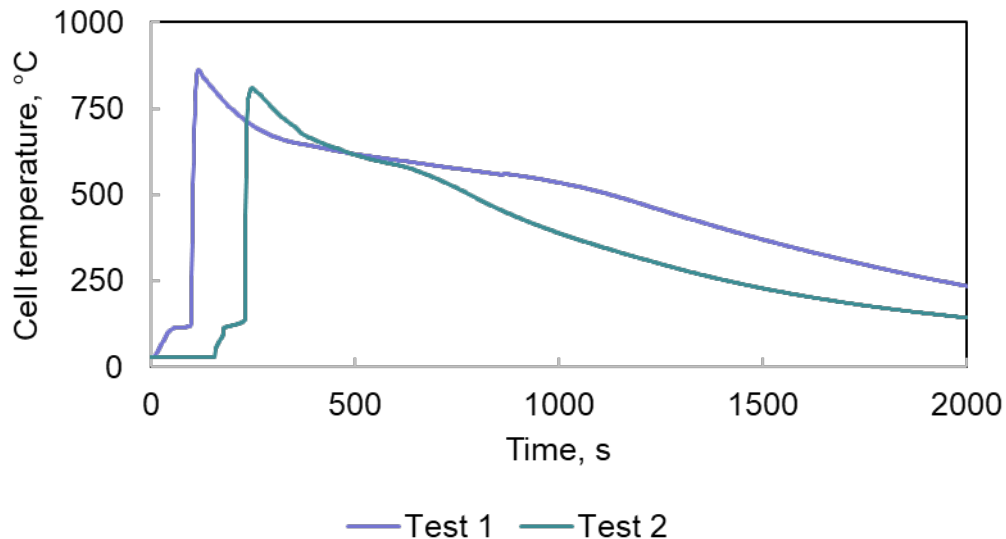


Figure 45 Temperature Monitoring of Lithium-Ion Cells During Thermal Runaway

Figure 46 shows the 5-20-minute moving average sensor response, with temperature measurements taken at the ceiling of the ULD using the 6.4mm mount. The system records the peak sensor response at 2.34°C for Test 1 and 0.65°C for Test 2. The difference in peak sensor response highlights a significant difference in the internal reaction of the cells. The significant sensor response in Test 1 aligns with the prolonged elevated temperature. The elevated temperature response suggests a more substantial ignition of flammable vent gases and a more extended release of thermal energy. The response of 0.65°C for Test 2 surpasses the activation threshold of 0.6°C, as established in Section 4.4.1. However, 0.65°C is well below the minimum sensor temperature response required to push smoke out of the ULD, as outlined in Section 4.4.2.

In contrast, the 2.34°C response from Test 1 far exceeds this threshold and reflects an intense thermal event. The high-temperature response suggests that Test 1 will push smoke out of the ULD while Test 2 will not.

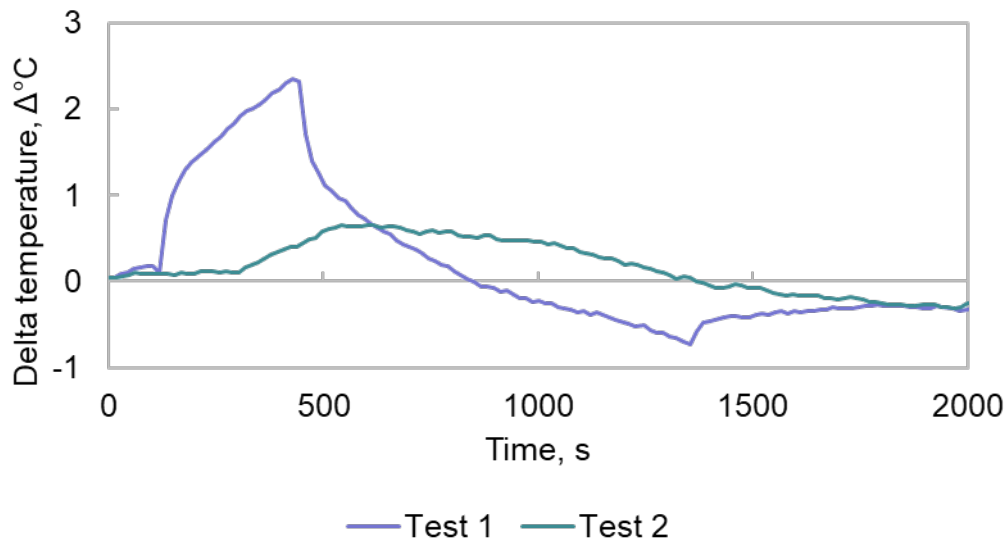
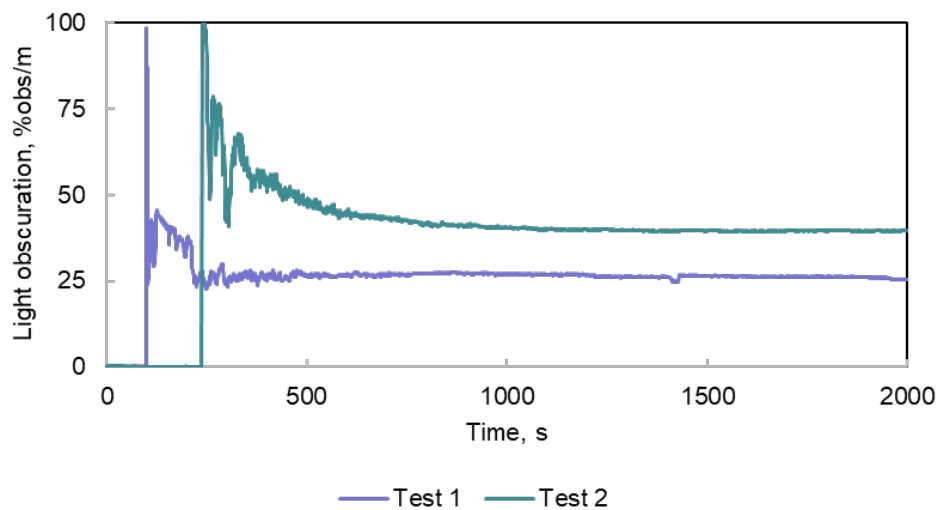


Figure 46 Sensor Response to Thermal Runaway (5-20-min MA Configuration)

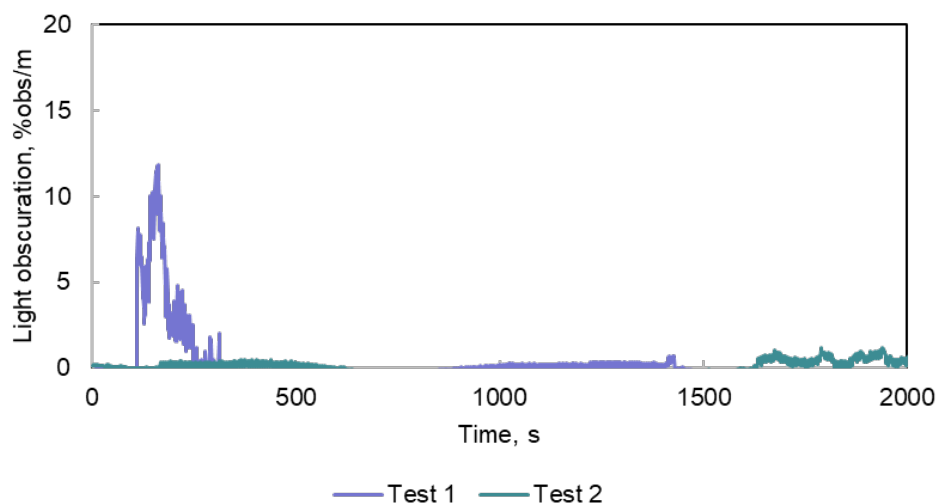
Figure 47 (a) and (b) examine light obscuration within and outside the ULD during thermal runaway tests of lithium-ion cells. In Figure 47 (a), both Test 1 and Test 2 initially exhibit elevated levels of light obscuration inside the ULD. The high light obscuration indicates intense smoke production at the onset of thermal runaway. However, the progression differs in each test. Test 1 demonstrates a rapid decrease in ULD light obscuration. The rapid decline in light obscuration in Test 1 suggests that smoke exits the ULD or a more complete combustion process. Conversely, Test 2 maintains elevated smoke levels for an extended period. The high light obscuration within the ULD indicates that smoke is not exiting the ULD or that the combustion process is less complete.

Figure 47 (b) demonstrates how smoke exits the ULD. Test 1 reaches a peak light obscuration of 11.8% obs/m. This measurement represents a substantial smoked density

but does not surpass the 12.5% obs/m activation threshold used in this report and UL 268 [43]. In contrast, the peak light obscuration in Test 2 is significantly below the smoke detection threshold. This confirms that the heat produced in Test 2 was insufficient to push smoke out of the ULD.



(a)



(b)

Figure 47 (a) Light Obscuration within ULD During Lithium-Ion Thermal Runaway (b) Smoke Detection in Cargo Compartment During Lithium-Ion Thermal Runaway

The experimental data is relevant to the analyses conducted in Section 4.4.2, which focused on the relationship between heat input and smoke exiting ULDs. The sigmoid function model presented in this section underscores the strong correlation between heat input and the effectiveness of external smoke detection systems. The tests detailed here offer practical validation of this model.

4.6.2. 20-50 and 5-20-min MA Heat Detection Analysis for Lithium-Ion Fires

The configuration of moving averages plays a significant role in determining the efficacy and timeliness of the response for lithium-ion fire detection within ULDs. The analysis here focuses on the 20-50 and 5-20-min MA configurations of the RFID-based heat detection system and their response to lithium-ion battery thermal events.

By design, the 20-50 min MA configuration is more attuned to capturing the gradual yet persistent temperature escalations typical of smoldering fires. This attribute was evident in Section 4.5.2, where the 20-50-min MA consistently signaled thermal events earlier than the 5-20-min MA setup.

Conversely, the design of the 5-20-min MA configuration is to respond rapidly to sudden temperature spikes. This sensitivity to abrupt temperature changes is essential for addressing the fast-paced nature of certain lithium-ion thermal events.

The test data reinforces these operational characteristics. As illustrated in Figure 48, the 5-20-min MA configuration displayed more prompt detection times than the 20-50-min MA configuration. The 5-20-min MA configuration reported 2.2- and 8.6-minute

detection times for Test 1 and Test 2, respectively. In comparison, the 20-50-min MA configuration reported detection times of 5.3 minutes for Test 1 and 16.3 minutes for Test 2. The average detection time across tests 1 and 2 for the 5-20-min MA setup was 5.4 minutes, whereas, for the 20-50-min MA setup, it was 10.8 minutes. The detection time difference average was 5.4 minutes between the two configurations.

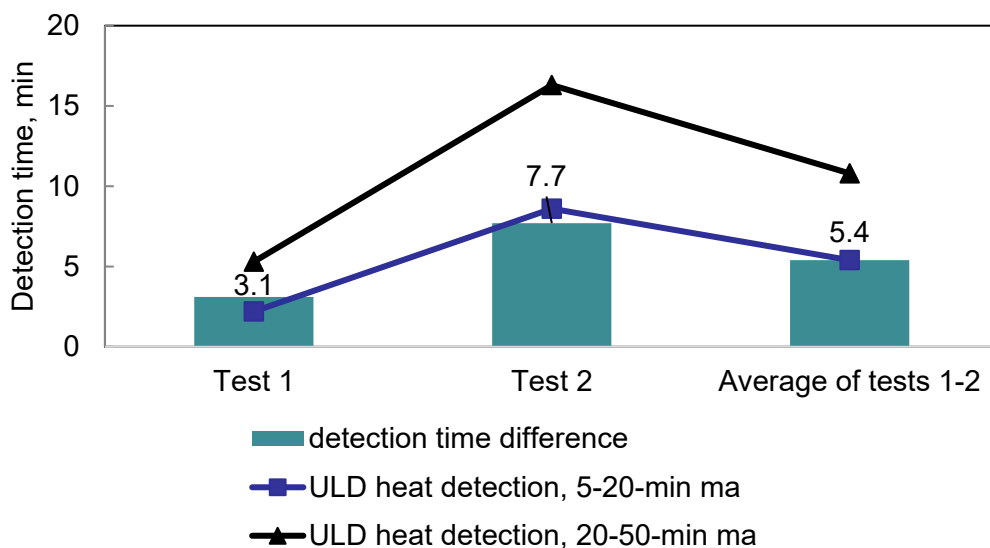


Figure 48 Comparison of Detection Times in Lithium-Ion Fires (5-20 vs. 20-50-min MA)

The choice between the two configurations must consider the specific fire risks associated with the cargo and the operational environment of the ULD. The data suggests that the 20-50-min MA is more adept at providing early warnings for gradually developing fires, while the 5-20-min MA is beneficial where more immediate detection is required. The analysis of detection times underlines the versatility of the RFID-based system in adapting to diverse fire scenarios.

4.6.3. Fire Detection Comparison for Lithium-Ion Fires

The efficacy of fire detection systems in lithium-ion fire scenarios is critical. This section compares the detection times between the ULD heat detection system and the aircraft smoke detection system.

Figure 49 indicates that the ULD heat detection system quickly identified the fires, with 2.2 and 8.6 minutes of detection time for Test 1 and Test 2, respectively. Quick detection is imperative, considering the aggressive nature of lithium-ion battery fires. Lithium-ion fires can propagate to more batteries or cells if not addressed promptly. In contrast, the exterior aircraft smoke detection system did not detect the fire in either test. The absence of detection from the smoke detectors could lead to delayed fire suppression efforts and flight diversions, potentially resulting in more severe outcomes.

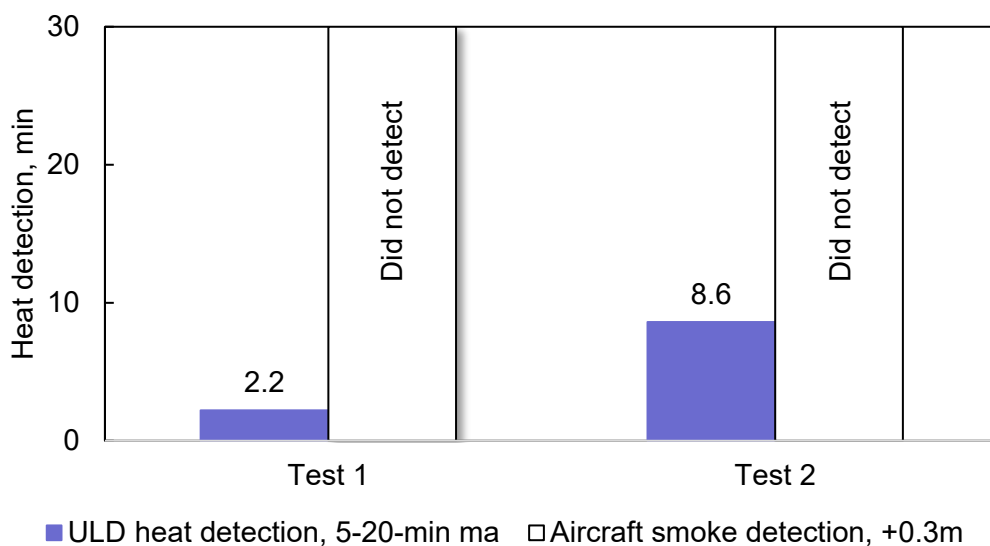


Figure 49 ULD Heat Detection vs. Aircraft Smoke Detection in Lithium-Ion Fires

This performance disparity highlights the need for advanced fire detection systems that can offer faster and more reliable detection of fires in cargo compartments. Furthermore, it suggests that the ULD heat detection system is more effective at early lithium-ion battery fire detection than traditional smoke detectors.

4.7. Results and Analysis Conclusions

This chapter presents a detailed analysis of the experimental evaluation of the RFID heat detection system within an AAY type ULD, focusing on optimizing the MACD algorithm for improved heat detection.

It examines the impact of sensor configurations, including UHF RFID heat sensors and light obscuration meters, and explores the effect of sensor placement on the system's sensitivity and response time.

A key part of the analysis involves assessing the system's performance in various fire scenarios, such as controlled, smoldering, and lithium-ion battery fires. This allows for a comparative assessment against traditional ceiling-mounted smoke detection systems.

Significant findings include the system's effectiveness in smoldering fire scenarios, which are difficult to detect early. Additionally, its rapid response to lithium-ion battery fires highlights its effectiveness in high-risk situations.

The chapter concludes that the RFID-based heat detection system represents a promising advancement in aviation fire safety, offering substantial improvements over traditional fire detection methods. By conducting extensive experimentation and analysis, this chapter lays the groundwork for further discussions on incorporating the system into aviation fire safety procedures.

5. Cost Benefit Analysis

A cost and benefit analysis provides a comprehensive view of a system's value. The cost analysis outlines the financial and operational burdens of implementing the system. In contrast, the benefit analysis highlights its potential to improve safety in air travel. The cost-benefit analysis is essential for stakeholders in aviation to make informed decisions about investing in and adopting advanced fire detection technologies.

5.1. Cost Analysis

While this report aims to address the development and implementation of an advanced fire detection system in aircraft cargo compartments, it is crucial to acknowledge the complexities involved in conducting a thorough cost analysis. A comprehensive cost analysis, such as the "Cabin Water Spray Systems Cost Analysis," would require extensive collaboration with a wide range of entities in the aviation industry, including airlines, manufacturers, and aerospace companies [94]. Given the current limitations in accessing this information and collaboration, a complete cost analysis is not feasible within the scope of this report. However, it is vital to outline what a cost analysis would consider.

A thorough cost analysis would involve examining various financial components. A comprehensive analysis includes expenses for engineering, design software, prototyping, and other essential resources necessary for the system's initial creation.

The next critical component would be a detailed breakdown of equipment costs. The study would involve itemizing the expenses for all fire detection system components, including UHF RFID temperature sensing tags, UHF RFID antennas, UHF RFID readers, and any associated hardware. This analysis also needs to consider the economies of scale, recognizing that unit costs may decrease as production volumes increase. As a baseline, the price paid for 100 units of Axzon 3200 temperature sensing tags is \$2.99 each. Additionally, the SensThys SensArray Core RAIN RFID reader costs \$1,527. Furthermore, the expense for one additional SensThys SensRF-101 antenna is \$524.

Another critical assessment is installation costs for integrating the fire detection system into different aircraft. This aspect of the analysis would vary depending on the size and design of each aircraft. The cost analysis would further investigate the expenses associated with retrofitting the system into existing aircraft, incorporating it into new aircraft during manufacturing, and designing new aircraft models with pre-installed systems. The installation cost assessment would give a comprehensive view of the financial implications across different implementation scenarios.

Maintenance costs form another part of the analysis. Maintenance costs include regular system checks and component replacements, software updates, and other routine maintenance tasks that ensure the system's continuous and effective operation. An important aspect to highlight in the cost analysis is the battery-free operation of the fire detection system. This innovative feature overcomes several challenges associated

with traditional battery-powered systems. Firstly, it significantly reduces maintenance requirements, as there is no need for regular battery replacements. This lowers maintenance costs and diminishes risks like thermal runaway inherent in battery-powered systems. Furthermore, the battery-free nature of the system contributes positively to environmental sustainability. It minimizes waste associated with battery disposal and reduces the environmental impact associated with battery production. By eliminating these factors, the system offers a more cost-effective and reliable solution and aligns with environmentally sustainable practices, an increasingly important consideration in modern aviation industry operations.

Evaluating direct operating costs is essential. This component would estimate the fire detection system's impact on the aircraft's overall operational costs. Consideration would extend to factors such as the system's impact on fuel efficiency due to additional weight, system monitoring and management costs, and any potential savings from improved fire safety.

The dual functionality of RFID tags in fire detection and asset tracking is a crucial component of operational expenses. RFID technology enhances cargo tracking capabilities by optimizing space utilization and inventory management. Implementing RFID technology for ULD tracking can significantly reduce the likelihood of lost or misplaced assets, a significant cost factor in cargo operations [77] [79].

Additionally, accounting for the expenses involved in creating detailed design documents, manuals, and support materials necessary for installing and maintaining the

system would be part of the process. These design costs and the cost of producing manuals and supporting documentation are vital for the system's successful deployment and operation.

5.2. Benefit Analysis

While this report primarily focuses on the system's development, it is crucial to outline what a thorough benefit analysis would contain. This section draws inspiration from "A Benefit Analysis for Cabin Water Spray Systems and Enhanced Fuselage Burnthrough Protection" [95].

A thorough benefit analysis would consider the NTSB investigations on the three catastrophic in-flight cargo fires that originated within ULDs and occurred between 2006 and 2011 [1] [2] [3]. These findings have led to NTSB recommendations aimed at enhancing early fire detection within cargo containers and pallets, improving the fire resistance of cargo container materials, and incorporating active fire suppression systems [4].

Another analysis component would be the growing risk of transporting lithium-ion batteries. From 2010 to 2020, the lithium-ion battery market had a compound annual growth rate (CAGR) of 23% [96]. Furthermore, experts predict the lithium-ion battery market will grow from 230 GWh in 2020 to 1300 GWh in 2030. This trend underscores the increasing importance of effective fire detection for lithium-ion batteries that undergo thermal runaway.

The analysis would compare the advanced system's detection times against traditional smoke detection methods in various fire scenarios. These sections highlight enhanced detection times and enable the estimation of life-saving potential. In addition, estimating the number of lives saved or the extent of damage mitigation achievable annually would rely on statistical models based on historical data on fire incidents.

5.3. Cost Benefit Analysis Conclusions

The cost benefit analysis section culminates in a comprehensive evaluation of the financial and operational aspects of implementing an advanced fire detection system within aircraft cargo compartments. This analysis juxtaposes the system's implementation costs against the tangible and intangible benefits it offers, particularly in enhancing aviation safety.

The cost analysis acknowledges the intricate financial considerations, from initial development expenses, including engineering and prototyping costs, to detailed equipment expenditures for components like UHF RFID temperature sensing tags and readers. Installation costs are examined, focusing on the variability across different aircraft types and the implications of retrofitting versus new installations. An essential aspect of this analysis is the recognition of maintenance costs, which are notably impacted by the innovative battery-free operation of the system, leading to reduced maintenance needs and aligning with environmental sustainability goals.

Direct operational costs are scrutinized, considering the system's influence on fuel efficiency and the operational efficiencies gained through the dual functionality of RFID tags in fire detection and asset tracking. This dual use enhances fire safety and optimizes cargo management, potentially leading to significant cost savings.

The benefit analysis underscores the system's potential to significantly improve air travel safety, drawing on historical data and NTSB recommendations following catastrophic in-flight cargo fires. The analysis highlights the escalating risk of transporting lithium-ion batteries and the system's capability to offer timely detection in various fire scenarios, potentially saving lives and mitigating damage.

In conclusion, the cost-benefit analysis serves as a pivotal tool for stakeholders in the aviation industry, offering a balanced perspective on the financial commitments and the safety enhancements provided by the advanced fire detection system. This comprehensive assessment aids in making informed decisions regarding adopting innovative technologies to bolster fire safety protocols in air cargo transport.

6. Conclusion and Future Directions

This report pursued three objectives to enhance fire protection in aircraft cargo compartments. The report first aimed to develop a cost-effective, battery-free fire detection system and successfully met this goal. The use of UHF RFID temperature sensing tags marked a significant economic advantage due to the low production costs of RFID tags and minimal infrastructure needs for operation. The fire detection system's battery-free operation overcomes the challenges traditional battery-powered wireless fire detection systems face. This feature reduces maintenance requirements and diminishes risks like thermal runaway. Additionally, this approach enhances the system's environmental sustainability by minimizing waste associated with battery disposal and reducing the environmental impact of battery production.

This research achieved the critical objective of developing a system that provides near real-time fire monitoring and early fire detection capabilities within aircraft cargo compartments, especially ULDs. This achievement involved directly installing UHF RFID temperature sensing tags in AAY type ULDs, which significantly differed from the traditional cargo compartment smoke detectors method. This strategic placement of RFID temperature sensing tags enhances detection speed by identifying temperature changes at the source of a fire event. The system employs the MACD algorithm, traditionally used in financial markets, for near real-time temperature trend analysis. This innovative application of the MACD algorithm increases detection speed while maintaining accuracy. This heat detection system can detect small smoldering fires that

are undetectable by traditional ceiling-mounted smoke detectors. Upon detecting a potential fire event, the system can promptly communicate vital data regarding the fire's status and location to the flight crew. This immediate transmission of information is instrumental in enabling flight crews to make crucial decisions, such as initiating fire suppression protocols or preparing for emergency measures.

The research successfully developed a false alarm resistant method for detecting fires in ULDs. By analyzing temperature fluctuations individually and within a communal framework, the heat detection algorithm can better detect anomalies by leveraging aggregated data to assess temperature trends. This achievement was validated through experimental testing. It involved using a multi-ULD configuration, which included a fire ULD equipped with UHF RFID temperature sensing tags for fire monitoring and a reference ULD with UHF RFID temperature sensing tags for baseline temperature data. This configuration effectively distinguishes genuine fire events from normal temperature fluctuations or environmental factors, reducing false alarms.

The NTSB determined that the design of ULD and its materials are crucial factors that impact the detection and suppression of fires within it [5]. This study specifically focuses on detecting heat in AAY type ULDs and the movement of smoke from fires that originate within them. However, the methodology used in this study can be applied to other ULD types and cargo configurations. The findings discussed in this study can also be used as general guidance.

6.1. Summary of Key Findings

Moving Average (MA) Intervals: The research emphasized the need to understand the interplay between activation thresholds, sensor responses, and detection times in various MACD configurations for fire detection in ULDs.

An increased interval of the short-term moving average significantly decreases the activation threshold. Thus, less pronounced temperature changes are required for the alarms to activate. However, adjusting the long-term moving average intervals slightly raises the activation threshold.

Increasing the short-term moving average intervals decreases the maximum sensor response. This contrasts with the effect of increasing the long-term moving averages, which increases the maximum sensor response.

Furthermore, lengthening the interval for short-term moving averages significantly prolongs the detection time, introducing a notable delay in the system's ability to respond to thermal events. Meanwhile, augmenting the long-term moving average intervals causes a moderate extension in detection time. However, this increase is less impactful than the adjustments in the short-term moving averages.

This analysis led to selecting two moving average configurations: the 5-20-min MA for quick detection of abrupt temperature increases and the 20-50-min MA interval for more accurate identification of slowly developing fires.

Heat Sensor Location: Placing the UHF RFID temperature sensing tags within ULDs improves sensor responsiveness and detection speed over externally placed temperature sensing tags. Temperature sensing tags were placed on mounts at varying heights from the ULD ceiling to minimize heat loss from conduction to the ULD surface. While the experiments suggested heights of 50.4mm for maximum response and 50.9mm for a minimum detection time, a 6.4mm sensor mount was chosen for its balanced attributes, ensuring high responsiveness and sensitivity with minimal impact on cargo space.

Smoke Sensor Location: Identifying the most effective location for smoke sensors was essential to the study. The study found that smoke displayed horizontal propulsion as it exited the ULD, directing itself toward the end of the mock cargo compartment before altering its direction. Based on these observations, the optimal placement for light obscuration meters was determined to be +0.3 meters from the ULD door.

Fire Detection in Controlled Fire Scenarios: This testing aimed to understand the correlation between heat input and sensor responses for heat and smoke detection in various controlled fire scenarios. The smoke production is constant during these tests, but the heat input varies. A notable aspect was establishing a linear correlation between heat input and the system's sensor responses. This correlation was captured by a linear function with a high R^2 of 0.97. This model also provided a predictive capability for near real-time fire management decision-making. It enabled fire scale or intensity estimations

based on heat input, allowing flight crews to make informed decisions about fire suppression and diversion strategies.

The smoke detection analysis established a sigmoid function that describes the connection between heat input and the observed smoke exiting the AAY type ULD. The study determined the minimum heat input required for smoke detection by conducting experiments and mathematical calculations. This information enables predictions about the heat for smoke escaping from the AAY type ULD.

Fire Detection in Smoldering Fire Scenarios: The study also addressed detecting smoldering fires, known for their slow heat release and minimal smoke production. These fires present unique detection challenges due to their gradual nature. The experimental setup included a smoke pipe filled with hardwood pellets to simulate smoldering materials. The RFID heat detection system consistently surpassed traditional cargo compartment smoke detection systems in detecting times. The enhanced fire detection was most evident in the 20-50-min MA interval, which showed better performance in early detection in most cases compared to the 5-20-min MA interval.

Fire Detection in Lithium-Ion Fire Scenarios: Another critical aspect of the study was evaluating the system's response to lithium-ion thermal runaway scenarios, characterized by their rapid escalation and high energy release. To simulate thermal runaway scenarios, the testing involved using two fully charged LCO pouch cells within a controlled environment. The 5-20-min MA configuration of the RFID heat detection

system demonstrated higher responsiveness than the 20-50-min MA configuration. Notably, the traditional smoke detection system failed to detect any of these fires.

6.2. Future Research

Future research should consider the advancement of RFID technology, focusing on enhancing the availability and development of robust gas sensing RFID tags. Gas detectors often demonstrate superior sensitivity compared to other fire detection methods due to their ability to detect the gases a fire produces at an early stage [45].

The variance between ground experiments and actual in-flight conditions represents a significant challenge in achieving optimal system performance. In flight, aircraft encounter unique environmental factors, including varying cabin pressure, temperature fluctuations, and vibrations, which can impact the system's sensitivity and reliability. These discrepancies highlight the need for further testing and validation under actual in-flight.

Investigating the impact of cargo compartment types, such as Class E and Class C, could present unique environmental conditions and challenges. Future research should explore ULD characteristics, including size, material, and the distinction between containerized and palletized loads. Additional testing should focus on examining the influence of ULD fillage levels and the arrangement of ULDs within cargo compartments. In fully loaded ULDs, the packed cargo impacts internal airflow, heat transfer, and the behavior of fires. Additionally, it is essential to analyze cargo compartment

configurations that incorporate a mix of ULD types, acknowledging that cargo compartments often contain a diverse array of ULDs.

The activation threshold, set at fifteen standard deviations, requires further research to validate its effectiveness in minimizing false alarms while maintaining sensitivity to actual fire events. Extensive field testing in operational scenarios and detailed statistical analyses would help refine this threshold. The analysis should evaluate the system's false alarm rates to optimize system performance considering environmental changes, cargo compositions, and flight dynamics.

The empirical selection of the 20-50-minute and 5-20-minute moving average intervals requires analytical justification. Future work should explore the mathematical foundations influencing these intervals' effectiveness, particularly how varying rates of temperature rise impact the selection of optimal moving averages for fire detection.

Developing strategies to mitigate potential interference with aircraft RF systems, especially automatic direction finders (ADF), is essential to seamlessly integrate RFID-based fire detection systems. Rigorous testing between the RFID system and existing aircraft communication and navigation systems is vital to maintaining safety and operational efficiency.

A comprehensive cost-benefit analysis is recommended to evaluate the financial implications and safety benefits of implementing advanced RFID-based fire detection systems. This analysis should balance installation and maintenance costs against the

advantages of enhanced safety, risk mitigation, and operational efficiencies, including the potential for reduced insurance premiums and the avoidance of costly liabilities.

Expanding on long-term operational studies involves thoroughly examining factors that could influence the system's performance over time. This includes studying the effects of wear and tear on the system components, changes in cargo handling practices, and the evolution of aircraft design and RF systems.

6.3. Extended Applications Beyond Aviation Fire Detection

The MACD algorithm, when combined with sensitive temperature sensors like RFID or thermocouples, has a wide range of applications beyond aviation fire detection. Its ability to detect subtle temperature trends early on is crucial when fast responses to heat anomalies are necessary for maintaining safety and efficiency. It is worth noting that using inexpensive, battery-free wireless sensors like RFID makes it easy to deploy them in areas where wiring is impractical.

The MACD algorithm can analyze sensor data in manufacturing settings to predict equipment malfunctions or fire risks. This approach would be vital in predictive maintenance. The MACD algorithm could be an essential safeguard, potentially detecting deviations from normal thermal patterns and signaling possible hazards.

In the agricultural sector, especially for grain silo monitoring, the MACD algorithm can play a significant role in enhancing safety. By alerting operators to early signs of heat accumulation, it enables the implementation of mitigation measures to

address conditions that could lead to a grain dust explosion. The system could also benefit chemical storage facilities, where it can detect exothermic reaction risks and trigger preventive measures.

In the automotive industry, particularly for electric vehicle (EV) battery management, integrating the MACD algorithm could potentially monitor for signs of thermal runaway. This integration can enhance safety by enabling early cooling measures or isolating affected battery cells before thermal runaway starts.

References

- [1] National Transportation Safety Board, "Inflight Cargo Fire United Parcel Service Company Flight 1307 McDonnell Douglas DC-8-71F, N748UP, Philadelphia, Pennsylvania February 7, 2006," Washington, D.C., 2007.
- [2] General Civil Aviation Authority of the United Arab Emirates, "Uncontained Cargo Fire Leading to Loss of Control Inflight and Uncontrolled Descent Into Terrain," United Arab Emirates, 2010.
- [3] Aircraft and Railway Accident Investigation Board, "Crash Into The Sea After An In-Flight Fire," Sejong Special Self-governing City, 2011.
- [4] National Transportation Safety Board, "Safety Recommendation A-12 -68 through -70," Washington, D.C., 2012.
- [5] National Transportation Safety Board, "Report No. 12-019," Washington D.C., 2012.
- [6] T. Wilk, "Smoke Detection Delay Inside a Cargo Container," Federal Aviation Administration (Unpublished), Atlantic City, NJ, 204.
- [7] S. Chin, "The Scalability of Smoke Detectors and the Viability of New Detection Methods in Aircraft," Federal Aviation Administration, Atlantic City, NJ, 2019.

- [8] J. Wood, "Strategies for Improved Fire Detection Response Times in Aircraft Cargo Compartments," Federal Aviation Administration, Atlantic City, NJ, 2020.
- [9] M. Petzinger, "Fedex Fire Suppression System," in *The Sixth Triennial International Fire & Cabin Safety Research Conference*, Atlantic City, 2010.
- [10] Telair, "CONTACT-LESS ULD TEMPERATURE SENSING WARNING SYSTEM," [Online]. Available: <https://telair.com/portfolio-item/contact-less-uld-temperature-sensing-warning-system/?nowprocket=1>. [Accessed 13 02 2022].
- [11] FAA Technical Center, Transport Canada Aviation, and Joint Aviation Authorities, "Proposed Cabin Safety Research Program (Transport Category Airplanes) DOT/FAA/AR-95/14," Department of Transportation, 1995.
- [12] Federal Aviation Administration, "Meetings," [Online]. Available: <https://www.fire.tc.faa.gov/meetings/meetings.asp>. [Accessed 12 03 2022].
- [13] "Code of Federal Regulations § 25.857 - Cargo compartment classification," 2016.
- [14] Federal Aviation Administration, "Revised standards for cargo or baggage compartments in transport category airplanes; Final rule. Federal Register, 63(31), 8032.," 17 February 1998. [Online]. Available: <https://www.govinfo.gov/content/pkg/FR-1998-02-17/html/98-3838.htm>. [Accessed 7 February 2024].

- [15] M. Burns, R. Hill, and F. Hahn, "Cargo Fire Suppression by Depressurization," FAA, Atlantic City, 2017.
- [16] "Code of Federal Regulations § 25.858 - Cargo or baggage compartment smoke or fire detection systems.," 1998.
- [17] Federal Aviation Administration, "AC 25-9A," 1994.
- [18] M. Karp and A. Freiling, "Characterizing Smoke Generator Smoke Transport for Aircraft Cargo Smoke Detection Certification," in *SUPDET*.
- [19] M. Karp, "False Alarm Smoke Detection and Smoke Generators," in *International Aircraft Systems Fire Protection Working Group*, Atlantic City, NJ, 2017.
- [20] M. Karp and R. Ochs, "Methods for Characterizing Artificial Smoke Generators for Standardizing Inflight Smoke Detection Certification," *Fire Technology*, no. <https://doi.org/10.1007/s10694-020-01060-3>, 2020.
- [21] M. Karp, "False Alarm Resistant Smoke Detection and Smoke Generator Standardization," in *International Aircraft Systems Fire Protection Working Group*, Cologne, Germany, 2018.
- [22] R.G.W. Cherry, "Research into Fire, Smoke or Fumes Occurrences of Transport Airplanes," Federal Aviation Administration, 2017.
- [23] Federal Aviation Administration, "Technical Standard Order Cargo Compartment Fire Detection Instruments TSO-C1e," Washington, D.C., 2014.
- [24] European Union Aviation Safety Agency, "Halon Replacement in The Aviation Industry," EASA, November 2019.

- [25] J. W. Reinhardt, "Minimum Performance Standard for Aircraft Cargo Compartment Halon Replacement Fire Suppression Systems," FAA, Atlantic City, April 2003.
- [26] J. G. Quintiere, Principles of Fire Behavior, Boca Raton, FL: CRC Press, 2017.
- [27] National Fire Protection Association, SFPE Handbook of Fire Protection Engineering, Quincy, MA: National Fire Protection Association, 2002.
- [28] Federal Aviation Administration, "VENTS WITH SMOKE, FIRE, EXTREME HEAT OR EXPLOSION INVOLVING LITHIUM BATTERIES," 30 June 2021. [Online]. Available:
https://www.faa.gov/hazmat/resources/lithium_batteries/media/Battery_incident_chart.pdf. [Accessed 6 July 2021].
- [29] International Air Transport Association, "2020 Lithium Battery Guidance Document Transport of Lithium Metal and Lithium Ion Batteries," 12 December 2019. [Online]. Available:
<https://www.iata.org/contentassets/05e6d8742b0047259bf3a700bc9d42b9/lithium-battery-guidance-document-2020.pdf>. [Accessed 6 July 2021].
- [30] T. Maloney, "Evaluation of Lithium Battery Thermal Runaway Propagation," Federal Aviation Administration, Atlantic City, 2022.
- [31] S. Summer and T. Maloney, "FIRE HAZARD ANALYSIS FOR VARIOUS LITHIUM BATTERIES," Federal Aviation Administration, Atlantic City, 2017.

- [32] Pipeline and Hazardous Materials Safety Administration, "Hazardous Materials: Enhanced Safety Provisions for Lithium Batteries Transported by Aircraft (FAA Reauthorization Act of 2018)," 21 December 2023. [Online]. Available: https://www.federalregister.gov/documents/2022/12/21/2022-27563/hazardous-materials-enhanced-safety-provisions-for-lithium-batteries-transported-by-aircraft-faa?utm_source=federalregister.gov&utm_medium=email&utm_campaign=subscription+mailing+list. [Accessed 5 January 2023].
- [33] International Air Transport Association, "2023 Lithium Battery Guidance Document Transport of Lithium Metal and Lithium Ion Batteries," 01 09 2023. [Online]. Available: https://www.iata.org/contentassets/05e6d8742b0047259bf3a700bc9d42b9/lithium-battery-guidance-document.pdf?Ref=email&dm_t=0,0,0,0. [Accessed 24 01 2023].
- [34] Federal Aviation Administration, *FAA Reauthorization Act of 2018 (Public Law No. 115-254) Section 333*, 2018.
- [35] M. Karp and J. Sica, "EVALUATION OF LITHIUM BATTERY THERMAL RUNAWAY VENT GAS COMBUSTION HAZARD DOT/FAA/TC-22/12," Federal Aviation Administration, Atlantic City, 2022.

- [36] M. Karp and J. Sica, "EXPERIMENTAL LITHIUM BATTERY THERMAL RUNAWAY COMBUSTION HAZARD TESTS BY GAS ANALYSIS," Federal Aviation Administration, Atlantic City, Unpublished.
- [37] M. Karp, "Thermal Runaway Initiation Methods for Lithium Batteries," Federal Aviation Administration, Atlantic City, 2019.
- [38] T. Maloney, "Impact of Lithium Battery Vent Gas Ignition on Cargo Compartment Fire Protection," Federal Aviation Administration, Atlantic City, 2016.
- [39] M. Karp, "Flammability limits of lithium-ion battery thermal runaway vent gas in air and the inerting effects of Halon 1301," FAA, Atlantic City, 2016.
- [40] Federal Aviation Administration, "2016," Advisory Circular 25.851-1.
- [41] R. Lyon and D. Blake, "Heat Release Rate of Objects Burning in Cargo Compartments," FAA, Atlantic City, NJ, 2005.
- [42] National Fire Protection Association, NFPA 72E: Standard for Automatic Fire Detectors, Quincy, MA: NFPA, 1990.
- [43] Underwriters Laboratories Inc., "Smoke Detectors for Fire Alarm Systems UL 268," 2009.
- [44] Siemens, "Aspirating Smoke Detection," 2015.
- [45] U. Hoefler and D. Gutmachera, "Fire Gas Detection," *Procedia Engineering*, vol. 47, pp. 1446-159, 2012.

- [46] A. McGill, J. Antevil, M. Anderson and D. Venezky, "Fire Detection by Surface Acoustic Wave Chemical Sensor Systems," Naval Research Laboratory, Arlington, VA, 1993.
- [47] C. Hongbin, C. Jiping, Z. Yunjun and W. Qing-M, "Large-scale Fabrication of ZnO Micro and Nano-Structures by Microwave Thermal Evaporation-Deposition," *Journal of Crystal Growth*, vol. 299, no. 1, pp. 34-40, 2007.
- [48] B. Rogers, ULD Explained, Hong Kong: ULD Care, 2016.
- [49] Society of Automotive Engineers, "Air Cargo Unit Load Devices - Performance Requirements and Test Parameters AS36100," 2005.
- [50] Federal Aviation Administration, "Cargo Pallets, Nets and Containers (Unit Load Devices) TSO-C90d," Washington, D.C., 2011.
- [51] International Air Transport Association, 2022 ULD Regulations (ULDR), 2022.
- [52] Society of Automotive Engineers, "Fire Containment Cover - Design, Performance, and Testing Requirements AS6453," 2013.
- [53] Society of Automotive Engineers, "Fire Resistant Container Design, Performance, and Testing Requirements AS8992," 2020.
- [54] D. Dadia, "Class E Cargo Compartment Mitigation Strategies Subjected to Class-A Fires," in *The 8th Triennial International Aircraft Fire and Cabin Safety Research Conference*, Atlantic City, NJ, 2016.

- [55] D. Dadia, "Class E Cargo Compartment Mitigation Strategies Subjected to Lithium Battery Fires," in *The 8th Triennial International Aircraft Fire and Cabin Safety Research Conference*, Atlantic City, NJ, 2016.
- [56] SensThys, "SensArray Enterprise Product Brochure," [Online]. Available: <https://www.sensthys.com/wp-content/uploads/2021/11/SensThys-SensArray-Ent-Product-Brief-2021-04-14.pdf>. [Accessed 10 03 2022].
- [57] SensThys, "SensRF-101 Specifications".
- [58] Axzon, "Reading Magnus-S Sensors," RFMicron, 2018.
- [59] RF Micron, "RFM 3200 Product Brief," Austin, Texas, 2016.
- [60] B. Tsirlina, *Passive xF RFID - A Practitioner's Guide for Selecting Hardware*, Middletown, DE, 2020.
- [61] D. M. Dobkin, "Introduction," in *The RF in RFID UHF RFID in Practice*, Oxford, Elsevier, 2013, pp. 1-4.
- [62] K. Finkenzerler, *RFID Handbook Second Edition*, West Sussex, England: John Wiley & Sons Ltd., 2003.
- [63] International Organization for Standardization, "ISO/IEC 14443-2:2020," 2020.
- [64] International Organization for Standardization, "ISO/IEC 18000-3:2010," 2010.
- [65] International Organization for Standardization, "ISO/IEC 18000-63:2015," 2015.
- [66] F. C. e. al., "Monitoring of temperature stress during firefighters training by means of RFID epidermal sensors," *019 IEEE International Conference on*

RFID Technology and Applications (RFID-TA), Vols. doi: 10.1109/RFID-TA.2019.8892269, pp. pp. 499-504, 2019.

- [67] M.-S. Joan and V. Xavier, "Ubiquitous moisture sensing in automaker industry based on standard UHF RFID tags," *2019 IEEE International Conference on RFID (RFID)*, 2019.
- [68] A. Rennane, A. Abanob and D. Kaddour, "Design of passive UHF RFID sensor on flexible foil for sports balls pressure monitoring," *IET Microwaves, Antennas & Propagation*, pp. 2154-2160.
- [69] H. T. Friis, "A Note on a Simple Transmission Formula," *Proceedings of the IRE*, vol. 34, no. 5, pp. 254-256, 1964.
- [70] S. Smiley, *The Insider's Guide to Working with RFID*, Birmingham, AL: atlasRFIDstore, 2020.
- [71] S. Farahani, *ZigBee Wireless Networks and Transceivers*, Oxford: Elsevier, 2008.
- [72] B. Graham, K. Hirasawa and J. H. Yeap, *Electromagnetic Fields and Waves*, 2019: IntechOpen, 2018.
- [73] NXP Semiconductors, "AN 1629 UHF RFID Label Antenna Design," Philips, 2008.
- [74] Omni-ID, "The Technology of On-Metal RFID," Omni-ID, Foster City, CA, 2009.
- [75] C. A. Balanis, *Advanced Engineering Electromagnetics*, New York: Wiley, 1989.
- [76] RFMicron, "White Paper WP001F17 Chameleon® Self Tuning," RFMicron Inc., Austin, TX.

- [77] N. Viswanadham, A. Praksam, and R. Gaonkar, "DECISION SUPPORT SYSTEM FOR EXCEPTION MANAGEMENT IN RFID ENABLED AIRLINE BAGGAGE HANDLING PROCESS," IEEE, Shanghai, China, 2006.
- [78] K. P. Koldkjær, "RFID for Baggage Handling and Tracking," Lyngsoe Systems, 2017.
- [79] Y. Chang, M. Son, and C. Oh, "Design and implementation of RFID based air-cargo monitoring system," Advanced Engineering Informatics, Republic of Korea, 2010.
- [80] International Air Transport Association, "Baggage Tracking IATA Resolution 753/A4A Resolution 30.53 Implementation Guide Issue 3.0," 2017.
- [81] International Air Transport Association, "Annual Review 2020 76th Annual General Meeting," November 2020. [Online]. Available: <https://www.iata.org/contentassets/c81222d96c9a4e0bb4ff6ced0126f0bb/iata-annual-review-2020.pdf>. [Accessed 02 06 2021].
- [82] State Information Technology Agency, "Baggage IT Insights 2020," 2020.
- [83] M. Santonino, C. Koursaris and M. Williams, "Modernizing the Supply Chain of Airbus by Integrating RFID and Blockchain Processes," International Journal of Aviation, Aeronautics, and Aerospace, 2018.
- [84] Federal Aviation Administration, "AC 25-9A - Smoke Detection, Penetration, and Evacuation Tests and Related Flight Manual Emergency Procedures," 1994.

- [85] Concept Smoke Systems, "Concept SDT Smoke Detector Testing System," Concept Engineering Ltd, Berks, UK.
- [86] Omega, "Revised Thermocouple Reference Tables Type K Reference Tables N.I.S.T. Monograph 175 Revised to ITS-90," Omega.
- [87] RFMicron, "Application Note AN006 Sensor and Temperature Measurements," RFMicron Inc., 2016.
- [88] Coherent, "PowerMax-USB UV/VIS Power Sensors," Coherent, Santa Clara, CA.
- [89] Coherent, "Miniature Diode Laser Modules," Coherent, Santa Clara, CA, 2017.
- [90] A. Ferraro, "Effect of Active Cargo Containers on Aircraft Smoke Transport," Federal Aviation Administration, Atlantic City, NJ, 2022.
- [91] J. Reeb, "Home Heating Fuels: Should I switch to firewood or wood pellets?," Oregon State University, 2013.
- [92] B. Hagen, "Onset of smoldering and transition to flaming fire, PhD Dissertation," University of Bergen, Bergen, 2013.
- [93] R. Mikalsen, "Fighting flameless fires Initiating and Extinguishing Self-Sustained Smoldering Fires in Wood Pellets," Universitaet Magdeburg, Magdeburg, 2018.
- [94] Civil Aviation Authority, "Cabin Water Spray Systems Cost Analysis," CAA, London, March 1993.

- [95] Civil Aviation Authority, "A Benefit Analysis for Cabin Water Spray Systems and Enhanced Fuselage Burnthrough Protection," CAA, April 2003.
- [96] C. Pillot, "The Rechargeable Battery Market and Main Trends 2020-2030," in *Batteries Event 2021*, Lyon, France, 2021.
- [97] Euroasian Cargo Solutions, "ULD Containers," [Online]. Available: <https://www.euascargo.com/en/useful-info/uld-containers/ake-dke-mke-qke-rke>. [Accessed 08 03 2022].